
# Smart Material Prosthetic Ankle

Employing material properties for variable stiffness

Heimir Tryggvason

**Faculty of Industrial Engineering, Mechanical Engineering and Computer Science**
**University of Iceland**

# Smart Material Prosthetic Ankle

Employing material properties for variable stiffness

Heimir Tryggvason

Dissertation submitted to the Faculty of Industrial Engineering, Mechanical Engineering and Computer Science, University of Iceland, in partial fulfillment of a Philosophiae Doctor degree in Mechanical engineering.

PhD Committee
Prof. Fjola Jonsdottir (Supervisor), University of Iceland
Prof. Sigurður Brynjólfsson, University of Iceland
Prof. Sigrún Nanna Karlsdóttir, University of Iceland
Mr. Magnús Oddsson, Össur hf., Iceland

Opponents
Dr. Peter G. Adamczyk, University of Wisconsin, USA
Dr. Elliott J. Rouse, University of Michigan, USA

Faculty of Industrial Engineering, Mechanical Engineering and Computer Science
School of Engineering and Natural Sciences
University of Iceland
Reykjavik, June 2021

Smart Material Prosthetic Ankle – Employing material properties for variable stiffness

Dissertation submitted in partial fulfillment of a *Philosophiae Doctor* degree in Mechanical Engineering



Faculty of Industrial Engineering, Mechanical Engineering and Computer Science
School of Engineering and Natural Sciences
University of Iceland
Hjarðarhagi 2-6
107, Reykjavik
Iceland
Telephone: 525 4000

Bibliographic information:
Heimir Tryggvason, 2021, *Smart Material Prosthetic Ankle*, PhD dissertation, Faculty of Industrial Engineering, Mechanical Engineering and Computer Science, University of Iceland.

Author ORCID: 0000-0003-0789-8338

ISBN: 978-9935-9579-5-5

Printing: Háskólaprent, Fálkagata 2, 107 Reykjavík
Reykjavik, Iceland, June 15th 2021

# Abstract

The inspiration for this research is the natural graduation in stiffness of the biological ankle, over a wide range of ambulation tasks. The goal is to achieve variable stiffness in the force response of a prosthetic foot, utilizing the properties of smart materials. This thesis presents the design and prototyping of a coupling that utilizes the discontinuous change in viscosity observed in shear thickening fluids. A speed dependent stiffness is achieved with the coupling installed in a system of springs. The coupling design presented is used in the modification of a commercially available prosthetic foot. The stiffness of the prototype foot depends on the rate of movement, ranging from a dissipating support at very slow walking speed, to efficient energy storage and return at normal walking speed.

Providing energy return during walking is an important design objective for passive prosthetic feet. The objective of this work is to design a prosthetic foot that provides a damped compliant support for slow ambulation without sacrificing the spring like energy return that is beneficial in normal walking. The function of the original prosthetic foot was analyzed in a finite element model to acquire the parameters for the improved design. The coupling was developed and characterized by uniaxial testing. A prototype prosthetic foot was designed and built, and the speed dependent stiffness measured mechanically. Furthermore, the prototype was tested by a user and body mechanics measured in gait analysis for varying walking speed, comparing the prototype to the original foot model. The results confirm speed dependent stiffness introduced by the novel device.

# Útdráttur

Innblásturinn að þessari rannsókn er náttúrulegur breytileiki í stífni líffræðilegs ökkla við mismunandi hreyfingu. Markmiðið er að ná fram breytilegri stífni gervifótar í svörun við álagi með virkum efniseiginleikum snjallefna. Þessi ritgerð lýsir hönnun og gerð frumgerðar á kúplingu sem nýtir sérstaka skerþykkjandi efniseiginleika vökva (e. shear thickening fluids) sem felast í skyndilegri, ósamfelldri breytingu á seigju vökvans. Hraðaháð stífni næst með kerfi af hlið- og raðtengdri fjöðrun, þar sem kúplingin er notuð við yfirfærslu krafta í kerfinu. Þekkt hönnun á gervifæti er endurbætt með kúplingu sem breytir virkni fótarins. Stífni fótarins veltur þannig á hraða hreyfingar notandans, allt frá því að veita dempandi stuðning á mjög hægum gönguhraða, að því að veita fjaðrandi endurgjöf á venjulegum gönguhraða.

Mikilvægt markmið í hönnun gervifóta er að hámarka orkunýtni þeirra. Markmiðið þessarar vinnu er að hanna gervifót sem veitir mjúkan stuðning við hægar hreyfingar, án þess að fórna þeirri orkunýtni sem hjálpar notandanum í venjulegri göngu. Virkni gervifótarins var greind með einingaraðferð (e. FEM) til að greina breytur og stærðir sem notaðar eru í endurbættu hönnunina. Kúplingin var þróuð og eiginleikar hennar staðfestir með prófunum. Frumgerð gervifótar var hönnuð og smíðuð, og hraðaháð stífni mæld. Ennfremur voru framkvæmdar notendaprófanir og göngugreining á mismunandi gönguhraða þar sem frumgerðin var borin saman við upprunalega gervifótinn. Niðurstöður prófana staðfestu hraðaháða stífni nýrrar hönnunar.

*“A path is made by walking on it” - Zhuangzi*

*This thesis is dedicated to the memory of Prof. Joachim “Joe” Paul (1947 - 2012). Joe is credited for seeding the idea, that my path would one day lead to this milestone.*

# Preface

This dissertation has been prepared for partial fulfillment of the requirements for a doctorate degree in Mechanical Engineering at the University of Iceland. The work presented here was carried out at the Department of Industrial Engineering, Mechanical Engineering and Computer Science at the University of Iceland and in the testing laboratories of Össur hf. in Iceland. This work represents a part of a larger research project, carried out in collaboration between the University of Iceland and Össur hf.

The overall objective of the project-group is addressing variable stiffness of prosthetic feet on wider terms. In addition to presenting novel designs of prosthetic feet, the grouped aimed to map out the need and preferences for stiffness change, in terms of how much change is needed, when it is needed and how it benefits the user.

The idea behind this sub-project was specifically using smart materials for producing stiffness change in prosthetic feet. This idea emerged, based on the notion that the special properties of smart materials make them useful in designing simple effective devices, providing solutions, free of complex mechanisms and control systems.

This work was funded by the Technology Development Fund (grant no. 163805-0613) and the University of Iceland Research Fund. Materials and parts for preparation of prototypes were supplied by Össur hf.

# Table of Contents

# List of Figures

# Nomenclature

| | | |
|---|---|---|
| $C_D$ | Damping coefficient | [Ns/mm] |
| $D$ | Piston diameter | [mm] |
| $D_p$ | Two dimensional axisymmetric pushed piston area | [mm] |
| $h$ | Gap height | [µm] |
| $K_{LS}$ | Stiffness of leaf springs | [N/mm] |
| $K_P$ | Stiffness of parallel spring | [N/mm] |
| $K_{sys}$ | System stiffness | [N/mm] |
| $K_T$ | Combined stiffness of serial connected springs | [N/mm] |
| $l$ | Piston length | [mm] |
| $p$ | Pressure | [Pa] |
| $P$ | Pressure gradient | [Pa/m] |
| $Q$ | Flow in annular gap | [$mm^3/s$] |
| $U_p$ | Piston speed | [mm/s] |
| $U_{p,cr}$ | Critical piston speed | [mm/s] |
| $u_x$ | Fluid velocity | [mm/s] |
| $v_x$ | System velocity | [mm/s] |
| $\gamma$ | Shear rate $\left(\frac{\partial u_x}{\partial y}\right)$ | [1/s] |
| $\gamma_{cr}$ | Critical shear rate (at DST) | [1/s] |
| $\mu$ | Fluid viscosity | [Pa s] |

# Abbreviations

| | |
|---|---|
| CF | Carbon Fiber |
| C-P | Couette – Poiseuille (flow case) |
| DST | Discontinuous Shear Thickening |
| ESR | Energy Storage and Return (of prosthetic feet) |
| EAP | Electro Active Polymers |
| FE | Finite Element |
| MR | Magnetorheological |
| PE | Piezo Electric |
| RoM | Range of Motion |
| SACH | Solid Ankle Cushioned Heel |
| SM | Smart Materials |
| STF | Shear Thickening Fluid |

# Acknowledgements

I would like to thank my advisor, Fjóla Jónsdóttir, for all the support and encouragement throughout the whole project, both on an academic level as well as personal. I have great appreciation for the detailed review and feedback on my work as well as the guidance she gave me to bring this project to a finish. Likewise, my gratitude extends to other members of the Doctoral committee, Sigrún Nanna Karlsdóttir, Sigurður Brynjólfsson and Magnús Oddsson, for their support and guidance.

I would also like to thank my colleagues in the project-group of the Variable Stiffness Project: Anna Lára Ármannsdóttir, Christophe Lecomte and Felix Starker for the deep interest they showed in my undertakings and their expert input to this work. Their partnership and collaboration really made the effort worthwhile.

I would like to thank Vilhjálmur Ívar Sigurjónsson for the technical assistance and for all the machining and assembling that went into facilitating the experiments performed in the hydraulic testing machine.

Finally, I would like to thank my colleagues in room 248 in VR-II for the company, the conversations and for making the daily grinding enjoyable.

# 1 Introduction

The objective of a prosthetic foot will always be to restore the function of the lost limb. While modern prosthetic feet perform well when it comes to replicating the walking function of a biological foot, they lack in other functions. The muscles, tendons and ligaments in the biological ankle work together to facilitate a high degree of adaptability. The advancements strived for in the design of prosthetic feet should be to imitate the dynamics of the natural ankle in order to provide comfort and natural feel for the amputee (Versluys et al., 2009).

It has been indicated that the performance of an energy storage and return (ESR) prosthetic foot, during diverse ambulatory tasks and conditions, could be improved further by varying the stiffness of the device (Hansen, Childress, Miff, Gard, & Mesplay, 2004; Shell, Segal, Klute, & Neptune, 2017). It can further be stated that adjustable, or adaptable stiffness could be beneficial to users, especially where a more optimal stiffness can be provided for tasks that differ from the normal walking motion. The progression of joint moment measured in a biological ankle for various ambulation tasks further supports this.

## 1.1 Background

Imitating the mechanical properties of the ankle joint, described in the curve of the ankle moment plotted against ankle angle in the sagittal plane, can be considered the main aim of prosthetic foot design. The slope of this curve in dynamic conditions is termed quasi-stiffness (Hansen, Childress, Miff, et al., 2004; Rouse, Gregg, Hargrove, & Sensinger, 2013). Such moment-angle curves have been measured for various tasks (Bayram & Bayram, 2018; Bovi, Rabuffetti, Mazzoleni, & Ferrarin, 2011; Collins et al., 2018; Hansen, Childress, Miff, et al., 2004; Kern, Papachatzis, Patterson, Bruening, & Takahashi, 2019) and ankle impedance, i.e. the differential change in position to angular moment, has been estimated for both the stance phase of walking and running (Rouse, Hargrove, Perreault, & Kuiken, 2014; Shorter & Rouse, 2020). A higher quasi-stiffness has been reported for faster walking, specifically during controlled dorsiflexion (Safaeepour, Esteki, Ghomshe, & Osman, 2014). In general, the curve of ankle moment versus angle shows a clockwise hysteresis at slow walking speed. At normal walking speed, the hysteresis disappears and progresses to a counterclockwise curve at faster speed (Hansen, Childress, Miff, et al., 2004) as the ankle provides positive work to the gait. Another characteristic of the biological moment-angle curve is an almost zero slope at heel strike to foot flat in the gait cycle, representing the shock absorption in the heel. For an effective ESR prosthetic foot, the moment-angle curve shows slight hysteresis, but a passive prosthesis lacks the dynamic push-off of the human foot in the late stance (Hansen & Starker, 2016).

Modern passive prosthetic feet can be described mechanically as designated and efficient spring systems. The ESR prosthetic feet, store energy in mid-stance of gait, that again is released for propulsion of the foot in late stance (Grimmer, 2015; Hansen & Starker, 2016). The flexible, energy-storing parts of ESR feet are generally leaf springs, fabricated from

fiber reinforced polymer materials. Stiffness curve and damping response is fixed and depends on material properties, shape, and thickness (Dziaduszewska & Wekwejt, 2018; Versluys et al., 2009). The fixed stiffness of ESR feet is generally optimized for normal, level ground walking, which in turn can be non-optimal for various other ambulatory tasks (Ventura, Klute, & Neptune, 2011). Feet are prescribed to patients in stiffness categories, primarily based on weight and activity levels (Beck, Taboga, & Grabowski, 2016; "Pro-Flex Catalog," 2019).

Increased energy return has been reported to benefit users with increased body propulsion and decreased sound limb loading (Childers & Takahashi, 2018). Research has indicated that prosthetic foot stiffness affects energy return and balance (Adamczyk, Roland, & Hahn, 2017; Hansen, Childress, Miff, et al., 2004; Shell et al., 2017). Deformation of the foot allows roll-over throughout stance, imitating the response of a biological ankle. Stiffness of the foot contributes to this roll-over, affecting the forces and moments exerted on the residual limb, and users' whole body kinematics (Adamczyk et al., 2017). The stiffness curve is aimed at imitating, as closely as possible, the reaction of the biological foot through the gait cycle (Hansen, Childress, Miff, et al., 2004; Hansen & Starker, 2016).

The variations in quasi-stiffness of the biological ankle during different tasks make the stiffness profiles of the prosthesis an important design factor to analyze. A number of researchers have studied the effect of prosthetic ankle stiffness on gait and body mechanics (Adamczyk et al., 2017; Childers & Takahashi, 2018; Fey, Klute, & Neptune, 2011; Hedrick, Malcolm, Wilken, & Takahashi, 2019; Koehler-McNicholas et al., 2018; Schnall et al., 2020; Ventura et al., 2011; Womac, Neptune, & Klute, 2019; Zelik et al., 2011). Although these studies give valuable insight into the design of prosthetic feet, it is complicated to construct an optimal stiffness curve as users have different requirements, depending on their physiology, activity and different tasks. However, it appears that a compliant foot is generally preferred as it provides greater energy return in late stance (Raschke et al., 2015).

Although an emphasis in design of ESR feet has been on energy return, a combination of spring and dissipative damping elements in series has also been shown to be beneficial to the mechanics of gait. For example, damping in early stance was found to increase self-selected walking speed of amputees (De Asha, Munjal, Kulkarni, & Buckley, 2013, 2014; Safaeepour, Eshraghi, & Geil, 2017). Damping characteristics of prosthetic feet have also been attributed to affect loading rates on uninvolved side in unilateral amputees (Jin, Adamczyk, Roland, & Hahn, 2016).

The objective of providing an adaptive walking experience has been investigated in the past and recent publications demonstrate an increased research interest in prosthetic feet that have adjustable stiffness and the effect of prosthesis stiffness on user in different tasks. Prosthetic feet with modular ankle stiffness have been proposed by Shepherd et al. (Shepherd & Rouse, 2017) and Glanzer et al. (Glanzer & Adamczyk, 2018). These devices alter stiffness by shifting a support in a beam deflection system, allowing a change in forefoot stiffness between steps. Shepherd et al. (Shepherd, Azocar, Major, & Rouse, 2018) reported that users could, on average, feel a stiffness change of approximately 8% and were consistent when choosing preferred stiffness. Adamczyk et al. (Adamczyk et al., 2017) showed the effect of forefoot and hindfoot stiffness on walking mechanics at different speeds on a prosthesis with adjustable component stiffness.

Another approach is achieving adaptable walking experience by incorporating active elements, such as actuators and motors. On one hand, powered prosthetic feet range from models that have actuated control of the ankle joint rotation to allow for adaption to inclines and provide toe-clearance in swing face without work input to the gait (Versluys et al., 2009). On the other hand, there are feet that actively provide positive power input into the gait and are capable of generating a push-off force (Herr & Grabowski, 2012; Versluys et al., 2009). The powered elements involved, introduce a cost in terms of weight and complexity, in the addition of sensors, control elements and power sources. Despite the drawbacks of added complexity and weight, these feet do provide active assistance in the gait cycle (Herr & Grabowski, 2012). The aim here is to achieve adaptability in stiffness, without the addition of weight and complexity that actuators introduce.

The innovative idea of this work is changing stiffness of prosthetic feet with the use of smart materials (SMs). Variable stiffness based on SM properties include, for example, dampers based on magnetorheological (MR) and electrorheological fluids. MR dampers in particular have been extensively researched (Wereley & Pang, 1998) and have been used to define a variable stiffness and damping system (Sun et al., 2015) by connecting an MR damper and a spring in parallel and controlling the force response in the system. A more of an adaptable change of fluid properties, rather than controlled, can be found in shear thickening fluids (STFs).

STFs are commonly colloidal suspensions of sub-micron sized particles, such as silica dispersed in a solution of polyethylene glycol. These concentrated suspensions of solid particles are known to show a non-Newtonian change in viscosity with changing shear rate (Barnes, 1989). Shear thickening can either be continuous, so that viscosity increases gradually with increased shear rate, or discontinuous. In highly concentrated suspensions (55-60 % vol.), the discontinuous shear thickening (DST) is seen as a sharp increase in viscosity, of several orders of magnitude, at a certain critical shear rate (Wagner & Brady, 2009). Our focus in this work is on DST, specifically designing a device in which the discontinuity is used to approach a step function in the force response.

## 1.2 Research objectives

The goal of this work is to design, prototype and test a variable stiffness prosthetic foot device. The objective is to utilize the state changing properties of smart materials to realize the stiffness change. The design is based on a commercially available foot that is modified to provide the function of adaptable stiffness. Two supporting, secondary objectives were identified:

- Review different SM's with the aim of identifying material properties, and changes in properties, that can be used to realize the change in stiffness.
- Construct a FEM to use as a tool to support the design of a variable stiffness prosthetic foot.

A review of different SM's concluded in employing the rate dependent properties of an STF to realize a non-linear element, that in combination with a system of springs will have speed dependent stiffness. The design of this element is aimed at providing a transition from

compliant damping at slow speed, to force coupling at fast speed. Connecting springs in series in a system, including the damping characteristics of the element, will provide the compliant action of the foot at slower movement. At faster movement, e.g. normal walking speed, the transition to rigid coupling parallel to one spring in the series, focuses the force response to the original leaf springs, that characterizes the energy return of the ESR system.

A FEM of the original prosthetic foot is constructed with the aim to both analyze the original system and to provide a tool to analyze design changes made on the system. The model is first validated against mechanical testing and then used to investigate the approach of variable stiffness through coupling forces over a spring connected in series. As the damping is in contrast with the energy storage and return of prosthetic feet it is also considered important to quantify the energy dissipation of the adaptable element.

The design objectives are damped, compliant response at slow movements while showing more efficient force transfer at faster movements. In a prototype prosthetic foot this should translate to a compliant support for slow ambulation and adaptability during leisurely activity, without sacrificing the spring like energy return, beneficial in normal walking, demonstrated in the characteristics of an ESR foot. The design tradeoff involved is striking the balance between compliance and maintaining sufficient recoverable energy for the level of activity.

## 1.3 Scientific contribution

The scientific contribution involved in the research work presented in this thesis, is stated as four-fold, all reflected in the three journal articles, published as a part of the work.

1. As a part of this work a FE model of the subject prosthetic foot was presented (Tryggvason, Starker, Lecomte, & Jonsdottir, 2020a). The model was used to simulate a standardized mechanical test ("ISO/TS 16955:2016 ", 2016), where the foot performs a full roll-over under a dynamic load profile. The construction of the model is meant to serve as a platform for iteratively modifying designs. A new spring and damper elements are defined in the modified model. Furthermore, the strain energy is analyzed, in order to quantify the dissipation of using damped force coupling for change in stiffness. The analysis surpasses the intricacy of previously published work by assuming the orthotropic properties of the carbon fiber (CF) material and by modeling a dynamic load profile in a transient analysis.
2. A novel design of a speed dependent piston damper is presented (Tryggvason, Starker, Lecomte, & Jonsdottir, 2020b), employing the special properties of DST in an STF. The damping coefficient approaches a coupling function at onset of DST at critical shear rate. The damper piston geometry and gap size are investigated experimentally and characterized. Previous work on STF filled piston devices have aimed at more aggressive damping (higher damping coefficients) at higher agitation frequency in more conventional damping applications (Yeh, Chang, & Chen, 2012; Zhang, Li, & Gong, 2008; Zhou, Yan, Jiang, Xuan, & Gong, 2016).

3. Further development of the STF filled piston design is introduced (Tryggvason, Starker, Armannsdottir, Lecomte, & Jonsdottir, 2020). With the objective of producing a stronger coupling effect, the STF's resistance to flow at critical shear rate causes increased pressure, that is meant to produce a geometric change in an elastic piston. Axial compression, and consequent radial expansion of the piston closes the fluid gap, resulting in a full force coupling. Experimental work characterizes the elastic material and the dynamic function of the device.
4. The incorporation of the novel damper/coupling into a system of springs, resulting in a speed dependent stiffness system is presented in both (Tryggvason, Starker, et al., 2020b) and (Tryggvason, Starker, Armannsdottir, et al., 2020). This concept was then incorporated in a prosthetic foot device and tested both mechanically and in user testing, confirming the variable stiffness of the prosthetic foot.

The following sections list the of published material produced as a part of the project, journal papers, conference papers and presentations, as well as posters.

### 1.3.1 Journal articles:

1. Tryggvason, H., Starker, F., Lecomte, C., & Jonsdottir, F. (2020a). Use of Dynamic FEA for Design Modification and Energy Analysis of a Variable Stiffness Prosthetic Foot. *Applied Sciences*, 10, 650.
2. Tryggvason, H., Starker, F., Lecomte, C., & Jonsdottir, F. (2020b). Variable stiffness prosthetic foot based on rheology properties of shear thickening fluid. *Smart Materials and Structures*, 29, 095008.
3. Tryggvason, H., Starker, F., Armannsdottir, A.L., Lecomte, C. and Jonsdottir, F. (2020). Speed adaptable prosthetic foot; concept description, prototyping and initial user testing. *Transactions on Neural Systems & Rehabilitation Engineering*, (Early access).

Author Contributions, applicable to all articles:
H.T. conceptualized the presented idea, H.T., F.S. and C.L. analyzed and validated the design. H.T. and F.S. conceived, carried out, and interpreted the results of experiments. A.L.A. performed gait analysis. Data curation and visualization was done by H.T. Prototype resources were provided by F.S. and C.L. Original draft preparation was done by H.T and all authors gave input to review and editing. F.J. supervised and acquired funding.

### 1.3.2 Conference papers:

1. Tryggvason, H., Starker, F., Lecomte, C. and Jonsdottir, F., "Modeling of stiffness characteristics in a prosthetic foot", ASME 2017 conference on Smart Materials, Adaptive Structures and Intelligent Systems, USA, Sept. 2017.
2. Tryggvason, H., Starker, F., Lecomte, C. and Jonsdottir, F., "Modeling and simulation in the design process of a prosthetic foot", SIMS 2017, Reykjavik, Sept. 2017.

3. Tryggvason, H., Starker, F., Lecomte, C. and Jonsdottir, F., “Variable Stiffness System Based on Rheology Properties of Shear Thickening Fluid”, 9th ECCOMAS Thematic Conference on Smart Structures and Material in Paris, July, 2019.

### 1.3.3 Conference presentations:

1. H. Tryggvason, F. Starker, C. Lecomte and F. Jonsdottir, “Modeling of stiffness characteristics in a prosthetic foot”, presented at the ASME 2017 SMASIS, USA, Sept. 2017.
2. H. Tryggvason, F. Starker, C. Lecomte and F. Jonsdottir, “Modeling and simulation in the design process of a prosthetic foot”, presented at the SIMS 2017, Reykjavik, Sept. 2017.
3. H. Tryggvason, F. Starker, C. Lecomte and F. Jonsdottir, “Enhancement of prosthetic foot design – Linking mechanical gait test method and FE model for simulation of stiffness response”, presented at OTWorld, Leipzig, Germany, May 2018.

### 1.3.4 Posters:

1. H. Tryggvason, F. Starker, C. Lecomte, and F. Jonsdottir, “Variable Stiffness System Based on Rheology Properties of Shear Thickening Fluid”, 9th ECCOMAS Thematic Conference on Smart Structures and Material in Paris, July, 2019.

## 1.4 Outline of the thesis

The thesis is divided into the following chapters.

**Chapter 2. Design of prosthetic feet**, offers a general overview of the type of prosthetic feet on the market today. Key design parameters and indicators in the gait of users of prosthetic feet are reviewed. Methods used for testing commercial feet and prototypes are described as well.

**Chapter 3. Material properties for variable stiffness**, outlines work that was done on reviewing different materials with respect to how the properties and the change in properties of different smart materials could be used in achieving variable stiffness. The conclusion is to explore the use of STF for the purpose of a speed adaptable stiffness prosthetic foot.

**Chapter 4. Stiffness change under dynamic loading**, presents the original foot model that was used as a basis for the prototype foot. The section includes the work on a FEM analysis made of the foot and the modifications made to quantify damping coefficients and spring stiffness. The system of springs connected in parallel and series to a damper/coupling is introduced as a speed dependent stiffness system. The chapter is largely based on the journal article (Tryggvason, Starker, et al., 2020a) as well as other material.

**Chapter 5. STF damper design**, describes the concept for variable stiffness and details the design of the initial damper used in the prototype. The damper is characterized in axial motion and a prototype foot is presented and mechanically tested in full roll-over test. The chapter is largely based on the second journal article (Tryggvason, Starker, et al., 2020b).

**Chapter 6. Improved coupling function**, explains the design and specification of an elastic piston device offering an increased coupling function. The geometrical changes of the elastic material are measured. The novel device is tested in axial displacement and the prototype is tested both mechanically in a rolling motion to measure stiffness and in user testing. The chapter is largely based on the third journal article (Tryggvason, Starker, Armannsdottir, et al., 2020)

**Chapter 7. Conclusions and future works,** finally some concluding remarks and discussions are put forth summarizing the thesis, as well as considerations and recommendations for future work.

# 2 Design of prosthetic feet

The objective of this chapter is to provide a general review of prosthetic foot design and the mechanical characteristics that affect the performance of the prosthetic device. A review of design features of recent commercial prosthetic feet and published research on models in the design stage are presented. Finally, methods of mechanical testing of prosthetic feet are discussed, as basis for testing of the prototype developed.

## 2.1 Background

The rate of lower limb amputations in western developed countries is 17.1 per 100,000 inhabitants (McGimpsey & Bradford, 2008) and the main causes for these amputations are complications in the vascular system, in particular diabetes related disease. In the USA it is estimated that in 2005, 82% of lower limb amputations were due to vascular disease, including diabetes related (Ziegler-Graham, MacKenzie, Ephraim, Travison, & Brookmeyer, 2008). In Canada, for years 2006-2011, this number is 90% (Imam, Miller, Finlayson, Eng, & Jarus, 2017). Studies agree that there is an increase in numbers of amputations due to aging and related increase in diabetes and vascular disease (Imam et al., 2017; McGimpsey & Bradford, 2008; Ziegler-Graham et al., 2008). It can be concluded that there is a growing need for prosthetics aimed at this group, allowing them mobility and necessary exercise due to health issues.

Prosthetic feet are generally categorized in three types, depending on functionality (and mechanical complexity):

- Solid Ankle, Cushioned Heel (SACH)
- Energy Storage and Return
- Powered Prosthetic Feet

The SACH foot is a solid shape of the foot that does not flex nor provide push-off at late stance of gait, with a bumper in the heel to dampen the force reaction at heel-strike. The ESR, on the other hand, has a range of motion and the main design criteria is to absorb the energy in early mid-stance and return it as push-off at late stance to toe-off. Powered prosthetic feet come in a range of models of varying function. Some provide actuated control of ankle joint rotation to adapt to inclines and provide toe-clearance in swing face, without work input to the gait (Proprio by Össur). Other models actively provide positive power input into the gait (emPower by Ottobock).

Despite the disability, amputees learn how to operate their prosthesis as a tool and get good at it. For example, trans-tibial amputees (TTA) show similar locomotor adaptability to able bodied during trials on split belt treadmill at different speeds (Darter et al., 2017).

## 2.2 Key properties of prosthetic feet

The performance of prosthetic feet is determined in clinical gait analysis of user's whole-body kinematics. Indicators in the gait of amputees that are examined to estimate the performance of the prosthesis are for example:

- Asymmetry in gait (e.g. step length and ground reaction force)
- Self-selected walking speed
- Load on residual leg
- Locomotor adaptation - balance

The design goals for prosthetic feet include increased self-selected walking speed, increased gait symmetry and stability in the gait. Additionally, the design objectives need to account for both more complex and simpler actions than level ground walking. This includes stair ascent/decent, walking up/down inclines, turning, standing up from a chair and still-standing. For the more complex tasks, like stair ascent/decent, the ESR prosthetics show limitation and worse performance than for level ground walking (Sinitski, Hansen, & Wilken, 2012). Furthermore, the design should take into account adaptability to uneven terrain and shock absorption at high impacts all according to specified needs.

The mechanical properties most often designated as the primary design parameters for prosthetic feet are as follows (Grimmer, 2015; Hansen & Starker, 2016):

- Force response
    - Flexibility / Stiffness
    - Damping
    - Roll-over shape
    - Push-off – energy return
- Range of motion (RoM) – in frontal and horizontal plane as well as in sagittal plane
- Toe-clearance during swing phase

The force related parameters are inherently linked in prosthetic feet that incorporate a spring action, like all commercial ESR and powered feet do. The rollover shape is dependent on the stiffness of the prosthesis. Damping is represented in the hysteresis of the deflection curve of the foot. Push-off is dependent on energy return of the spring action, and the range of motion in the sagittal plane (and for some foot models in the frontal plane) is increased with increased flexibility of the spring mechanism. The toe-clearance is, on the other hand, a property that is subjected to other restrictions. In a passive prosthetic it is not possible to affect the toe-clearance as it is impossible to dorsi-flex the foot without work-input to the standard ESR foot (or accept reduced propulsion from the foot's spring system).

Figure 2.1 presents the normalized ankle moment vs ankle angle in the sagittal plane of a biological ankle, through the walking cycle, shown for two walking speeds. These curves show a function of the biological foot that prosthetic design aims to imitate. The moment vs angle curve for the ankle describes the quasi-stiffness through the stance phase. The curves show the cycle starting at heels-strike (A) and weight acceptance, through plantar flexion to foot flat (B). The controlled dorsiflexion and foot loading through mid-stance (B-C) to push-off (C-D). Finally, the swing phase, with no load (C-D). The quasi-stiffness is represented

in the slope of the curves (moment/angle). Higher quasi-stiffness is seen for faster walking through mid-stance and towards push-off (B-C). The same curve for a passive ESR foot will be a close to linear curve, going through the center point, not changing for different walking speeds.

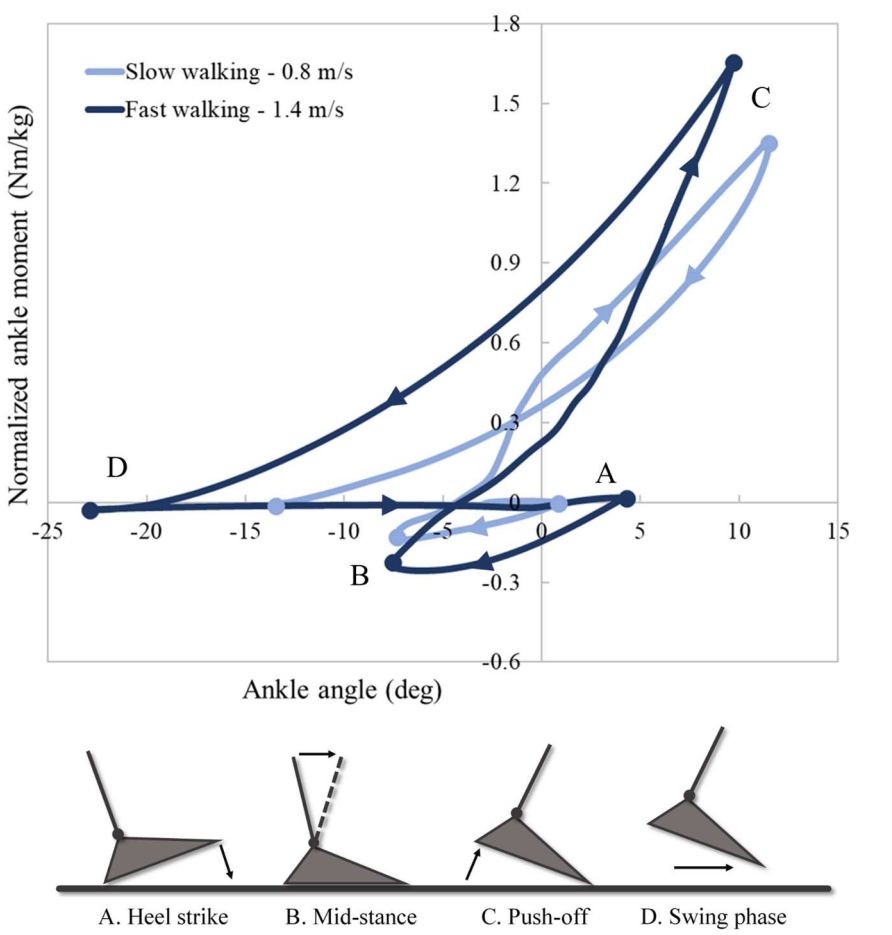


*Figure 2.1 Ankle moment vs ankle angle in the sagittal plane, of a biological ankle, for two different walking speeds. Letters indicate the start of each phase of gait as described by the infographics (Gait analysis data from the able side of a unilateral amputee, courtesy of Anna Lara Armannsdottir).*

Hysteresis is seen in the clockwise curve of slow walking speed in Figure 2.1 while the counter-clockwise curve of the fast walking indicates power input to the gait (curve direction in C). It can therefore be concluded that the ankle function can be imitated quite closely with an effective spring system for walking speed below normal walking (1,1 m/s for the test subject of Figure 2.1), i.e. where hysteresis present in the moment curve. It also follows that the optimal walking speed of amputees is lower than that of able bodied. (Genin, Bastien, Franck, Detrembleur, & Willems, 2008).

## Force response

One of the most characterizing aspect of a prosthetic foot is how it responds to forces acting on it through the stance phase. How much does it flex, how much of the energy is dissipated in damping, how is the spring energy of the leaf springs deflection returned in push-off.

From a user perspective, the optimal response for most of these features is not in a maximum or a minimum but somewhere in between and where exactly is highly dependent on the individual user.

One of the key features of prosthetic feet is the stiffness of the foot in the sagittal plane. A simple measure for stiffness is the force reaction for fixed deflection for the toe and heel. This is discussed further in section 2.4.1. For most ESR feet this relation is progressive. Flexibility of the prosthesis provides the energy transfer from absorption at mid-stance deflection to energy release at the toe at late stance. Added flexibility also enables the user added maneuverability and range of motion, but too much flexion can cause an uneven progression of the center of pressure (CoP) throughout the stance phase of a gait that will affect the forward propulsion (Klenow, Kahle, & Highsmith, 2016). In able bodied, the foot adapts to changes in gait by maintaining a similar roll-over shape (Hansen, Childress, & Knox, 2004). Additionally, an excessively flexible forefoot will result in shorter effective foot lengths leading to reduced ankle moments in the prosthesis and an increased load on the sound side (Klodd, Hansen, Fatone, & Edwards, 2010).

Another significant feature of the ESR foot is the storing of energy with deflection of springs in the foot. For maximum energy return of the foot for forward propulsion, the damping effect should approach zero. Research on comparison of similar prosthetic feet with low and higher damping effect have shown that damping leads to smoother, more consistent progression of CoP throughout stance phase of gait (Hansen & Starker, 2016). In contrast, increased damping effect in prosthesis have also been shown to have an increased internal abduction moment and loading rates in the uninvolved knee (Jin et al., 2016).

### Range of Motion (RoM)

As stated before, most prosthetic feet are optimized for level ground walking. For the walking action the emphasis is on the rotation about the ankle joint in the sagittal plane. Effects of other joints in the feet are neglected or not presented to the same extent. The source of deflection varies between different foot models; in some, a mechanical joint facilitates the movement, while in others a deflection of leaf springs provides a virtual joint. Generally, higher RoM is beneficial and less active patients may benefit more from increase RoM, due to better stability, rather than increased energy return (Zmitrewicz, Neptune, Walden, Rogers, & Bosker, 2006).

Designs of feet have also addressed mechanical adaptation of the prosthetic foot to inclined surfaces. Prototype has been made of a foot design that enables control of the engagement of the main spring mechanism to the shank movement. A deflection in the mechanism after the initial dorsiflexion between heel-strike to foot-flat locks the shank and the spring at the variable foot-flat angle of the ankle depending on angle of incline (Williams, Hansen, & Gard, 2009).

Research also shows benefits of adaptable torsional stiffness in connection between residual foot and prosthetic foot. This has been shown for both stance phase of walking as well as in turning and maneuvering (Stuhlenmiller, Schuy, Beckerle, & Rinderknecht, 2017).

### Toe clearance

Problems with toe-clearance are in some extent connected to the type of amputation. If the amputation is trans-femoral and the patient has a prosthetic knee in addition to the foot, the function of the knee is also limited to assist with the bending of the leg in the swing phase to provide toe clearance.

For foot design, the powered feet are the only type that address this in any substantial way. Powered feet do actively dorsiflex the ankle joint during swing phase to provide this clearance (e.g. Proprio by Össur). The dorsiflexion needed in the foot to provide the clearance is not available in the passive ESR feet without compromising other characteristics. Passive feet with hydraulically damped joint attachment have been shown to provide increased toe clearance (Johnson, De Asha, Munjal, Kulkarni, & Buckley, 2014). The dorsiflexion of the foot is partially retained in the damped joint at toe-off, at the cost of reduced push-off and overall damping through the stance phase. For an ESR to be dorsiflexed during swing phase, this kind of adjustment of the neutral state of the foot must be set to that dorsiflexion.

## 2.3 Features of current commercial feet

### SACH – Solid Ankle, Cushioned Heel

Despite the development in design of prosthetic feet, the simple design of the SACH foot is still in demand. The price of a prosthetic foot is and will be a big factor in choosing a foot. The SACH foot is the most economical choice available and prostheses manufacturers are still developing the simple design of a SACH. The demand for SACH feet is more from lower active amputees that suffer from underlying disease.

Design of more affordable feet is moving towards an effort of applying the ESR technology in a more cost-effective manner, achieved by using cost-effective materials and production methods. An example of this is the Niagara foot (Kandil, 2016) where a spring blade shape is cast using a thermoplastic elastomer. Another example is the Balance Foot S (Össur, Reykjavík) where a polymeric foam heel is attached to a fiber laminate leaf spring keel. Both represent robust designs with the use of materials that exhibit a greater hysteresis in force/displacement curves.

### ESR – Energy Storage and Return

ESR feet have been on the market for over 40 years and have over that period developed from simple bent leaf spring designs to more sophisticated spring systems. Different designs have added functionality, allowing more range of motion and/or specific response of the spring system. Following are some examples of specific designs that attempt this.

- Split leaf springs – enabling inversion/eversion of the foot for increased stability in uneven surface. Most leaf springs models feature this.
- Leaf springs connected with a hinged joint – increased range of motion and a more concentrated center of rotation (ankle joint) in the sagittal plane (Pro-Flex Pivot – Össur)

- Dual keel that engages and provides a force vs. displacement curve that is more progressive at maximum deflection (Thrive foot by Freedom Innovations)
- Adaptation to angles of inclined surfaces, mechanically or with hydraulic control (Echelon by Endolite)
- Joints allowing medial/lateral movement, inversion/eversion.

Some producers of prosthetic feet focus on active users and feet are designed with certain activities in mind, like skiing etc. where foot maneuverability and durability is needed for more complex eversion and torsional movement than in walking on flat surfaces. An example of this is the RUSH foot (Ability dynamics, USA), marketed for highly active people that need a robust foot that can endure use in sea-water and sand conditions. The leaf springs are made of fiberglass (FG) which has higher density than carbon fiber (CF) as well as a lower Young's modulus and tensile strength. Hence, for the same stiffness and strength a thicker, heavier blade is needed. On the other hand, it is more durable as it can be brought repeatedly closer to its breaking point with less risk of delamination than is the case with CF. Blades are glued together, eliminating the need for bolted joints – less weight and pinching points for dirt.

Also emerging are commercial feet that negotiate some of the characteristics for more cost-effective solutions to bring down manufacturing costs and produce more robust feet. The target markets are low income countries and war victims. An example of this is the previously mentioned Niagara foot (Kandil, 2016).

### Powered feet

In recent years, several designs have emerged that have a powered control over the movement of the prosthetic ankle joint. The following lists some types of feet that are commercially available and gives a short description of their function.

- Élan – Endolite: Hydraulic joint, joint resistance is actively controlled via hydraulic system to adjust to uneven terrain and slopes.
- Proprio – Össur: Ankle joint is driven with a DC motor that will adjust the angle to slopes and provide toe-clearance in swing phase.
- emPOWER – Ottobock. emPOWER is the second generation of this foot. This is the only foot that is claimed to provide work into the gait. A DC motor drives the ankle joint with a ball screw. Adjusts to slopes and terrain, normalizes gait and restores function of lost muscle. (Herr & Grabowski, 2012).

Additionally, there is ongoing testing on models that have not yet been made commercially available that promise positive work input to the gait (Cherelle, Grosu, Cestari, Vanderborght, & Lefeber, 2016). As seen above, the first two types of powered feet listed, solely accommodate/control the movement and posture of the foot without adding work into the step.

Development in robotics has been very rapid the last decade or so. Robotic hands controlled by myoelectric signals are on the market now. The most perceptible difference on criteria for design of prosthetic hands and prosthetic feet is that much of the use of a hand can be restored without restoring the full force or power of a nominal human hand whereas the feet

nominal use is under a much higher load of the erected human body, presenting one of the biggest challenge for prosthetic foot design.

To increase energy efficiency and compensate for lacking energy density of electrical motors designers are building feet that work on principles of storing energy from motors over a period in the stride/step to release late in the stance-phase to provide push-off (Cherelle et al., 2016; Darter et al., 2017).

Research has shown positive effects of work input from the prosthesis to the gait. Increased self-selected walking speed, ankle plantarflexion at push-off and toe clearance in comparison with ESR feet has been reported in TTA patients, but the additional power does not normalize the joint kinematics at knee or hip in irregular surfaces (Gates, Aldridge, & Wilken, 2013). Powered feet result in higher RoM and increased ankle power in gait, but does not eliminate the hip-strategy of TTA patients in stair ascent (Aldridge, Sturdy, & Wilken, 2012). Furthermore, there is no significant difference in range of whole-body angular momentum, link to balance, in stair walking between passive and powered prosthesis (Pickle, Wilken, Aldridge, Neptune, & Silverman, 2014).

### Cost of prosthetic feet

One of the key design criteria to be considered in any product development is the cost of the product. In prosthetic design this has an added complexity to it, as the reimbursement rules for prostheses are very different between countries and this influences how affordable the product is to the consumer. Cost of prosthetic feet vary greatly with how advanced the technology being used is and in the USA, range from approx. $5000 for a basic prosthetic foot that will able the amputee to walk on level ground and up to $70.000 for a powered prosthetic ankle, not taking reimbursement into account (Ziegler-Graham et al., 2008).

Affordable prosthetic feet are increasingly low-cost designs of ESR feet rather than SACH feet. In the development of ESR feet, compromises must be made between features to be emphasized; increased damping will affect energy-return, more robust designs often call for added weight etc. The design goal will either be to do better at a specific feature with a specific user group in mind or do better at combining different features for a better all-around foot.

The current commercial DC-motor technology does not fulfill the requirements for driving a prosthetic ankle directly coupled. The models on the market, and that reported on design stage, all depend on spring systems in conjunction with the power input. These systems are less robust than ESR feet and although considerable effort is being made in developing powered feet, the cost of these prosthesis is high and will be in the foreseeable future.

## 2.4 Mechanical testing of prosthetic feet

While performance of prosthetic feet is evaluated through clinical gait analysis, key mechanical properties can be determined by using simpler mechanical testing methods. Standardized mechanical testing methods are generally aimed at testing structural integrity and service-life and are based on assumptions on real life load conditions. Test methods aimed at analyzing other mechanical characteristics, like stiffness and efficiency, are largely

based on these, and the two test methods described here are presented as relevant for the following work.

### 2.4.1 Force deflection testing

Semi-static force-deflection testing is common in the development and production of prosthetic feet. As a quality check, individual blades are tested as simple cantilever beams. These tests are not standardized, but rather a method to standardize production. Standardized testing of prosthetic feet aimed at testing for ultimate strength and fatigue is represented in ("ISO 10328:2016," 2016). The load configurations described by the standard are illustrated in Figure 2.2. The foot is rigidly attached to a uniaxial test machine above an angled free rolling plate. The plate is sloped, -15 deg for testing on the hindfoot and 20 deg for the forefoot testing. A force is applied to the plate, pushing against the foot sample, measuring the resulting displacement. The results from these tests, carried out as quasi-static tests at fixed displacement velocity, give a curve representing the stiffness of the prosthetic foot.

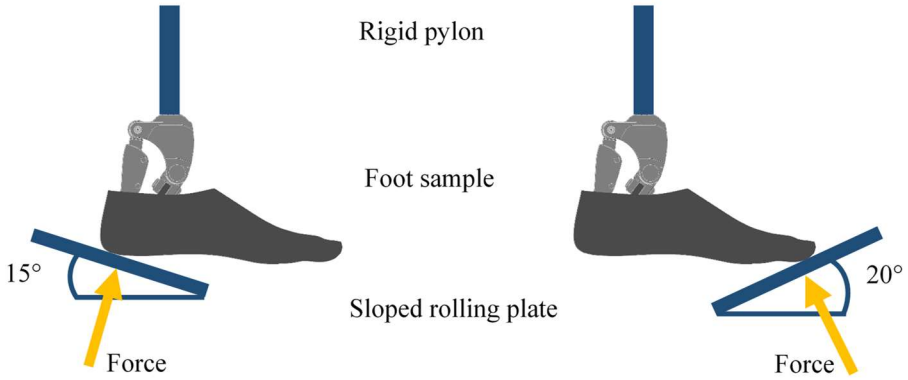


*Figure 2.2 Schematic image of the setup in mechanical testing of maximum hindfoot and forefoot loading, according to ISO 10328. Foot sample is rigidly attached to the pylon and a force is applied perpendicular to the sloped rolling plate, measuring force value and displacement of plate.*

### 2.4.2 Dynamic load testing

Technical specifications specifying quantitative methods to evaluate prosthetic foot performance in a mechanical test setup have been standardized in ("ISO/TS 16955:2016 ", 2016). Figure 2.3 shows the schematic setup of the test equipment and control functions described in the standard. The investigated cycle consists of the dynamic stance phase of a single step. The foot sample is attached to a rod and force applied to a ball joint at the other end. The rod and attached foot sample are thus free to rotate around the ball joint. The M-shaped force curve represents the ground reaction force of heel-to-toe walking; see Figure 2.3 c). The maximum force peak is set to 824 N, representing the typical ground reaction force of a 70 kg person walking at normal speed.

The sample is pushed vertically down on a rotating plate (tilt table). The rotation is constant displacement controlled according to a synchronized profile; see Figure 2.3 b). The heel

contact at the start of the cycle is at a −20 deg decline, rolling over to 40 deg incline and pushing the foot up at the toe. A load cell positioned at 500 mm above the foot (about the height of the anatomical knee joint) on the rod measures the resulting forces and moments. The stance phase time is 0.6 s, corresponding to a 1.0 s normalized step time.

The heel-to-toe profile of the standard does not fully represent normal walking, as it exaggerates the angle at initial contact through foot flat and the loading response of stance phase, resulting in higher moments and anterior-posterior forces than would be expected from clinical gait analysis results of a prosthetics user.

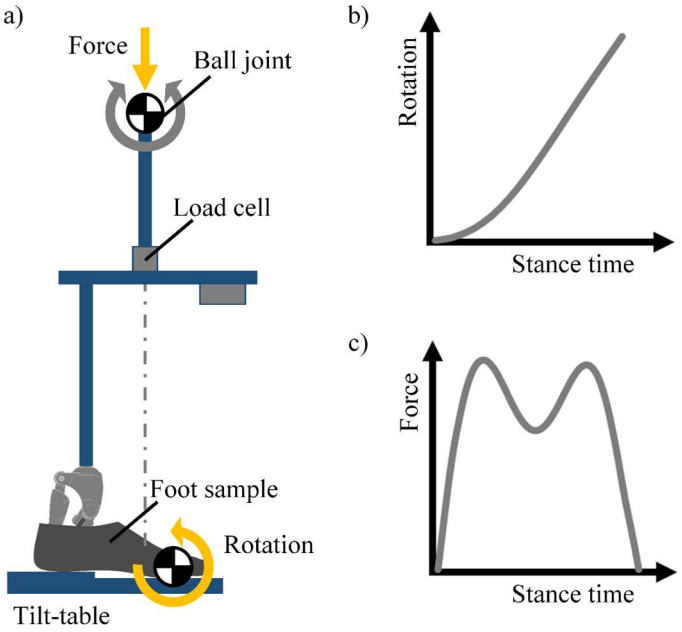


*Figure 2.3 a) Schematic image of the setup for mechanical testing according to ISO/TS 16955. Control functions, b) rotation of tilt-table and c) vertical force on ball joint, as functions of stance phase time (yellow arrows).*

# 3 Material properties for variable stiffness

While the primary goal of this work is to realize a variable stiffness prosthetic foot, the novelty introduced is the use of smart materials (SM) to reach that goal. The approach taken was to explore the broad spectrum of various smart materials and evaluate them for use in variable stiffness. The following review of some different materials is presented as a short summary of this background work. The aim is to identifying properties that are relevant for the use in an active element in a prosthetic foot design. Material function and characteristics are briefly discussed as well as previous research on applications significant to prosthetics and robotics. The materials reviewed here are: magnetorheological (MR) materials, piezoelectric (PE) materials, electro active polymers (EAP) and finally, shear thickening materials (STM).

## 3.1 Background

The general definition of SMs is an engineered or designed material that undergoes a change of properties as a result of certain external stimulation. The property change is partially, or fully reversible and the materials exhibit hysteresis through cycles of these changes. These materials can be composites of materials with different properties where the external stimulation effects which properties are governing. Others are materials whose structure on the micro or nano scale changes alignment according to external stimulation, sometimes through phase changes.

Examples of variable stiffness is exhibited in many biological materials and systems e.g. in plants, trees, shellfish etc. The mechanisms behind the stiffness change are of various nature; Velcro like sacrificial bonds on the molecular level, glass transition due to change in temperature or moisture levels, pressure of water within the structure, to name a few. These examples are in some cases fast acting while others happen over a longer period of time (Saavedra Flores, Friswell, & Xia, 2013).

Several attempts have been made on producing a variable stiffness element; from variable material properties, mechanically varying systems, variable layer bonding etc. The requirements for such an element have been established but yet the majority of the technology presented has not reached the levels of maturity, stability or reliability needed for commercial success (Kuder, Arrieta, Raither, & Ermanni, 2013).

## 3.2 Magnetorheological materials

MR materials are composite materials that exhibit a change in rheological properties under a magnetic field. MR materials are suspension of ferromagnetic particles on the micro scale

that are dispersed in a non-magnetic carrier material. The carrier material is, as indicated, a fluid or soft solid that will deform under shear and can be described with the principles of rheology. The particles have an unsubstantial effect on the properties of the carrier material under normal conditions. In an external magnetic field, the iron particles form a structure, independent of the carrier materials micro structure, which inhibits movement in the material (Muhammad, Yao, & Deng, 2006); see Figure 3.1. The iron particle size is on the micro scale (1-10 µm) (Phulé, 2001). The carrier material of MR materials is primarily fluids, oil or water based, but compliant materials like elastomers and foams that have rheological properties are also available. The MR technology is well established and used in various mechanical systems for actuation, mainly in active vibration control (Carlson & Jolly, 2000). A good example is the commercially available MR damper. These are standard hydraulic piston dampers with a magnetic circuit in the piston-head around the orifice. As the circuit is activated it affects the viscosity of the MR fluid as it is pushed through the orifice increasing the damping effect.

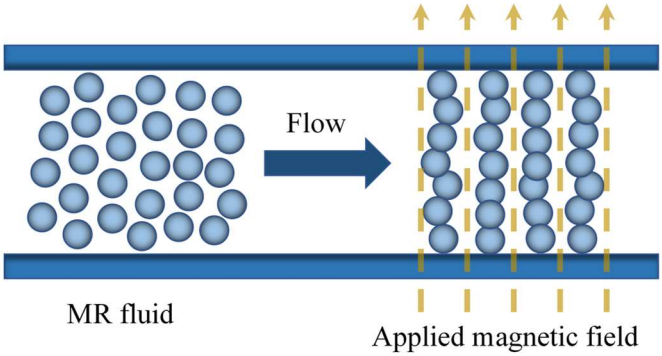


*Figure 3.1 Scematic illustration of the micro structure in MR fluid flow. As the MR fluid is subjected to an external magnetic field the particles form a chain-like structure, indipendent of the carrier fluid.*

MR technology has been used commercially in prosthetic knees with good results (K. H. Gudmundsson, Jonsdottir, Thorsteinsson, & Gutfleisch, 2011). Furthermore, MR dampers have been suggested in prosthetic feet for control of prosthetic knee joints (Gao, Liu, & Liao, 2017; Park, Yoon, Kang, & Choi, 2016).

Gao et al. (Gao et al., 2017) recently published a study on development of a prototype powered knee prosthesis that uses MR damper. The prototype did not include the MR damper though and did not demonstrate the hypothetical function of the foot. Gudmundsson et al. (I. Gudmundsson, Jonsdottir, & Gudmundsson, 2011) proposed and formulated a spring actuator based on an MR elastomer. The resulting design was bulky and the controllable effect not considerable enough to realize a product.

Objective with MR actuators is often damping of vibration. In the case of prostheses, as the examples above show, the objective is more of an impedance control over two sections around joints. In prosthetic feet the objective in normal gait is to be able to return as much of the energy absorbed by the foot prosthesis in early stance, back to the foot in late stance. Damping effect will reduce this energy return. The damping effect is useful in some ambulation instances to make the movements more life-like with softer reactions (or reduce shock).

Characteristics such as fast response time, damped engagement, low operating voltage, limited number of moving parts and silent operation, make MR actuators suitable for prostheses. Controllability, with simple interface between electrical input and mechanical output in MR technology is also an advantage (Olabi & Grunwald, 2007). On the other hand, MR actuators call for an external power source and the use of materials with high values of electromagnetic permeability for an effective magnetic response. These materials are dense and are not the desired materials for use in prostheses where the emphasis is on making the device as light as possible. For an MR actuator to be feasible in prosthetic design the benefit would have to be considerable to justify the weight addition.

Potentially an MR damper could be used in a prosthetic foot as a controlled element between, and parallel to spring acting elements. Controlled damping like that could be beneficial in prosthetic feet where the actuator could be controlled on a range from very compliant to close to fully rigid. Actions that require maneuverability would utilize the compliant mode and actions that require a spring reaction would use the stiff mode. The MR actuator response is quick enough to adjust the stiffness response of the actuator for certain parts of the walking phase as required.

MR technology has good potential for more utilization in damping application and coupling of machine parts where dissipation of energy is important (Spaggiari, 2012). The question is if these actuators can be dimensioned and prepared light enough and with an effect on their controlled spectrum that is non-energy dissipative to fit the needs in prosthetic design.

## 3.3 Piezoelectric materials

Piezoelectric (PE) materials develop an electric charge in reaction to strain due to externally applied mechanical stress. This is what is referred to as the direct effect, but the process is reversible so that the inverse PE effect produces strain in the material as a reaction to applied electrical fields. Both effects are well known and used in everyday applications. The inverse effect is e.g. used for precision control actuators like ink ejectors in ink-jet printers. One of the better-known applications for the direct effect is the piezo ignition for gas appliances.

The PE effect can be found in many diverse materials from natural crystals to soft polymer foams. All piezoelectric materials are anisotropic dielectric materials. In general terms, the source for the effect is the deformation of a structure of/within the material resulting in an asymmetry of charges; see Figure 3.2. In the case of piezoelectric crystalline materials, it is the arrangement of charged ions in the crystal structure that causes an electric field as the structure is stressed. Ferroelectric materials, like one of the most effective piezoelectric materials lead zirconate titanate (PZT), are ceramic materials that require a poling process to arrange their anisotropic structure along a desired direction.

Ceramics are by far the most commercially used piezoelectric material and are used in various equipment. These have a very high force capacity at a low displacement and operating voltage of up to 1000 V. Stacking of the actuator increases the displacement available and commercially available stacked actuators can produce a displacement of 300 μm and generate a force of 80 kN in milliseconds ("Piezoelectric Actuators," 2014).

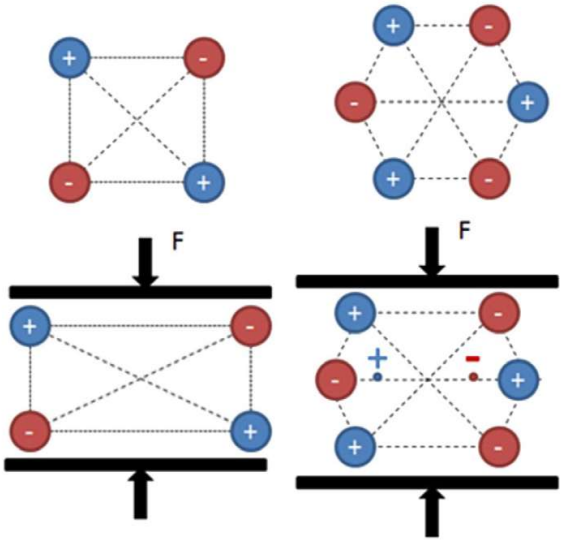


*Figure 3.2 Example of piezoelectric effect, left: symmetric arrangement of charges hence non-piezoelectric, right: asymmetric arrangement of charges and electric field formed under strain conditions (Ramadan, 2014).*

Tests have been made where ceramic piezoelectric actuators have been introduced in carbon fiber epoxy structures, to either effect the stiffness of the structure or morph it. Giddings P. et al. (Giddings, Bowen, Salo, Kim, & Ive, 2010) attached a piezoelectric PZT macro fiber actuator of on a slightly concave shaped carbon fiber plate of two plies. The concave structure was bi-stable and could be snapped between two stable states. The actuator was placed so that contraction of the patch increased the bend when actuated. The blocking force in a 3-point bend was measured as a function of applied voltage to the piezoelectric patch as well as the free deflection, characterizing the actuator properties. Considerable creep was produced in the structure but no significant increase in stiffness was measured.

Other similar tests have been made where piezoelectric patches are embedded between carbon fiber plies with measurable actuation properties, but the order of magnitude lower Young's modulus of the piezoelectric patches weakens the structures. Piezoelectric actuators have been introduced into fiber composites to reduce vibration by creating vibration in an opposite phase and been made commercially available in sporting equipment.

Mei et al. (Mei, Guerrero, Kowalik, & Chung, 2002) examined the reverse piezoelectric effect of a carbon fiber composite using piezoelectric matrix of nylon-6. The sample showed strain in the through thickness of a laminate as a result of applied electric field, although the reaction time was measured in minutes.

Various attempts have been made of embedding piezoelectric material into carbon fiber composites. Lin et al. (Lin, Shaffer, & Sodano, 2010) coated single carbon fibers with concentric PZT for fabrication of a piezoelectric carbon fiber composite. Piezoelectric effect was measured, but the mechanical properties of this composite material were not mapped. Ray et al. (Ray & Batra, 2009) proposed a hybrid piezoelectric composite of parallel aligned carbon nanotubes and piezoelectric fibers in a polymer matrix. Significant piezoelectric effect was measured in a composite with an increased elastic modulus from previous piezocomposites. Villani et al. (Villani et al., 2016) introduced a piezoelectric transducer

integrated into carbon fiber laminate by growing zinc oxide nano-rods directly on the carbon fiber before embedment in epoxy resin. The device showed change in dielectric permittivity indicating piezoelectricity without severely compromising the inter-laminar shear strength of the composite material.

These demonstrate that a number of attempts of fabricating a piezoelectric composite are ongoing. The aim seems to be a material that matches the structural properties of carbon fiber composites and exhibits a piezoelectric effect that is significant enough to serve a load bearing member, with adjustable tensile and compression module. This is though still to be realized. Despite this, all these materials also serve as sensors in the direct piezoelectric effect and even could be evolved to be used for structural health monitoring. It is though difficult to see that the increased complexity in manufacturing of the carbon fiber material would be weighed out with gains from this added functionality. Especially as piezoelectric strain gauges are commercially available for direct attachment to carbon fiber laminate structures.

## 3.4 Electroactive polymers

EAP have been under development since the 1990's and there is still a keen research interest in the field although they are not an established technology in the industry. These are often referred to as artificial muscle because of similarity of their behavior to biological muscle operation and many of the researches are orientated towards advances in robotics. (Belluco, 2007).

EAPs can be categorized in two by their electromechanical operating principle; electronic and ionic. Ionic EAPs are activated by displacement of ions within the material. The most common type is the ionic polymer-metal composite where a polymer membrane is sandwiched between two electrodes. These operate on a relatively low voltage and produce large bending displacements as mobile cations are force to the negative electrode side. Downside of the ionic EAPs is e.g., that the operation requires an electrolyte, response is relatively slow and actuation force is low, are relatively complex to manufacture and have a low efficiency.

The electronic EAPs are of a different nature whereas the activation is due to electrostatic manipulation of dipoles in the material. The group counts a variety of different structured materials of different electrical activation; dielectrics, electro-strictive, piezoelectric, ferroelectrets etc. (Harrison & Ounaies, 2001; Ramadan, Sameoto, & Evoy, 2014; Wegener, 2010). In contrast these materials are fast acting, induce a relatively large actuation force but are limited to operation in moderate temperatures and require high voltages for operation 20-150 MV/m (Belluco, 2007).

The interest in the electromechanical effect in polymer materials can be explained with the interest to counteract the flaws of the more conventional inorganic piezoelectric materials discussed above. Inorganic piezoelectric materials have a more complex and, in most cases, costlier production process, high processing temperature, poling process and toxicity. In contrast to the inorganic materials, polymers are mechanically flexible, span a range of electrical conductivity for different applications (Ramadan et al., 2014). Inevitably this also

implies that polymers are not suited for being used in high force applications where rigidity is of importance.

Main applications for EAPs presently and in development are physical sensors, inertial sensors, acoustic transducers, and energy harvesting devices (vibration and tactile). Moody et al. (Moody, Marvin, & Hutchison, 2016) developed a piezoelectric polymer foam with molecular dopants of large dipole moments showing large piezoelectric effect, suggesting use in energy harvesting devices amongst other. Cellular foam electrets used as key/touch-pads and experimental use in producing facial expressions in polymer foam masks on robots. Despite the advances in the development in piezoelectric polymer foams as well as other EAPs, the low force and lack of rigidity of the presently developed materials excludes them from use in as load bearing members in applications like prosthetic feet.

## 3.5 Shear Thickening Materials

Similar to the MR materials, STMs are composite materials of solid particles suspended in a carrier fluid or embedded in a compliant solid medium. Such suspensions are known to have non-Newtonian properties (Barnes, 1989). These materials react to the rate at which shear stresses are applied to the material, so the more rapidly the stress is applied, the higher the apparent viscosity or shear modulus of the material. The particles are generally sub-micron sized and form a colloidal suspension with the carrier medium, often because of repulsive forces between particles. Some highly concentrated suspensions (55-60 % vol.), exhibit a step wise increase in viscosity, of several orders of magnitude, at a certain shear rate value. This specific material property has sparked interest of use of these materials in variable stiffness actuators.

Figure 3.3 shows schematically the microstructure of particle interactions affecting the apparent viscosity of a shear thickening fluid (STF). At very low shear rates the fluid flows in an equilibrium and the random collisions of particles causes increased viscosity of the suspension, compared to the viscosity of the carrier fluid. As the shear rate is increased, the particles are forced in an ordered layer structure that causes lower viscosity or shear thinning. For a certain critical shear rate, the particle-particle interactions at this high packing

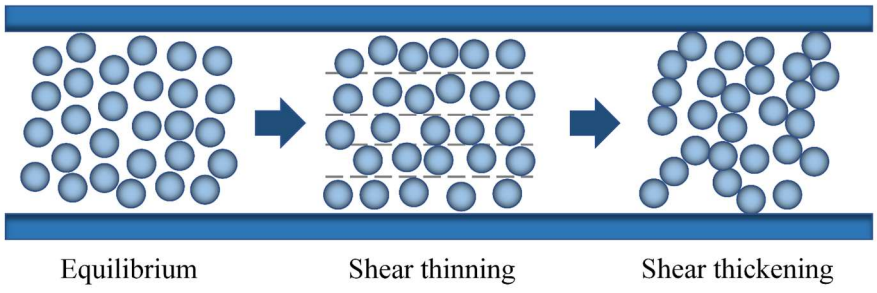


*Figure 3.3 Schematic illustration of particle interaction in a shear thickening fluid for increasing shear rate. At low shear rates the particle interaction are at an equlibrium, then forming a layered structure as shear rate increases. At a critical shear rate the particle collision and confinement cause particle jamming (Wagner & Brady, 2009).*

fractions, will cause a particle jamming or discontinuous shear thickening (DST) in the suspension, seen as a sharp increase in viscosity of several orders of magnitude (Wagner & Brady, 2009).

Figure 3.4 further shows the effective viscosity in the different regions of a DST fluid. In the equilibrium the fluid behavior is close to Newtonian, followed by a region of decreasing viscosity as the particles are forced into the layered structure (shear thinning). At a certain critical shear rate, particle jamming occurs, and the viscosity rises sharply in a discontinuous manner by an order of magnitude. Following the shear thickening is a second shear thinning region characterized by the breakdown of the particle structure of the DST (Galindo-Rosales, Rubio-Hernández, & Sevilla, 2011; Tian, Nakano, & Li, 2018).

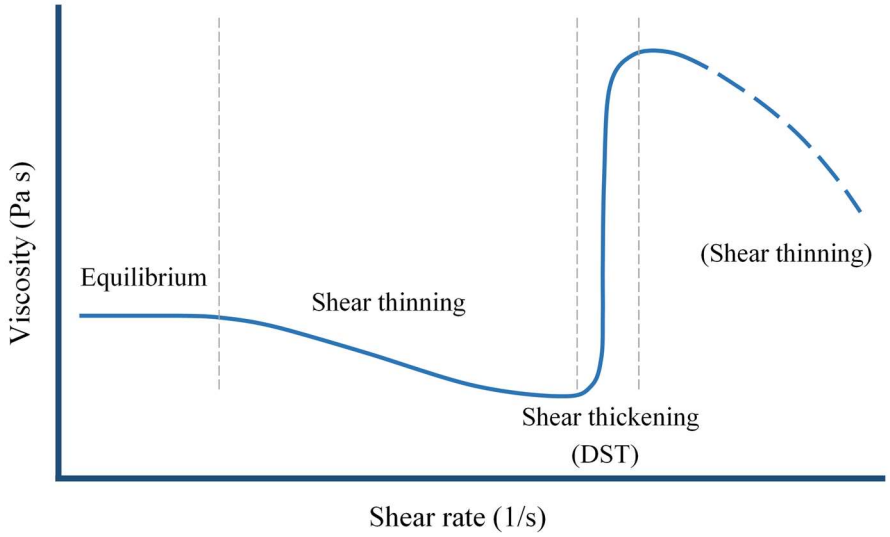


*Figure 3.4 Schematic illustration of the viscosity regions of a DST fluid.*

The properties of DST fluids have been observed, see for example; (Guy, Hermes, & Poon, 2015; Lee & Wagner, 2003; Maranzano & Wagner, 2001). However, there are conflicting theories about the underlying microscopic mechanisms at work. Several mechanisms have been proposed. An early explanation for shear thickening is hydroclustering (Brady & Bossis, 1985; Wagner & Brady, 2009), that is, at high shear rate, hydrodynamic forces overcome inter-particle forces, causing particles to produce clusters. This mechanism is believed to explain continuous shear thickening, but not the significant increase in viscosity in DST (Brown & Jaeger, 2012; Brown & Jaeger, 2014). Another proposed mechanism is dilatancy, in which the effect of volume expansion and resulting forces against the boundary cause the DST effect (Brown & Jaeger, 2012). More recently, it is believed that the effect is caused by frictional contact between the particles as particles are rarely completely smooth (Comtet et al., 2017; Mari, Seto, Morris, & Denn, 2014; Peters, Majumdar, & Jaeger, 2016). Still, it has been demonstrated that for rough surface particles, the DST effect can be explained by hydrodynamics (Jamali & Brady, 2019).

The change in properties, seen in DST is reactive rather than controlled, considering the externa stimuli involved (shear rate). As such the STMs fall outside of the informal definition of smart materials stated above. Being engineered materials designed especially for the function they introduce; they are generally included in the category of smart materials.

The onset of shear thickening in an STF is affected by several parameters of the composite. The volume fraction of particles in the fluid as well as particle size and shape, influence greatly the critical shear rate and the intensity of shear thickening. Another important factor is the viscosity of the carrier fluid (Barnes, 1989; Tian et al., 2018; Wagner & Brady, 2009). At a lower viscosity of the fluid phase the critical shear rate will increase, and shear thickening intensity decrease (Tian, Li, Ding, Alici, & Du, 2013). Consequently, as the viscosity of the carrier fluid is temperature dependent, so are these shear thickening properties of STFs. The critical shear rate is expected to increase with higher temperature and the DST effect will decrease.

Commercial use of STM is known for example in personal protective equipment e.g. for sporting activities ("D3O: Impact protection," 2019) in the form of shear thickening elastomers. The elastomers are mixed with shear thickening additives and formed into flexible padding designed to stiffen when affected by impact forces, spreading the force through the padding. Kalman et al. (Kalman, Merrill, Wagner, & Wetzel, 2009) did research on Kevlar fabric intercalated with shear thickening materials. The results showed improvements in resistance of ballistic penetration and spike puncture.

Zhou et.al (Zhou et al., 2016) reported an STF damper that showed damping characteristics varying highly with frequency and amplitude in a sinusoidal excitation. The damper showed a sharp increase in damping force on a relatively narrow range of velocity, exhibiting the jamming effect in the flow of the STF. Similar research was conducted by Zhang et al. (Zhang et al., 2008) and showed the same rise in damping coefficient of the proto-type damper at a critical velocity where the viscosity of the STF rises dramatically at a critical shear rate.

A velocity sensitive actuator based on STFs property dependency on shear rate could be used to affect the stiffness of the rotation around a prosthetic ankle joint. As stated above, these fluids show a stepwise reaction to change of the rate of the movement at a critical shear rate. The actuator can then be adjusted so it is in the high viscosity regime above the critical shear rate as movements are rapid, but more compliant when the movement is slower. This can be translated to a more rigid response in movements at a velocity of normal and hurried walking but softer in slower movements, like when the foot is being adjusted before you stand up off a chair or other relaxed ambulation.

Figure 3.5 shows the ankle angle and rotational speed of a prosthetic foot (Fey & Hargrove, 2014). In normal gait the rotation of the ankle joint goes from negative between heel-strike to foot flat. After this initial rotation of the ankle there is a controlled/even positive direction rotation ending with a negative rotation leading up to toe-off. A STM based actuator could be adjusted to variate stiffness between different phases through the gait cycle and actuate the spring elements when energy storage and return is needed.

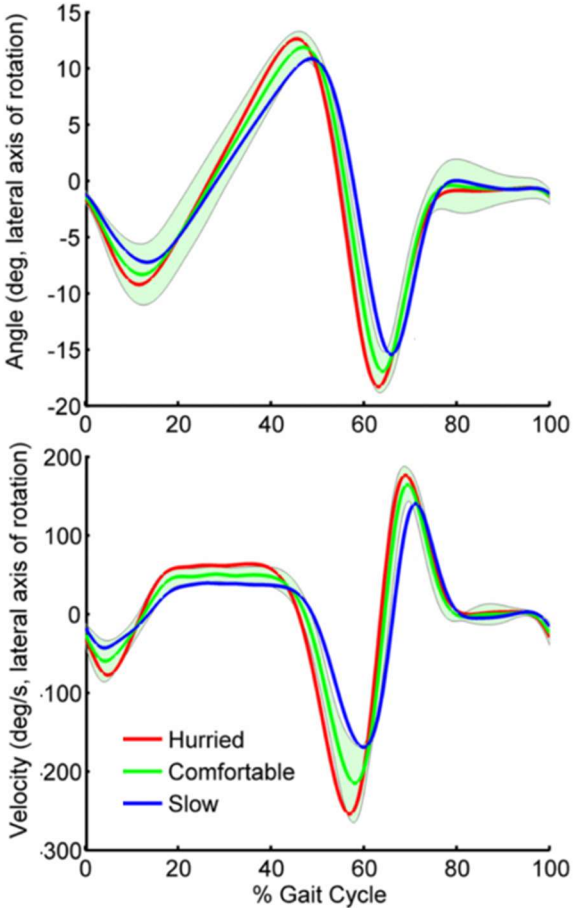


*Figure 3.5 Prosthetic ankle joint angle and angular velocity through a step for three walking speeds on level ground (using an active knee and ankle prosthetic) (Fey & Hargrove, 2014).*

## 3.6 Summary

In the examples above the reaction of SMs is always associated with energy dissipation. This effect contradicts the design objective of ESR prosthetic feet that are being optimized for energy return in a normal walking cycle. However, the damping of the impact forces is needed to some degree in prosthetic feet to reduce negative effect to the upper parts of the lower extremities of the body and ensure comfort for the user.

Table 1 summarizes the above review of the four material groups in a general assessment against key attributes, deemed relevant for the application. EAP and STF are marked as unfavorable against maturity of technology as they do not have a widespread commercial application. Added weight of components and the requirement of external power and control system are likewise considered unfavorable for the application. Even though the added complexity of a control system is considered undesirable, a fully reactive solution could prove hard to adapt to the use in the prosthetic foot.

*Table 1. Assessment of materials against key attributes, relevant for the application; assessed as favorable (+), and considered unfavorable (–).*

| Attributes | MR | PE | EAP | STF |
|---|---|---|---|---|
| Maturity of technology | + | + | – | – |
| Weight of components | – | + | + | + |
| Requires external power/control | – | – | – | + |
| Relative change in property | + | – | – | + |
| Robustness | + | + | – | + |
| Independent of environmental conditions | + | + | – | – |

The main interest in this review is materials that exhibit a change in strain behavior as a result of external forces (i.e. stiffness or rigidity). For these materials, fluid state and other compliant materials show more difference in behavior than soft solid materials. The more compliant the base state is, the more of a jump the material exhibits in its properties. This can be seen in the comparison on materials in the same category e.g. MR-Fluid vs. MR-Polymer and STFs vs. ST-Elastomers. A variable stiffness actuator in a prosthetic foot, will ultimately be connected both in parallel and series to spring elements. Hence, a noticeable effect will be needed to affect the overall response of the system.

The piezoelectric and electroactive materials are either suitable for high force / low strain or high strain / low force applications, as seen in the properties of examples taken of ceramic piezoelectric and piezoelectric polymers, respectively. The recent research on softer piezoelectric polymers addresses the technology mainly for its capability at sensing strain and energy harvesting. The more developed and commercially available ceramic

piezoelectric actuators are mostly high frequency precision devices. Neither category seems to suit as the active element in a variable stiffness actuator.

Actuators based on MR and STF technology could on the other hand be used as the active material in controlled or reactive actuators to provide variability in stiffness. While the viscosity of an MR fluid will be affected by temperature like in the case of STFs, the property change is induced by a magnetic field and is unaffected. The temperature dependency of STFs could be expected to affect a prosthetic device both with change in ambient temperature and through potential heating of the fluid due to shearing.

Chapter 4 describes the variable stiffness system as it is presented here. The damper/coupling function involved can be resolved for example with an MR damper as well as an STF damper. The decision here is to proceed with an STF damper as a lightweight solution as well as being the simple solution with regards to control and need of external power supply. The ambient temperature will be controlled, and potential heating of the fluid due to shear will be observed.

# 4 Stiffness change under dynamic loading

This chapter introduces the design concept for a variable stiffness foot. The design is based on a commercially available prosthetic foot. A finite element (FE) model is constructed of the foot and used for structural analysis through a standardized load cycle. The concept for the variable stiffness function is described and the model used to analyze parameters for the design of the variable stiffness element to be implemented in the original model.

The objective is a proof-of-concept, achieved by applying the modifications on the foot in a simulation on the computational model. Design changes include the addition of a controlled damping element, connected in parallel to an additional spring and in series to the leaf springs of the ESR foot. The aim is to change the stiffness of the device under dynamic loading, by applying a high damping constant, approaching force coupling, for the given boundary conditions. The dynamic modeling simulates mechanical test methods used to measure load response in full roll-over of prosthetic feet (see section 2.4). Activation of the element during loading of the foot justifies the damped effect.

## 4.1 Background

The objective with the modeling is twofold. First, to simulate the dynamic force reaction of a prosthetic foot throughout the gait cycle. The purpose here is to track shifts in function as the design is modified. Secondly, to induce a change in stiffness with a controlled damping element, using the model to verify the change in function of the modified design. Abrupt changes in the force response of a prosthetic device during loading will affect the foot roll-over shape. It is stipulated that a change in force response of a prosthetic device under load, needs to be gradual or damped, to ensure continuity in the roll-over. Therefore, our methodology is to induce stiffness change, by introducing high damping coefficients in a system of springs connected in parallel and series.

It is considered important to quantify the energy dissipation that damped force coupling introduces and the consequential effect on energy return. An element with a high damping coefficients is used to simulate what could be described as a combination of viscose and frictional damping in a functional force coupling. The assumption is made that the functional element has a low off-state damping coefficient and a high on-state damping coefficient.

The modeling is done using finite element analysis (FEA). Earlier work on the application of FEA in prosthetic foot design has focused on investigating structural characteristics of components, rather than function. These works range from stress analysis of individual mechanical components to models of the whole prosthesis, focusing on the force response in the anisotropic carbon fiber material. Omasta et al. (Omasta, Paloušek, Návrat, & Rosický, 2012) studied the load bearing response of a prosthetic foot, from spring blade and foot cover deflection, to stresses in foot-pylon connection. Several studies also utilize force values from

gait analysis data (Bonnet, Pillet, Fode, Lavaste, & Skalli, 2012; Mahmoodi, Aristodemou, & Ransing, 2016; Omasta et al., 2012; Saunders et al., 2003). The use of FEA for direct design purposes is also common, as seen in (Ke et al., 2017), where different curvatures of a spring blade prosthetic foot are investigated, and (Kandil, 2016), where shapes of a solid plastic foot (Niagara foot) are evaluated. In addition, there has been interest in FE modeling of the interface between residual leg and prosthetic socket since the early 90s (Quesada & Skinner, 1991) and is ongoing (Cagle et al., 2018).

FEA that focuses on the dynamic modeling and damping response of ESR prosthetic feet are most notably modal and frequency analysis of sprint feet. Vinney et al. (Vinney et al., 2012) evaluated the suitability of FEA as a method to study dynamic characteristics of prosthetic feet. Noroozi et al. (Noroozi et al., 2014) studied the damped elastic response to impulse synchronization of running feet, where it is suggested that user performance can be enhanced by optimizing the prosthetics design to this parameter. A recent study from Rigney et al. (Rigney, Simmons, & Kark, 2017) uses FEA for mechanical characterization of several types of sprinting feet, including damping under dynamic loading. Furthermore, work done by Shepherd et al. (Shepherd, Gunz, Lecomte, & Rouse, 2019) uses an FEA to validate methods of describing and characterizing the mechanics of running feet. The use of FEA has also proven useful in more complex studies of the prosthetic gait for design purposes. Mahmoodi et al. (Mahmoodi et al., 2016) used FEA to optimize design parameters of three types of prosthetic feet to estimate optimal stiffness based on gait analysis data, such as ground reaction forces and roll-over shape. Bonnet et al. (Bonnet et al., 2012) used kinetic data from gait analysis combined with FEA to calculate stress, strain, and energy storage in a prosthetic foot.

## 4.2 Subject prosthetic foot

The prosthetic foot model studied as basis for a prototype is a Pro-Flex Pivot® (Össur, Reykjavík, Iceland) (size 27, Category 5) ("Pro-Flex Catalog," 2019), a proven energy efficient ESR foot (Childers & Takahashi, 2018) with a high ankle range of motion (RoM) (Heitzmann et al., 2018). The foot is a system of connected carbon fiber (CF) leaf springs, articulating around a pivot joint; see Figure 4.1. The three CF composite leaf springs; top blade, middle blade, and sole blade, are the elastic parts of the foot. The blades are unidirectional CF, with thin layers of bidirectional woven material on top and bottom. The three blades are a split blade design, allowing for inversion and eversion of the foot. The blades are fixed together, bolted with wide washers, clamping the CF material.

The blade assembly is connected to the main body and the mechanical link with clamped connectors. The top blade connects to the main body in the articulating joint, in a pin bearing. The mechanical link connects to the middle blade and the main body, in ball joints with bushings. The main body is milled out of aluminum alloy and the mechanical link is made of stainless steel.

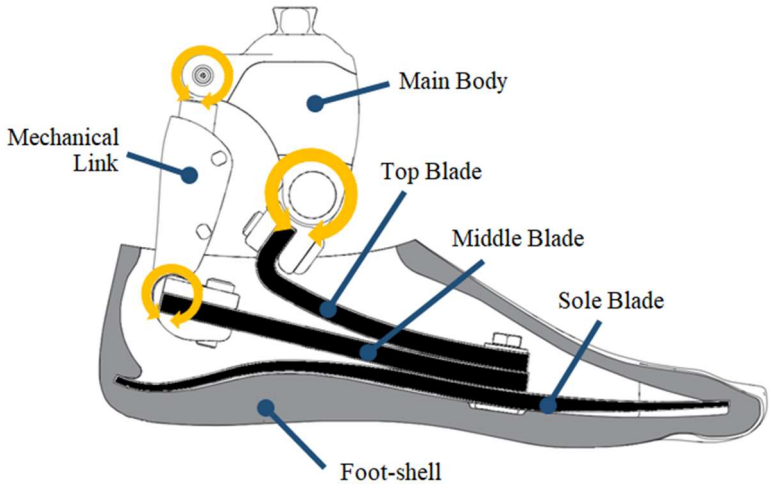


*Figure 4.1 Schematic of the prosthetic foot (Pro-Flex Pivot), yellow circular arrows showing rotational degrees of freedom in joints, carbon fiber leaf springs colored black.*

A force acting on the hindfoot (heel) will result in a compressive force in the mechanical link, of roughly the same magnitude as the ground reaction force. The resulting strain in the leaf springs is mainly the mid- and sole-blades strained against each other, while the top blade is largely unaffected. Counteractively, a force acting on the forefoot (toe) will result in tension in the mechanical link, pulling the mid-blade against the top-blade. Due to the extended moment arm to the pivot joint, the tension force is in the order of three times the ground reaction force working on the forefoot (for size 27). The overall stiffness of the foot is thereby largely affected by the stiffness of the middle blade

Prosthetic feet are prescribed to patients in foot size and stiffness categories, generally based on factors like body weight and activity level (Beck et al., 2016). The stiffness change between categories varies between foot models. For the Pro-Flex Pivot, in the category range considered, this change is 10 – 15%.

## 4.3 Model Development

### 4.3.1 Preparation of FEA

The model is made using ANSYS Workbench® (Canonsburg, PA, USA). The model is constructed in three steps and each step is validated against mechanical testing to confirm assumptions on material properties and contact behavior. Transient structural analysis is carried out for the 3D geometry model of the foot, where a mechanical testing standard ("ISO/TS 16955:2016 ", 2016) (see section 2.4.2) is simulated to allow for real time function of the foot in a continuous step cycle.

The three CF leaf springs are defined as flexible bodies, while other components are assumed fully rigid. The blade thickness is retrieved from the layup recipes of the CF composite material and implemented in the model geometry. The blades are meshed with a sweep method and modeled with solid/shell type elements (ANSYS; SOLSH190). These are solid

type elements that are free from locking in bending dominated conditions and specially designed to model thin to moderately thick plates and shells. The element type allows for definition of layers with different material properties through the thickness of the body ("ANSYS Mechanical APDL Element Reference," 2018)

The layer thickness, material properties, and fiber angle are assigned to each layer of the blades. The tensile and compressive moduli in the fiber direction of the unidirectional CF composite dominates the force response of the blades in bending, although the shear modulus is also important in a high deformation condition (Mujika, 2007). To get an accurate estimate of the moduli, a three-point bend test was performed on 5 mm thick, unidirectional CF composite samples. The flexural modulus was found to be 97 GPa and set as the Young's modulus for the material in fiber direction. Other values on material properties were taken from ANSYS pre-defined "Epoxy Carbon (230 GPa) Prepreg".

Rigid parts are connected by joint elements and assigned a rotational degree of freedom, imitating the actual rolling joint and ball joints of the prosthetic foot. Bonded contact is defined for the connection between the three blades and the connection of blades to the clamps. Frictionless contacts are defined at the wedging of the blades in bending and frictional contact between sole blade and tilt table; see Figure 4.2. Friction factor is adjusted so that no slip occurs. Contact formulation and normal stiffness settings are adjusted to imitate the physical conditions of each case.

### 4.3.2 Model Validation

The model is validated in three steps. First, the in-line production tests of the blades in cantilevered beam loading, are simulated and compared to measured values. This comparison confirms assumptions made on material properties. Second, simulations are done of static toe and heel deflection testing, described in section 2.4.1, and compared to measured values. Herein, the sample foot is rigidly attached to a uniaxial test machine and aligned at a fixed angle, −15 deg for the heel and 20 deg for the toe, against a free rolling plate. The foot is compressed for a set displacement and the resulting force is measured. In this process, the model assumptions on contact and joint element settings between different parts are adjusted. Lastly, a simulation of the roll-over task of the technical specification ("ISO/TS 16955:2016 ", 2016), described in section 2.4.2, is done and compared to measurements for final validation of the model. Figure 4.2 a) shows the FE model displaying strain energy in the flexible parts in maximum forefoot loading and the sequence of the roll-over is shown in Figure 4.2 b).

Every-day use ESR prosthetic feet are used with a cosmetic foot shell, made of soft elastomers. The foot shell was excluded in the FE modeling as the visco-elastic member would increase the complexity and reduce reliability of the model. In contrast to the standard ("ISO/TS 16955:2016 ", 2016), the comparison mechanical measurements were also executed without a foot cover to allow for direct comparison.

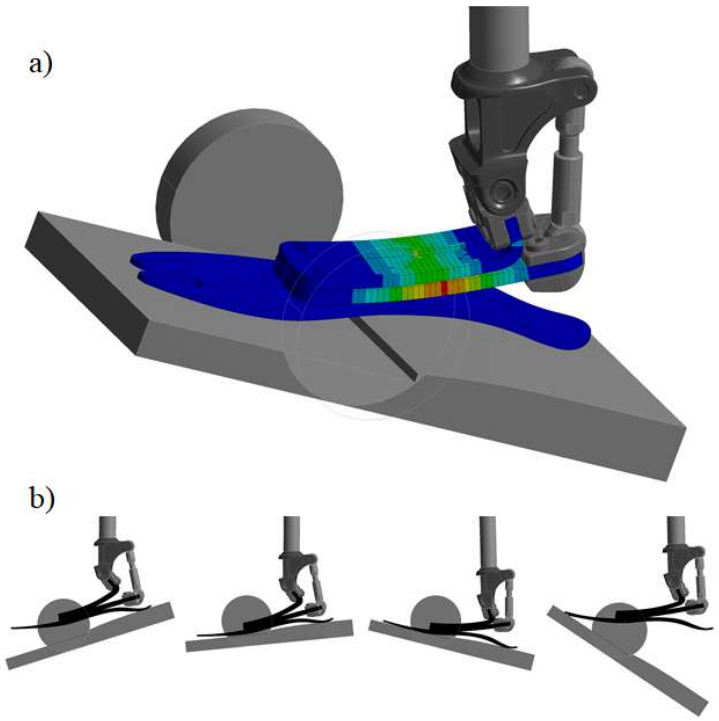


*Figure 4.2 FE model of the prosthetic foot. a) Three-dimensional (3D) view of the model showing strain energy at 0.45 s. b) Stance phase sequence showing movement and flexion in the model at stance times; 0.1, 0.25, 0.4, and 0.55 s.*

Results of the roll-over simulations are compared to the mechanical testing and presented in a quasi-stiffness curve; see Figure 4.3. The angular moment in the sagittal plane is calculated for the ankle system in the rotational joint between the main body and top blade. This moment reaction is plotted against the ankle angle, characterizing the quasi-stiffness of the ankle system throughout stance phase. In the mechanical testing, the force and moment reaction in the load cell are used to calculate the moment in the ankle joint. The ankle angle is measured between the sole blade and the pylon with a 2D video analyzing software, TEMA (Image Systems, Linköping, Sweden). The curve starts at a 0 deg angle with no moment reaction, then through plantarflexion, back through the zero point at mid-stance, through positive values in dorsiflexion, and then returns to the starting position.

The difference between the model and measured values is most noticeable at maximum plantarflexion, where the measured quasi-stiffness is 5.7 Nm/deg but the model results are 6.5 Nm/deg (14% higher). The results are sensitive to sample alignment and this difference is believed to be due to the shift of foot sample in the dynamic measurements. The coefficient of determination of measured values against the model results was calculated as 0.987. As the measurement data is retrieved at 1000 Hz, the data points are not evenly distributed throughout the curve in Figure 4.3. This will exaggerate the coefficient of determination, mainly as the curve for mechanical testing consists of relatively few data points in the relaxation from peak moment, where it deviates from the FE results. The primary objective

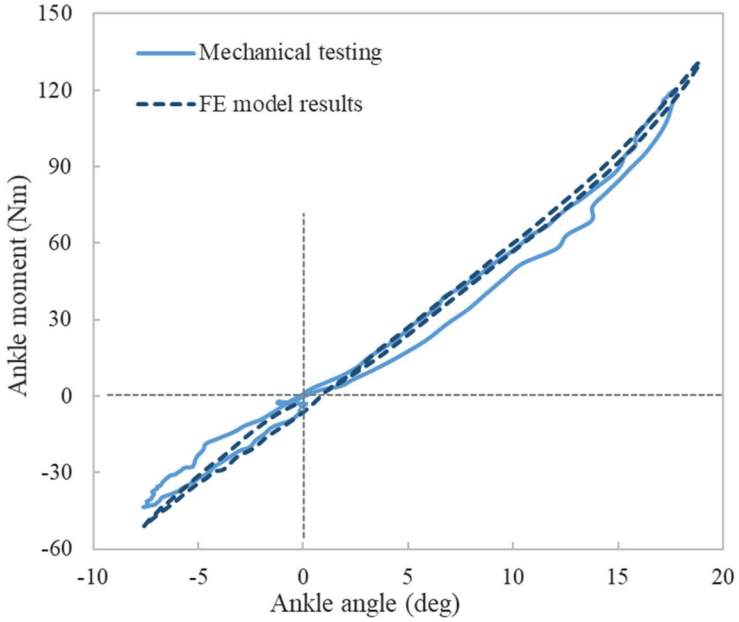


*Figure 4.3 FE model validation. Ankle moment vs. ankle angle, measured values compared to results from the FE model.*

of the modeling is to track the effect of design changes. Overall, this difference between measured values and simulation is considered within requirements for a valid comparison and valuation of shifts in results as the model is modified.

The main source of convergence difficulties in the FE model is related to the instability of the solution in periods of the cycle where abrupt contact changes occur. This is apparent as the heel rolls over the tilt table in the beginning of load response and as the forefoot comes in contact with the tilt table just before mid-stance. A three-point moving average filter was applied to smooth the results before further calculations are made, where abnormal fluctuations in the simulation results occur.

### 4.3.3 Strain Energy

From the FE analysis, we can retrieve the reacting forces and moments in all parts of the prosthetic foot. Figure 4.4. shows the total strain energy for the leaf spring system, as well as, for each individual blade. The results show how each blade is strained and unloaded over stance phase. During early stance, the energy is stored in the middle blade and sole blade. However, during late stance when only the toe is loaded, the strain energy is primarily in the top blade and middle blade. Over the stance phase, the middle blade has the greatest effect on the overall stiffness of the device.

The work at the boundaries is calculated from the force and displacement of the pylon, summed with product of torque and rotation on the tilt table at the sole. Total work at the boundary will equal the system energy. If we assume that frictional losses in moving parts are negligible, the boundary work will equal the strain in the spring blades and losses due to material damping. These damping losses are seen as hysteresis in the quasi-stiffness curve from mechanical testing (see Figure 4.3). The model does not account for material damping, causing the boundary work to be equal to the strain energy curve over the cycle time.

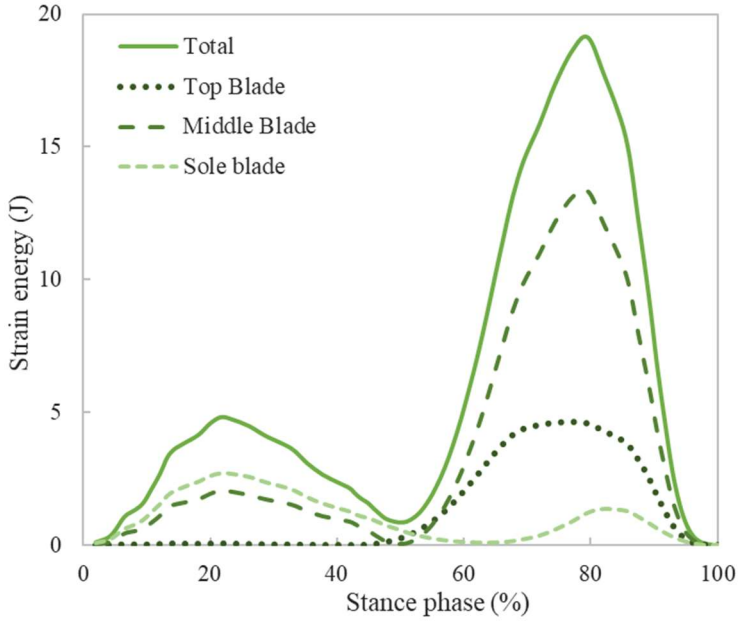


*Figure 4.4 Strain energy of flexible spring blades compared to work at boundaries. Dotted lines show strain energy for individual blades of the prosthetic foot for the load case in the step cycle.*

## 4.4 Concept system for variable stiffness

The first objective of design modification in the model is to produce a change in the characteristic quasi-stiffness curve. The stiffness change in the system is achieved by coupling the force acting on the system over a spring connected in series. A schematic illustration of the simplified system is presented in Figure 4.5. A parallel connected spring ($K_P$) and damper (coupling) ($C_D$) are connected in series to a second spring ($K_{LS}$). At a low damping coefficient, the stiffness of the system is governed by the two springs connected in series. If the coefficient is low enough relative to the spring constants, we can ignore the damping effect and the overall system response can be approximated to the combined stiffness constant of the springs in series, $K_T$.

$$\frac{1}{K_T} \approx \frac{1}{K_P} + \frac{1}{K_{LS}} \tag{4.1}$$

At a value on the damping coefficient that approaches a full coupling of the force over the parallel connected spring, the system stiffness approaches the stiffness of the spring in series, $K_{LS}$.

In this simplified system, let us assume a fixed spring constants and varying damping coefficient. The energy dissipation of the system in given excitation conditions will increase with higher damping coefficient, to a maximum for a given value of the damping coefficient. For coefficient exceeding this, the reaction of the damper will approach coupling function and the energy dissipation decreases.

For the prosthetic foot, the carbon fiber leaf springs of the original ESR foot are represented in $K_{LS}$, in the simplified system above. The modification of the foot involves introducing a parallel connected spring and coupling, working in series with the leaf springs.

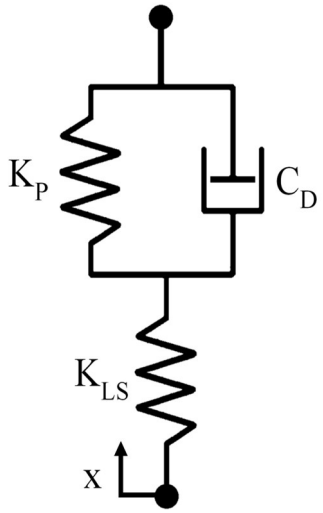


*Figure 4.5 Speed dependent stiffness. $K_P$ is the stiffness of the spring connected in parallel with the damper/coupling of damping coefficient $C_D$ and $K_{LS}$ is the stiffness of the leaf spring connected in series with spring and damper.*

## 4.5 Simulating Design Modification

The modelled foot is of stiffer category than recommended for the weight that the load profile of the test cycle assumes (89-100 kg vs 70 kg). The intention is to make changes in the model that make the foot more compliant and then increase stiffness with a controlled element, preferably to the original stiffness. The aim is to change the stiffness with an element that is purely damping and evaluate the damping factor needed for an efficient force transfer. This could be frictional damping or otherwise damped force coupling. The assumption made is that abrupt force coupling would have adverse effects on the user as discontinuity in the foot roll-over. The simulation assumes an active element that is actuated from mid-stance to late stance, in order to affect the forefoot stiffness. The timing of the actuation is also varied to study the effect of actuation under load. The second objective is to quantify the effect of the energy dissipation as a result from the damping on the energy return.

The model is initially made more compliant by defining a new degree of freedom in the foot design. Instead of a rigid mechanical link connecting the middle blade to the main body in rotational joints (see Figure 4.1), this component is modeled as two parts, connected by a translational joint. The translational joint has a degree of freedom of movement in one axis, defined in the axial direction between the two connection points. Allowing this movement between the pivot points on the main body and the mid-blade makes the system unsupported, so a linear spring element is defined over the joint, shown schematically in Figure 4.6. The spring stiffness is set at 500 N/mm after iterative simulations, aiming for a 30% overall

increase in RoM for the given boundary conditions. The introduction of a new spring element that acts both in series and parallel with the existing spring system lowers the overall spring stiffness of the system.

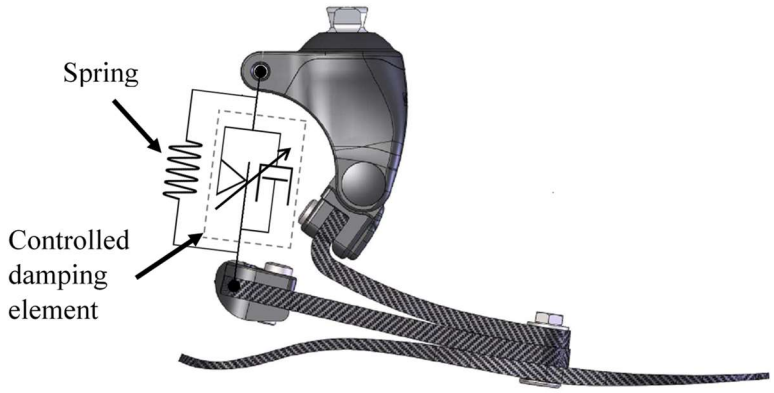


*Figure 4.6 Schematic representation of the linear spring and active damping element defined between top pivot on main body and bottom pivot on mid-blade.*

The resulting angular stiffness of the compliant model of the foot is compared to simulation of the original prosthetic foot design. The angular stiffness curve shows a slight decrease in moment and 25.9 % increase in RoM on the hindfoot (plantarflexion). The effect is more on the forefoot, as RoM is increased from 18.9 to 26.3 deg and the resulting ankle stiffness is decreased by 42% (6.9 to 4.0 Nm/deg). A damping element is defined parallel to the spring, with the assumption that a controlled element will have an off-state damping effect, represented with a low damping coefficient of 1 Ns/mm. The effect of this damping is negligible on the hindfoot, but a small hysteresis effect appears in the forefoot reaction curve, see curve for compliant setup in Figure 4.7.

### 4.5.1 Active damping

For the actuated element, a second controlled damping element is included in the model and is defined parallel to the spring and off-state damping, previously defined in the mechanical link. The element is inactive at the start of the cycle and activated at mid-stance (0.3 s). It is then turned off shortly before the end of the cycle, at 0.56 s (93% of stance), allowing for the spring energy to be released. The resulting quasi-stiffness curves for four values of damping coefficients for the active element are shown in Figure 4.7, compared to the FE simulation of the original prosthetic foot and the simulation of the compliant model with no active element. The damping coefficients are set to 25, 50, 100, and 300 N s/mm. The quasi-stiffness approaches the original rigid link model as the damping coefficient is increased. Quasi-stiffness evaluated at maximum moment in dorsiflexion increases up to 51% when applying 300 Ns/mm damping compared to the compliant setup (from 4.0 to 6.1 Nm/deg). In Figure 4.7, the curves for actuated damping are cut off at peak ankle angle to clarify the plot, excluding the return curve showing the hysteresis due to damping. The energy dissipation is shown and quantified in more detail in Figure 4.8.

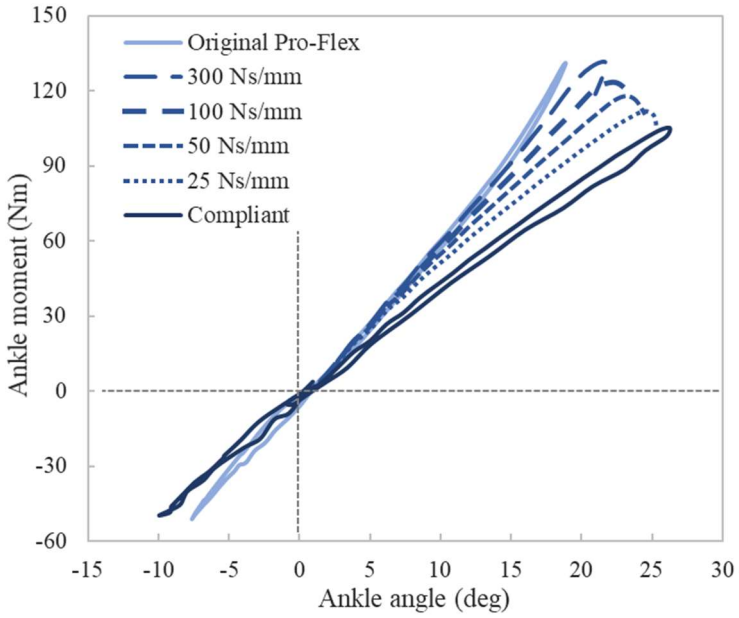


*Figure 4.7 Design modification - Ankle moment vs. ankle angle results from the FE model. Comparison between original foot simulation (light) and resulting curves for the modified designs; compliant mechanical link (dark) and actuated damping with four different damping coefficients (dashed). Damping element is activated at mid-stance at 0.3 s.*

To track the effect of the energy dissipation in the actuated element, the energy and work is calculated for model components. Figure 4.8. shows the stored and dissipated energy in the model for the simulation of the actuated damping element for three damping coefficients. The lowest damping coefficient (25 Ns/mm) is disregarded, as it induces the least change in stiffness. The plot shows the recoverable energy and damping energy for the three cases. The recoverable energy is the combined strain energy from the strain in the CF blades and the spring energy from the additional defined spring element. The strain in the CF blades increases with higher damping coefficients. The difference between the combined strain energy curves is primarily the higher spring energy, as a result of increased displacement of the spring element for lower damping coefficients.

The damping energy from the actuated damping model rises at mid-stance, as the element is activated, showing the total dissipated energy at the end of the cycle. Dissipated energy for the cycle increases when increasing the damping coefficient from 50 to 100 Ns/mm but decreases when damping coefficient is further increased to 300 Ns/mm. This confirms a maximum dissipation for the given system and boundary conditions at a damping coefficient between 100 and 300 Ns/mm.

The dissipated energy reduces the strain energy available for foot propulsion in late stance phase, decreasing the efficiency of the foot as an energy returning spring system. The sum of the strain energy and damping dissipation equals the work done on the system at the boundaries. As the simulations are investigated under constant displacement conditions, the dissipated energy adds to the boundary work rather than decrease the recoverable strain energy. The efficiency can be represented by a ratio between recoverable energy and work at the boundaries. This ratio between peak values at roughly 80% of the stance phase show

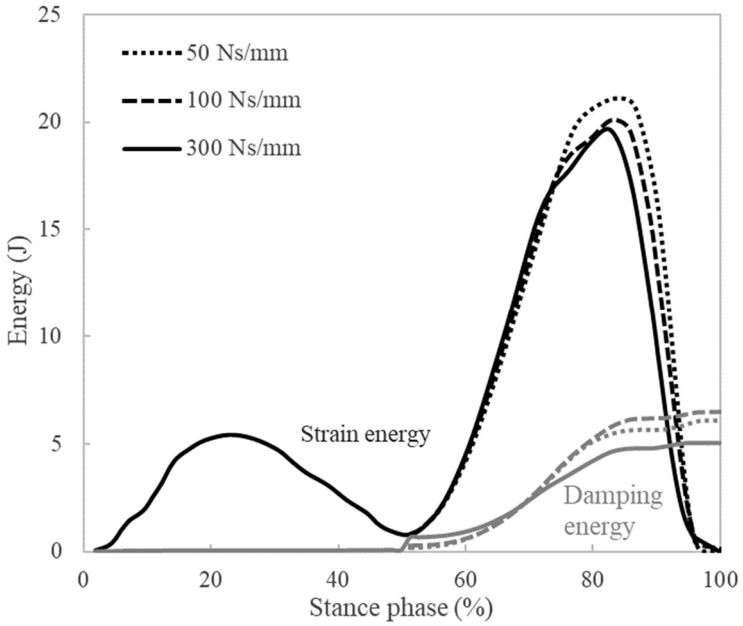


*Figure 4.8 Dissipated damping energy (grey) and recoverable strain energy (black) development in the foot over the stance phase for different damping coefficients used in the actuated element, strain energy being from CF blade strain, and spring element strain.*

that efficiency is in line with the absolute value of dissipated energy, or 77.6%, 75.6%, and 79.6% for 50, 100, and 300 Ns/mm damping, respectively.

To further study the effect of the actuated damping, simulations are made where the actuation time for the damping is delayed into the terminal stance. Figure 4.9 shows the results for the 300 Ns/mm damping coefficient for two additional actuation times. As before, the curves are compared to the simulation of the Pro-Flex Pivot and the compliant model. In addition to actuation at mid-stance (0.3 s) the element is actuated at 0.35 and 0.4 s (58% and 67% of stance phase, respectively). These results show that even as the element is activated during considerable loading of the foot, at 67% of stance phase, the moment versus angle curve is continuous. This supports the hypothesis that damped actuation of change in load support will result in a gradual stiffness change that will not cause a breakpoint in the roll-over of the foot.

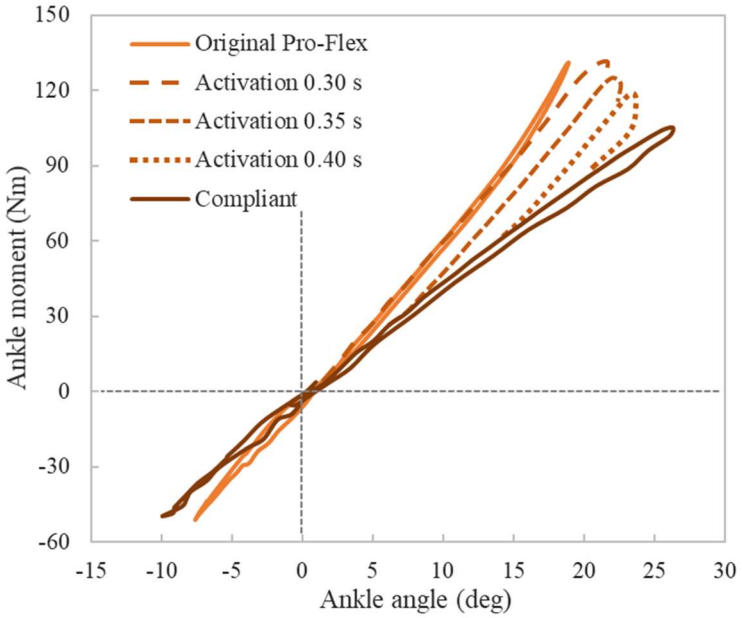


*Figure 4.9 Ankle moment vs. ankle angle results from the FE model. Comparison between different activation times of the functional element (corresponding to 50%, 58%, and 67% of the stance phase).*

## 4.6 Summary

An FE model of a prosthetic foot was presented and validated against actual measured values on a physical prosthetic foot. The model can be used to predict mechanical reactions to forces, moments, and displacements. It also proved to be a useful tool to analyze the functional characteristics of the prosthetic foot. Furthermore, the model can be used to simulate the response of the device when modifications are implemented in comparison to the original design. As focus in prosthetic design is increasingly shifted towards actuated elements and microprocessor-controlled function, the need arises for a robust method to assist with identifying the best parameters for both sensing and control. These results also demonstrate the effectiveness of using FEA in such tasks.

The design case shows how the stiffness of a system of series and parallel springs can be altered by introducing a pure damping element. Quasi-stiffness change of 51% was demonstrated. Although the change achieved is less than demonstrated in previous work (Glanzer & Adamczyk, 2018; Shepherd & Rouse, 2017) it is considerably higher than the reported user perception of 8% (Shepherd et al., 2018). Furthermore, for the given system and boundary conditions, it was presented that the dissipation of a damping element will reach a maximum at a given value of damping coefficient. For higher values, the energy dissipation decreases due to decreased velocity, causing the element to be better described as force coupling, becoming more efficient at transferring the forces as the coefficient is higher. The dissipation in the damping element, given a large enough damping coefficient, has been shown to reduce the recoverable energy by over 20% for the utilized load profile. The benefit of being able to change or adapt the foot stiffness during loading, needs to outweigh the effect of this lost energy.

For the load condition of constant displacement, change in the system function such as the increased damping in the case presented, will have more impact on work on the boundary than how the foot deforms. The strain energy does therefore not vary as much as might be expected in gait analysis of a user walking on the foot, where it is expected that the reaction would be more complex. It is anticipated that users will adjust their gait to the force response of the foot, affecting both deformations, as well as reactive forces and moments.

As stated previously, the force and rotation input functions for mechanical testing ("ISO/TS 16955:2016 ", 2016) differ from what is seen in clinical gait analysis when investigating amputee gait at normal walking speed. This is apparent when the strain energy curves are compared to earlier work. The strain energy results presented here, compare quite well with results for fast walking speed presented by Bonnet et al. (Bonnet et al., 2012), while it differs for normal walking speed in the same work. The load in early stance phase is higher than for normal walking speed and the mid-stance minimum occurs later in the stance phase.

# 5 STF damper design

The topic of this chapter is the design of a load-rate dependent element, to serve as an adaptable damper/coupling in the design of the prototype foot. The source for load-rate dependency is the stepwise, discontinuous change in viscosity of an STF (DST). Connected in parallel to the additional spring and in series to the leaf spring system of the ESR foot, the STF based element can influence the stiffness of the prosthetic foot dynamically over the gait cycle. The device described, prototyped, and tested in this work is an STF filled symmetric piston/cylinder design. The objective is a velocity dependent force response over the piston motion. Ranging from damped, compliant deflection at low velocity, jumping to a more efficient force transfer (coupling) at critical speed.

The rapid viscosity increase in the STF at a critical shear rate is used to approach a stepwise force response, thereby enabling adaptive response of the foot for different load rates. The adaptive response results in a greater range of motion with easier rollover for slow movement, for instance standing up from a seated position and adaptation to inclined surfaces, without sacrificing the energy return favorable for normal walking.

## 5.1 Background

The unique rheological properties of DST have been employed in various engineered applications in recent years and are actively being researched (Ding et al., 2013; Tian et al., 2018). One commercialized field of use is impact protection for various applications, e.g. personal protective equipment and protectors for sensitive devices ("D3O: Impact protection," 2019; Palmer & Green, 2008). Of similar category is the embedding of STF in textile, e.g. for puncture resistance of body-armor (Decker, Halbach, Nam, Wagner, & Wetzel, 2011; Wagner & Brady, 2009). The use of STFs for damping in structures has also been a research topic. Guo et al. (Guo et al., 2018) used STF to dampen flange connections on pipe assemblies and Yeh et al. (Yeh et al., 2012) proposed an STF filled piston damper designed for earthquake protection of buildings. Furthermore, Zhang et al. (Zhang et al., 2008) and Zhou et al. (Zhou et al., 2016) designed and built STF filled piston dampers with rate dependent damping characteristics. Devices working on the principles of STF properties have also been proposed in torque brakes (Tian & Nakano, 2017).

The design proposed here is a linear piston damper, comparable to the ones referenced above, with the objective being transition from damping to force coupling and adjustment of the velocity at which the transition occurs. The gap, between piston and cylinder wall in the damper, serves as the orifice. The dimension and geometry of the gap is varied to investigate the change in reacting force as a function of velocity. The challenge is to design the device so that the velocity at which the function changes can be adjusted. Analysis of the application, discussed in chapter 4, revealed specific rates at which the reaction forces are required to increase. The required force values in the element were also mapped.

## 5.2 Concept

### 5.2.1 System description

The proposed design change of the subject foot, involves replacing the rigid mechanical link with a parallel arranged STF damper and spring, connected in series to the mid blade of the leaf spring system. The effect is a more compliant pivoting movement, as a new degree of freedom is introduced in the system. Figure 5.1 shows, the variable stiffness system described in section 4.4. Now including the functions as intended for rate dependent coupling and resulting stiffness function. The damping coefficient is a function of velocity, dependent on the properties of the STF; see Figure 5.1 b). Initially, at low velocity deflection the coefficient is at a low level. As the velocity of movement over damper reaches a critical value ($U_{cr}$) that translates to the DST of the STF and particle jamming occurs, the coefficient rises accordingly.

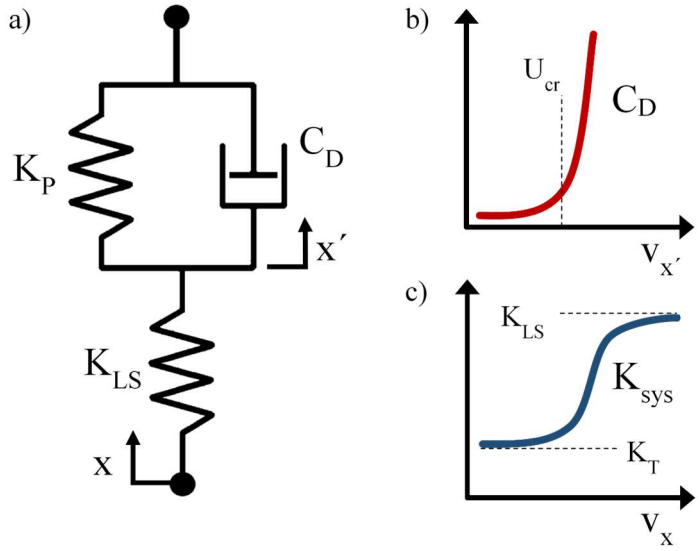


*Figure 5.1 Speed dependent stiffness. a) System diagram previously shown in Figure 4.5. b) Speed dependency of damper/coupling, $C_D$ as a function of velocity. c) The resulting system stiffness, shifting from stiffness of two springs connected in series and approaching the stiffness of the leaf springs.*

At increasing velocity, the piston will couple the force over the element. The intention is that this coupling will make the whole system response approach the effect of the original rigid link and thus approach the stiffness of the spring in series, $K_{LS}$; see Figure 5.1 c). Here it should be noted that the stiffer the parallel spring is compared to the leaf spring, the less influence the damper has. A softer spring stiffness $K_P$, will increase the displacement over the damper and the change in damping will have more effect on the system response. The stiffness change aimed at for the prototype, is defined as the change in stiffness of one category, as defined for the original model. The objective is a more compliant foot, enabling better surface adaptation and easier roll over at lower activity, without sacrificing too much energy efficiency in normal walking.

The parameters for the design goals of the STF damper are determined by the results from simulation of the prosthetic foot system in chapter 4. The compliant damping forces prior to DST should be minimized while the coupling force after DST were evaluated to exceed at least 2 kN. The damping force, and thereby the calculated damping coefficient, should approach a step function where the value rises rapidly at a critical piston velocity of ~4 mm/s and remain high. Furthermore, it would be beneficial to have the damper adjustable to adapt the device to different user preferences. The aim is to characterize the piston design and to approach these operating values.

### 5.2.2 STF properties

The STF material used is a commercially available suspension of sub-micron sized silica particles, in a hygroscopic glycol (STF Technologies, Delaware, USA) ("Data Sheet: STF SG - Standard," 2015). The silica content in the STF is 68 wt.% ("Safety Data Sheet: STF," 2015). The shear thickening properties of the STF can be adjusted by diluting the suspension with carrier fluid. Viscosity of the STF, given by the supplier is shown in Figure 5.2, measured in a standard plate and cone rheometer. The dilution of the STF will result in a shift in critical shear rate and lower viscosity. Although it is not shown in the chart, the viscosity is expected to drop quite rapidly after the maximum value of DST is reached, as indicated in literature (Galindo-Rosales et al., 2011). Measurements of varying gap dimensions are done on undiluted STF. To investigate the effect of fluid properties, two mixtures are made for testing of diluted STF; 4.0 and 8.0 wt.% diluted.

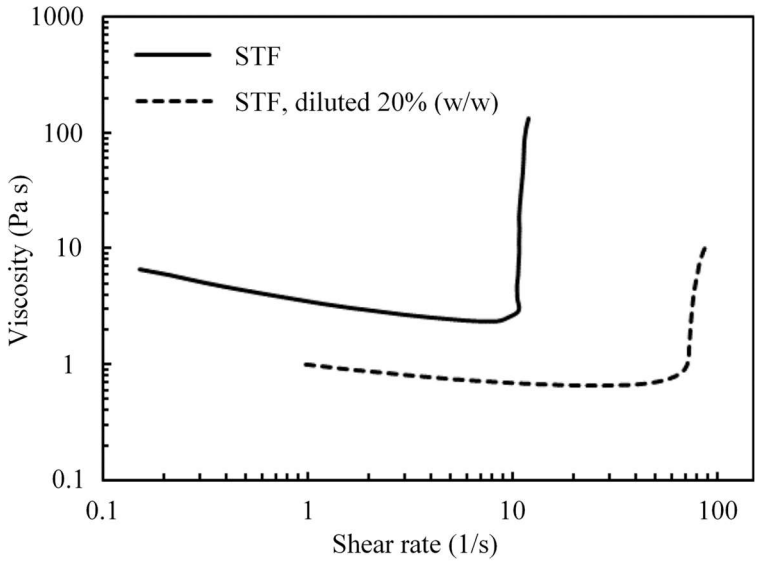


*Figure 5.2 Steady state shear rate viscosity of the STF, Showing undiluted and diluted fluid ("Data Sheet: STF SG - Standard," 2015).*

### 5.2.3 Orifice flow case

A forward displacement of the damper piston inside the cylinder, at a velocity $U_p$, pushes the STF back through the annular gap between piston and cylinder. For an analytical model of the flow in the gap, we consider the combined Couette-Poiseuille (C-P) (pressurized Couette) flow between a moving and a fixed, parallel plates. The velocity profile of the developed flow is a superposition of the linear profile due to the moving plate and the parabolic profile due to the pressure gradient of the pushed flow. For all test setups of the piston damper; dimensions, velocity and fluid properties, the Reynold's-number for the orifice flow fulfils, Re < 1. Hence, laminar flow through the gap is assumed. Furthermore, it is assumed that for shear rates below the critical shear rate of DST, the flow is fully developed of homogeneous properties and that entrance/exit effects can be neglected. Figure 5.3 shows a schematic representation of the two-dimensional, axisymmetric flow between the piston and cylinder wall.

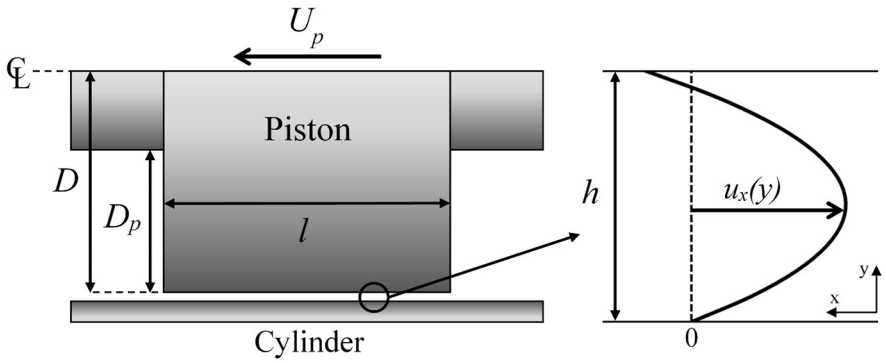


*Figure 5.3 Schematic illustration of the Couette-Poiseuille flow-case assumptions for the orifice gap.*

The velocity profile $u_x(y)$, derived from the momentum equation and the no-slip boundary conditions, is well known and adapted here from (White, 1991). The first term, in equation (5.1), is due to the flow being driven by the pressure gradient in the x direction, $P$. The second term is due to the wall driven flow,

$$u_x(y) = \frac{P}{2\mu} y(h-y) + U_p \frac{y}{h} \quad \text{where} \quad P = -\frac{dp}{dx} \tag{5.1}$$

where, $\mu$ is fluid viscosity and $h$ is the gap height.

The flow through the gap is the integral of the velocity profile over the full gap width. Assuming that the flow is incompressible and continuous, the flow, $Q$, equals the product of pushed area of the piston, $D_p$, and the piston velocity.

$$Q = \int_0^h u_x(y)dy = \frac{Ph^3}{12\mu} + \frac{U_p h}{2} = D_p U_p \tag{5.2}$$

Solving for $P$ and noting that the force acting on the piston, $F$, is a product of the pressure gradient, piston length and area pushed by the piston $(F = PlD_p)$;

$$P = \frac{12U_p\mu}{h^3}\left(D_p - \frac{h}{2}\right) \text{ and } F = \frac{12U_p\mu l D_p}{h^2}\left(\frac{D_p}{h} - \frac{1}{2}\right) \tag{5.3}$$

where $l$ is the piston length.

Of interest is the shear rate of the flow and relations to onset of DST. The shear rate is given by;

$$\dot{\gamma}(y) = \frac{du_x}{dy} = \frac{P}{2\mu}(h - 2y) + \frac{U_p}{h} \tag{5.4}$$

It is furthermore assumed that the DST phenomena initiates at highest shear conditions, at the boundaries, (y = 0 and y = $h$). Evaluating the shear rate for these by inserting expression from equation (5.3) in for $P$ in equation (5.4);

$$\dot{\gamma}(y)\Big|_{\substack{y=0\\y=h}} = \pm\frac{6U_p}{h^2}\left(D_p - \frac{h}{2}\right) + \frac{U_p}{h} \tag{5.5}$$

The onset of shear thickening at the critical shear rate is thus assumed to depend on the piston speed, pushed area and gap dimension. Accordingly, assuming that the critical shear rate is constant, then solving for the critical piston velocity yields;

$$\dot{\gamma}_{cr} = \pm\frac{6U_{p,cr}}{h}\left(\frac{D_p}{h} - \frac{1}{2} \pm \frac{1}{6}\right) \quad \text{then} \quad U_{p,cr} \approx \left|\frac{\dot{\gamma}_{cr}}{6}\frac{h^2}{D_p}\right| \tag{5.6}$$

Here, the expression for the critical piston velocity is simplified by ignoring the second and third terms in the parenthesis, originating from the wall driven flow. The relevance of these can be seen by comparing them to values of $D_p/h$ for the current cases in Table 2. These range from 3.6 for the largest gaps to 12.0 for the smallest. The smaller the gap, the less significant the approximation is.

For velocities below the onset of DST the viscosity is shear thinning, but the flow can be assumed fully developed and of homogeneous properties. For velocities above DST these assumptions are disrupted. As stated, the shear thickening is assumed to initiate at the boundaries, but the development of the shear thickening through the flow regime is unknown and the effect on the velocity profile. This also raises concerns if entrance/exit effects need to be considered in this case.

The intention is not to apply the model in direct comparison to experimental results as the model is not expected to give a fitting result. The purpose is rather to highlight the relations of force and critical velocity to the geometry of the damper orifice represented with $D_p$ and $h$. Later, in section 5.3.3 empirical relations are presented from the results for critical piston velocity and piston force for constant velocity, and are compared to the assumptions drawn from this model on ratios of geometric variables $D_p$ and $h$.

### 5.2.4 Piston damper design

The STF damper design is a symmetric piston damper with an axial piston-rod, eliminating the need for a compensator; see Figure 5.4. The cylinder and endcaps are made of aluminum alloy, but the piston/rod and insert for seal/bearing are of stainless steel. Low friction seals and bearings are selected to minimize forces at low velocities. The cylinder inner diameter is 20 mm and the rod diameter is 12 mm.

Ten different piston designs were tested, aimed at mapping the effects of changes in $D_p$ and $h$. Four pistons of different diameter were prepared for varying gap dimension. These result in a dimensions of the annular gap (orifice) between piston and cylinder in the range of 250 to 720 µm. Another three pistons were prepared with corresponding cylindrical inserts, reducing the cylinder inner diameter, but keeping the orifice gap constant by changing the piston diameter accordingly; see Figure 5.4 c). The purpose being to map further the effect of reduced volume being pushed. Finally, three pistons were prepared with piston diameter 19.5 mm (250 µm gap) and 250 µm wide radial slits along the length of the piston. Evenly distributed over the circumference of the piston; 10, 20 and 30 slits, see example in Figure 5.4 d). These were prepared to investigate the effect of increased gap area while keeping the gap dimension constant. Dimensions of the different pistons are listed in Table 2. The piston length is l = 16 mm. The available piston stroke is 11 mm.

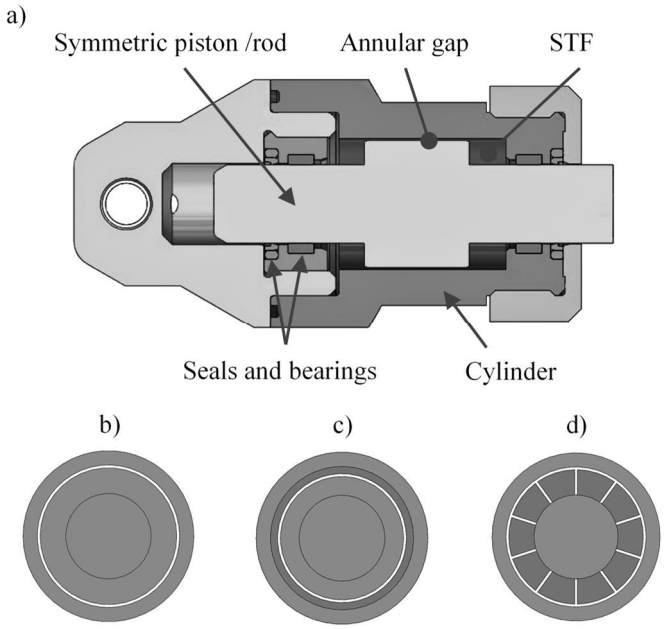


*Figure 5.4 STF damper and piston design. a) Section view of STF damper. Schematic representation of piston design tested, b) varying piston diameter, effecting gap dimension. c) varying cylinder diameter with cylindrical inserts and d) varying gap area with radial slits in piston.*

The process of introducing the STF in the damper aimed at minimizing air-bubbles in the fluid and effects from the environment. In addition to the low friction piston seals, (Figure 5.4 a), the lids on each end are sealed with rubber O-rings. The fluid was injected through two filling holes on one end of the cylinder and fluid used to flush out air-bubbles. Syringes

were used in the filling process to limit fluid exposure and parts primed with fluid before assembly to reduce risk of trapping air.

## 5.3 STF damper characterization

### 5.3.1 Force-displacement measurements

The force-displacement of the damper was measured with a hydraulic testing machine, Instron 8503 (Instron, Norwood, USA). The damper was fixed in the test machine with a ball joint on top and free to rotate in one plane at bottom, to avoid any horizontal forces; see Figure 5.5.

*Figure 5.5 Test setup of the STF damper in a dynamic test instrument.*

The control settings were displacement at constant velocity. For each test, the piston was displaced for 37 runs at incrementing velocity. For each run the piston was pulled a displacement of 7 mm and then pushed back to the original position. To allow the fluid to recover from thickened state and to limit risk of temperature increase during testing, the instrument was paused after each displacement. The pause time was 1 – 5 seconds, increasing for higher velocity setting. All testing was done at room temperature (22 +/-1 °C).

The velocity increments between runs varied from 0.2 mm/s, at low speeds, up to 3 mm/s at higher speed. The increments at low speed were small to capture the DST effect, or the velocity at which the force increase occurs. The displacement was placed over the mid-range of the piston stroke, to avoid potential end-effects.

Data for negative direction (push) was omitted as it is symmetric to the positive direction. An average value was calculated for each run. Some flexion was present in the fixtures for the damper, especially at high force. Due to this, data for the first 0.4 mm and the last 0.1 mm of each stroke are not included in the average.

### 5.3.2 Varying gap dimension

The results from force-displacement testing are reviewed as damping force vs. piston velocity. In the following plots, the data points of each test are plotted in same color (light colored dots) captured at a sampling frequency of 100 Hz. For each run, the average value is plotted in a larger dot of a darker color. Inserts are included in the plots, showing average results in a larger scale for the velocity range up to the sharp increase of DST.

Results for varying gap dimensions of the piston damper are shown in Figure 5.6. The characteristic property of the fluid is observed in the resulting force measurement. Initially the force is ~50 N and decreases slightly with increased piston velocity. This decrease is coherent with the initial decrease in viscosity at low shear rate as shown in Figure 5.2. The initial force is affected by the friction of piston rod sliding in the seal and bearings. Due to this, it is difficult to draw conclusions from the force measured in the range before DST. At a certain velocity for each piston, the force rises dramatically, indicating the onset of DST.

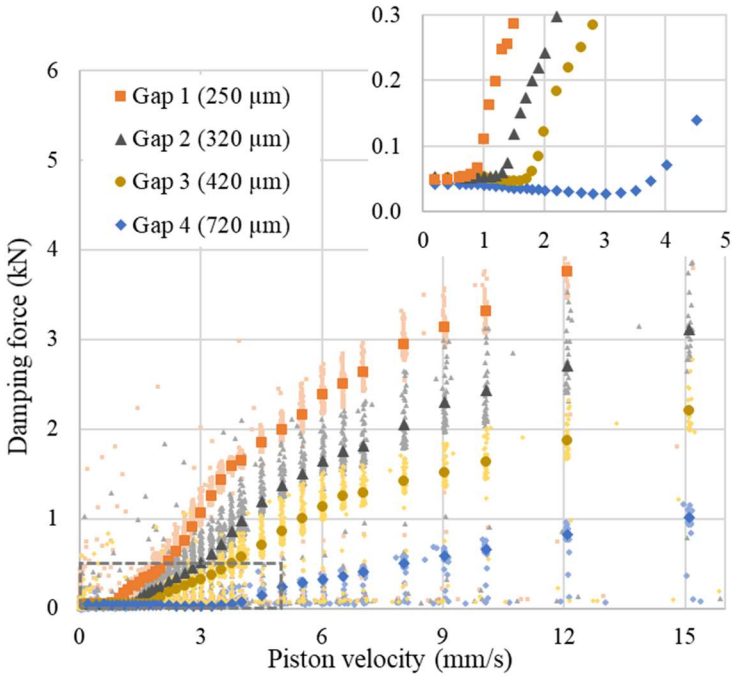


*Figure 5.6 Damping force vs. piston velocity for different gap dimensions. Measurements shown in small gradient dots and average for each velocity setting shown in larger, dark dots. Average data points shown in more detail in upper right corner, underlining critical piston velocity.*

The piston velocity at DST is evaluated from the plots for each piston setup and listed in Table 2, as critical piston velocity, $U_{p,cr}$. Although the assumption is made here, that the rise presents the onset of DST, the force profile is not discontinuous in all cases (see data for Gap

4) so the critical velocity is determined in the approximate intersection of linear viscosity curves before and after DST.

As anticipated, an increase in damping force and decrease in critical velocity is seen with decreasing gap dimension. For the application studied, the 250 and 320 µm gap arrangements generate damping forces that meet the criteria of $F > 2$ kN. As detailed further in Table 2, the transition for these occurs at a piston velocity that is below the value aimed at.

### 5.3.3 Varying piston cross-sectional area

Two approaches were made to investigate the effect of varying the ratio between pushed area and the gap cross-sectional area ($D_p/h$ in axisymmetric formulation). First, by reducing the piston and cylinder diameters, while keeping the gap dimension constant at ~ 250 µm. Cylindrical inserts were used to reduce cylinder inner diameter (see Figure 5.4 c). The purpose is to map the resulting increase in critical velocity as it is foreseen that the force will be reduced. The second approach was to make radial slits in the piston to increase the cross-sectional gap area, keeping a constant gap dimension, $h$. The objective was to maximize force response with a narrow gap, while increasing the critical velocity by increasing the gap area.

Figure 5.7 and 5.8 show the result for the pistons with inserts and slit pistons. These are compared to the results of the 250 µm gap in Figure 5.6 (Gap1). As listed in Table 2, the critical velocity changes proportionally with the ratio between pushed area and gap area ($D_p/h$) for both types of pistons. In contrast, there is a more rapid drop in damping force, at higher velocity for the insert piston, due to less pushed area, $D_p$.

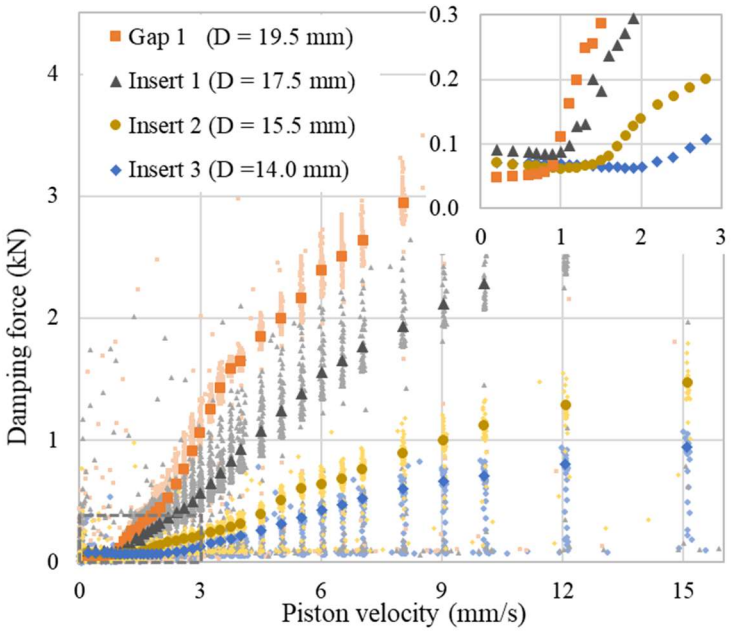


*Figure 5.7 Damping force vs. piston velocity where piston diameter is varied but gap between cylinder and piston kept ~ 250 µm with inserts, changing inner cylinder diameter. Scaled up inserts show variance in forces at low velocities due to frictional forces.*

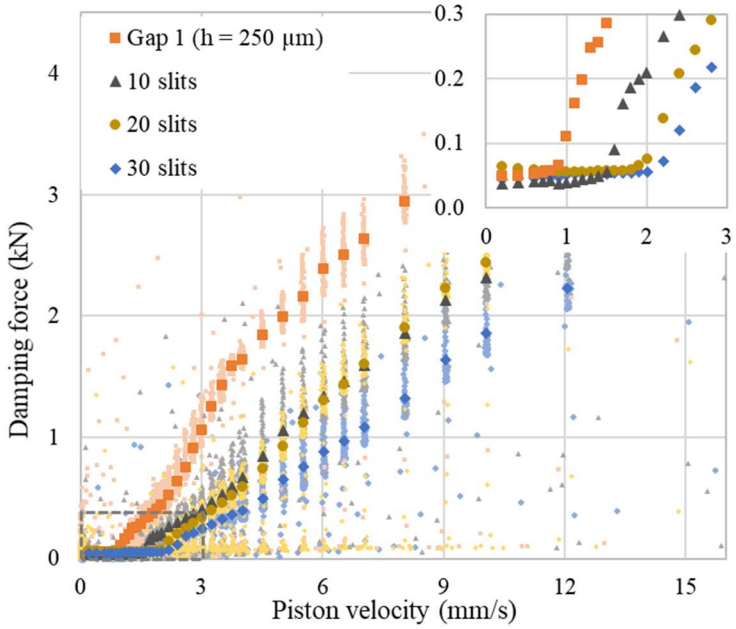


*Figure 5.8 Damping force vs. piston velocity for different number of 250 µm slits in piston compared to no slit.*

Table 2 further lists the average fluid velocity, $\bar{u}_x$, calculated from the piston velocity and the ratios calculated for geometric variables, $D_p$ and $h$, considered in derivations from the C-P model in section 2.3.

*Table 2: Critical velocities for different gap dimensions and ratio between gap and pushed area by piston (representation of ratios is according to two dimensional case, values are calculated for the actual case).*

| Piston | Gap dimension $h$ [µm] | Piston diameter $D$ [mm] | Piston area/ gap area $D_p/h$ [-] | Critical geom. point (C-P) $h^2/D_p$ [mm] | Critical piston velocity $U_{p,cr}$ [mm/s] | Critical fluid velocity $\bar{u}_{x,cr}$ [mm/s] |
|---|---|---|---|---|---|---|
| Gap 1 | 250 | 19.50 | 12.0 | 0.021 | 0.8 | 9.6 |
| Gap 2 | 320 | 19.36 | 9.2 | 0.035 | 1.2 | 11.0 |
| Gap 3 | 420 | 19.16 | 6.8 | 0.062 | 1.6 | 10.9 |
| Gap 4 | 720 | 18.56 | 3.6 | 0.199 | 3.5 | 12.6 |
| Insert 1 | 280 | 17.50 | 8.1 | 0.034 | 1.0 | 8.1 |
| Insert 2 | 270 | 15.50 | 5.6 | 0.048 | 1.3 | 7.3 |
| Insert 3 | 250 | 14.00 | 3.6 | 0.069 | 2.0 | 7.2 |
| 10 slits | 250 | 19.50 | 7.2 | 0.035 | 1.5 | 10.7 |
| 20 slits | 250 | 19.50 | 5.0 | 0.050 | 1.9 | 9.4 |
| 30 slits | 250 | 19.50 | 3.7 | 0.067 | 2.1 | 7.8 |

Figure 5.9 shows the critical piston velocity (a) and force (b) at a constant piston velocity, as functions of these geometric representations, presented here as empirical relations. In Figure 5.9 a) $U_{p,cr}$ shows a close to linear relation to $h^2/D_p$ from the approximation in equation (5.6). The value for the piston of the largest gap dimensions, 720 µm, deviates the most from the trend line drawn through the other values. Lowering of the exponential of $h$ would however render this to a straight line with the other values. This is an indication that the critical velocity is less dependent on the gap dimension than the model describes. It can further be stated that the calculated critical piston speed, using shear rate values from Figure 5.2, is lower than the measured values of a factor ~20. We conclude from this that the development of particle interaction, or jamming, through the thickness of the flow profile

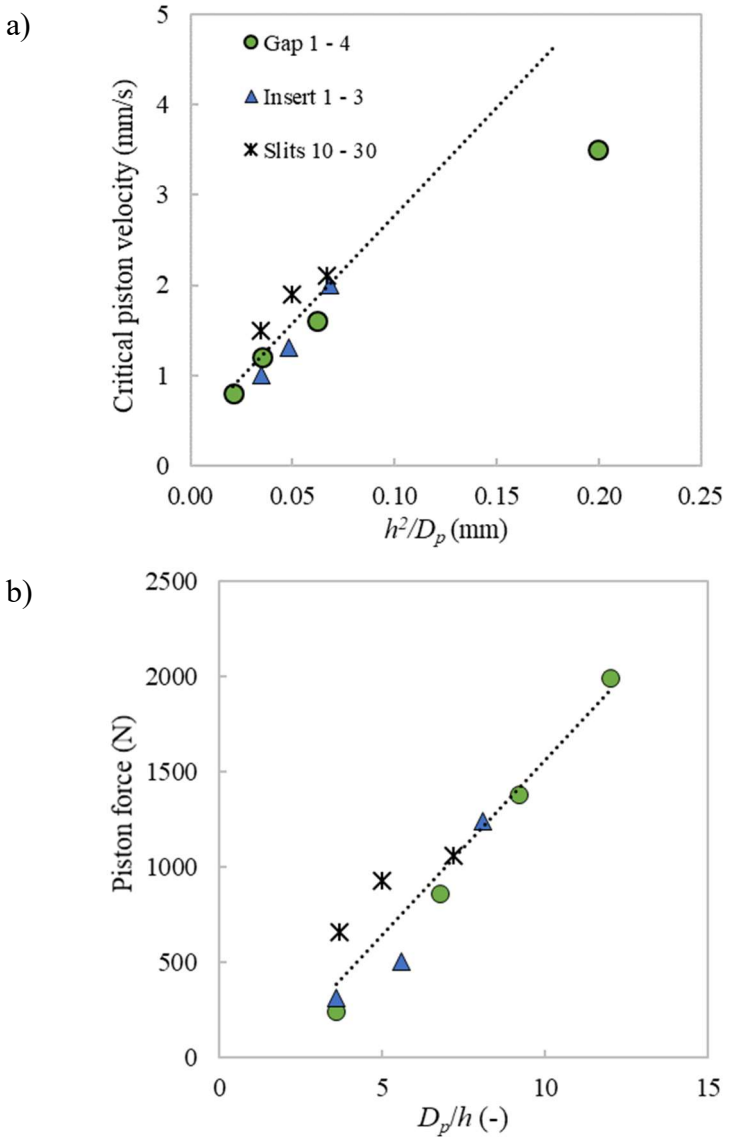


*Figure 5.9 a) Evaluated critical piston velocity for different piston designs plotted as a function of geometric dependency according to C-P model (Gap 4 excluded from the trend line). b) Piston force measured at piston velocity of 5 mm/s compared to the ratio $D_p/h$.*

will be gradual and that the discontinuity in the force–velocity profiles represent a full DST of the fluid through the profile.

In Figure 5.9 b) the piston force at $U_p$ = 5 mm/s for all piston types from Figures 5.6 to 5.8 show a close to linear relation to the ratio between pushed area and gap area, $D_p/h$. Value on the piston speed is chosen with respect to the requirements of the application. It should be noted that the given piston velocity is after the DST occurrence for all cases. The linear relation is strong for the pistons of a regular annular gap, but data for the more complex slit piston design, with the combined C-P and pure Poiseuille flow, differs slightly.

This representation of relation of the force to the geometric variables presented here, is over an order less dependent on geometry than described in equation (5.3). Empirically, the data correlates better with this relation. As the values in Figure 5.9 b) are for a constant piston velocity, the shear rate and therefore the viscosity for each case is a function of the geometric values. The viscosity of STFs is known to decrease for increasing shear rates after the DST (Galindo-Rosales et al., 2011). This relation could reduce the dependency of the force to the geometric variables in the small range this data covers and effect the results above. These empirical relations of force and critical piston speed help in the further design process of the damper.

### 5.3.4 Varying STF properties

To study the effect of change in STF particle concentration on damper characteristics, the damper was further tested with varying dilutions of the supplied STF. Considering the fluid properties presented in Figure 5.2, it is anticipated that the damping force will decrease as the concentration is lowered and viscosity of the fluid decreases. The shift in critical shear rate of the DST effect could indicate increased critical piston velocity at increasing dilutions. While the lower damping forces are undesirable for the application in the STF damper there could be benefits of increased critical piston velocity.

The force vs. piston velocity results for undiluted STF are compared to those from tests of fluid diluted 4 and 8 wt.%. The tests were made with a piston of 19.36 mm diameter, or an annular gap of 320 μm. The results are shown in Figure 5.10. As expected, the force reaction drops with increased dilution of the STF. The critical piston velocity or onset of DST is not as clearly depicted in the 8% diluted sample as it is in the other two. The diluted samples show a clear minimum in the force measured at $U_p \sim 1.0$. This could be indication of the start of weak, or not fully developed, shear thickening. The critical piston velocity at the discontinuity for the undiluted sample is determined $U_{p,cr} \sim 1.2$ mm/s (see Table 2) and the same value can be concluded for the 4% diluted sample. The corresponding value for the 8% diluted sample is only slightly higher or ~1.6 mm/s.

This shift in critical velocity is less than would be anticipated from the shift shown in the viscosity measurements in Figure 5.2. The shift in critical shear rate is though highly nonlinear as seen for example in silica glycol mixtures in (Moriana, Tian, Sencadas, & Li, 2016).

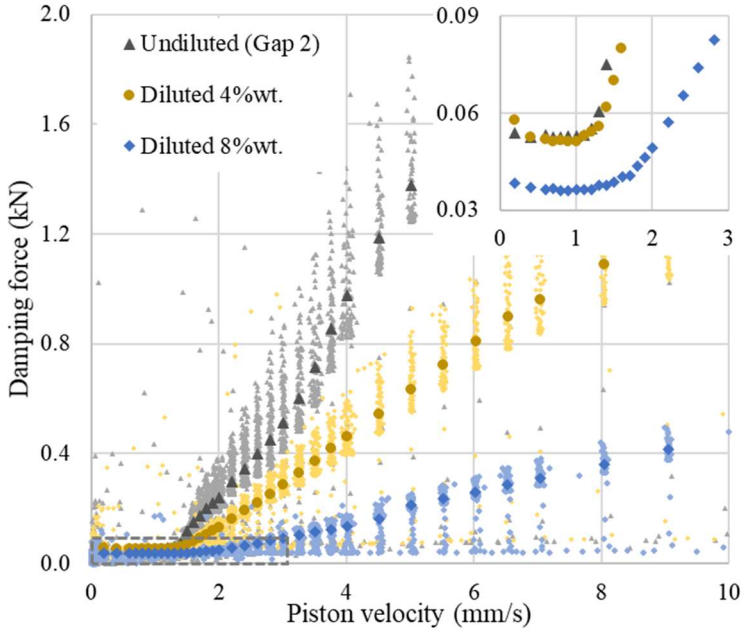


*Figure 5.10 Damping force vs piston velocity for varying STF dilution. 4% and 8% diluted compared to undiluted in damper with 320 µm piston gap.*

## 5.4 STF prosthetic foot prototype

### 5.4.1 Prototype preparation and testing

Figure 5.11 shows the modified Pro-Flex Pivot (original model) (Össur, Iceland) In the prototype, the rigid link connecting the main body to the mid-blade has been replaced with the STF damper and two parallel connected C-springs, allowing movement between main body and mid-blade connection.

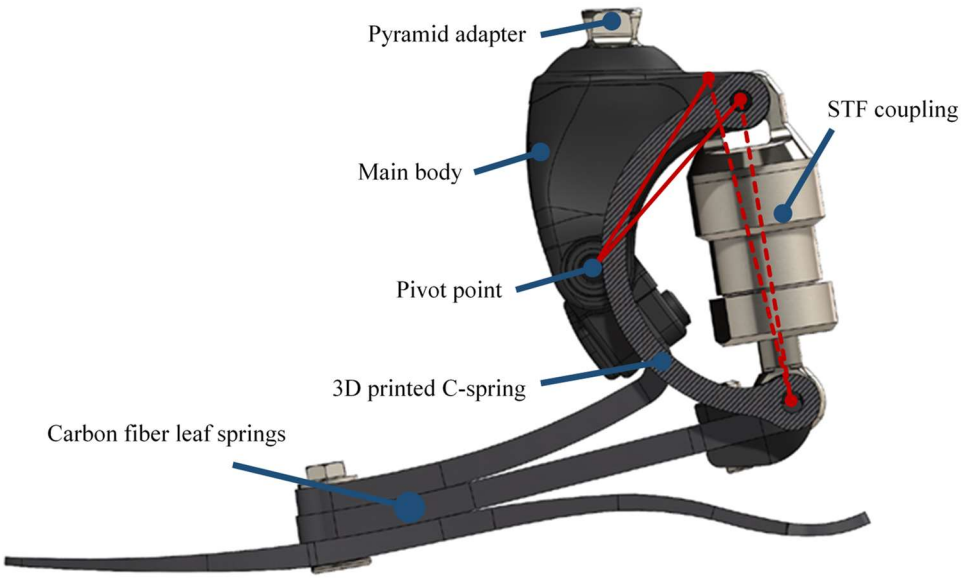


*Figure 5.11 The prototype prosthetic foot based on Pro-Flex Pivot. Red markings show relation between the length over the coupling and rotation around the pivot point.*

The desired base stiffness of the prototype is intended for a user weighing 89-100 kg, referred to as category 5 by the manufacturer for the original model ("Pro-Flex Catalog," 2019). As the new mechanism will make the foot more compliant, the prototype is set up with blades of higher stiffness (cat. 6 sole-/top-blade and cat. 7 mid-blade). For testing purposes, the prototype is compared to a cat. 5 original model. Basic trigonometry is applied to find the relation between the length over the coupling and rotation around the pivot point, see markings in red in Figure 5.11. In the range of available coupling displacement, the relation can be considered linear so that the displacement of the link of ± 5 mm results in a rotation around the pivot point of ± 6 deg.

The piston selected for the prototype was a slit design with 20 radial slits. The critical piston velocity of 1.9 mm/s is slightly higher than for the pistons with a smaller gap area and damping force exceeds 2 kN at a piston velocity below 9 mm/s. Figure 5.12 shows the damping coefficient for the damper setup calculated from the averaged force and piston velocity measurements. The coefficient increases rapidly for piston velocities higher than 2 mm/s and is relatively high for velocity above 4 mm/s. The high values at velocity below ~1.0 mm/s are highly affected by the friction in the damper.

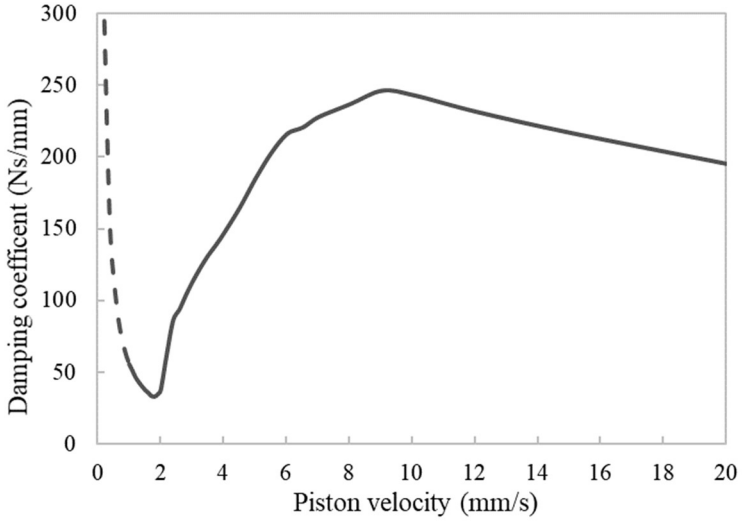


*Figure 5.12 Damping coefficient for the 20 slit piston design used in the prototype foot.*

The damper connects to the main body at top in a hinge connection and the mid blade in a ball joint. Two simple C-springs were connected parallel to the damper, at each side, connected to the main body and mid-blade with the same pins holding the damper. The springs were 3D printed out of nylon composite material, reinforced with continuous carbon fiber filament (Markforged, Watertown, USA). The spring constant for each spring was determined to be 125 N/mm, resulting in a combined 250 N/mm spring. This is considerably lower than 500 N/mm, used in the modeling in chapter 4. With only half the force required for the same deflection, this softer spring is meant to increase the potential stiffness change in the system.

To test the prototype for variable stiffness, the foot is tested in standard force-deflection on heel and toe, as described in section 2.4.1. In the current case, the dynamic response of the STF damper needs to be captured. Therefore, instead of the quasi-static fixed displacement rate, the test was carried out at different force rates, 200 (normal rate), 1000 and 2000 N/s.

The prototype foot was also tested in full heel to toe roll-over according to technical specification ("ISO/TS 16955:2016 ", 2016), discussed in section 2.4.2. According to the test standard, the cycle rate is set to 1.0 Hz, representing the rate of normal speed walking. Thereof, stance phase is 0.6 s and swing phase 0.4 s. To capture the rate dependency of the prototype the cycle is slowed down to imitate slower walking. In addition to a 1.0 Hz cycle, the prototype was also measured at 0.5 and 0.25 Hz.

The ankle angle, between sole blade and shank, is measured graphically using a 2D video analyzing software, TEMA (Image Systems, Linköping, Sweden). The moment is calculated for the pivot point from the force and moment reaction in the load cell. Plotting the ankle moment vs ankle rotation gives a dynamic quasi-stiffness representation (Hansen, Childress, Miff, et al., 2004) for the foot throughout the stance phase.

### 5.4.2 Heel/toe deflection

Figure 5.13 shows the results for linear displacement testing on heel and toe. The curvature of the plots shows the non-linearity in the force deflection profile of the leaf springs, especially in the forefoot flexion. In comparison to the testing of the prototype foot at different force rates, the original foot with a rigid link is tested. The test on the original foot (cat. 5) was performed at 200 N/s force rate, shown with a dotted line in Figure 5.13. Energy dissipation is seen in the hysteresis loops, higher in the damped prototype than the rigid link setup of the original foot. Test were performed with a foot cover.

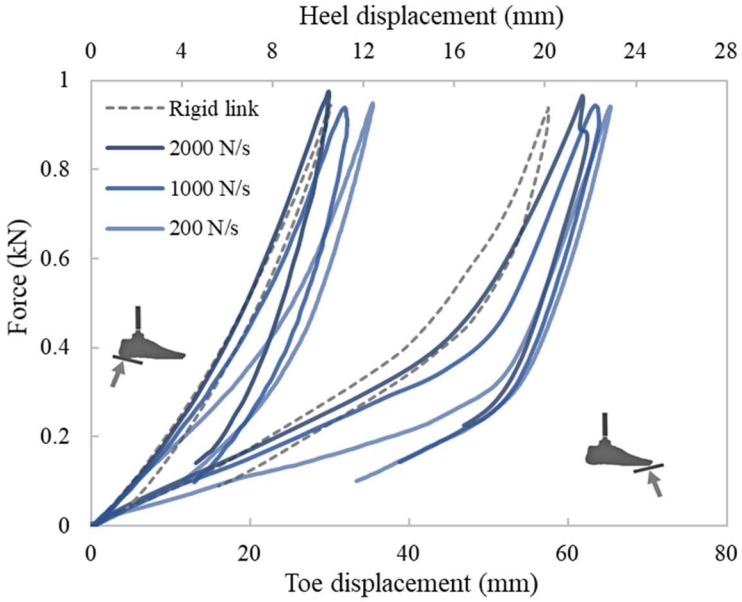


*Figure 5.13 Foot stiffness shown on a force vs displacement plot, in heel and toe deflection for three force rates, compared to a foot with a rigid link. Displacement values for heel on upper horizontal axis and toe on the lower.*

First taking into consideration the rate dependent stiffness of the prototype, linear stiffness is calculated from maximum force vs deflection. On the hindfoot, the stiffness increase between the highest and lowest force rates is roughly 23%. The increase on the forefoot is less, as the damper is fully extended at ~50 mm deflection. The overall stiffness increase is 12% in this case. Looking only at the range where the damper is active, in 0 – 40 mm deflection, the increase in forefoot stiffness, calculated from slope of the curve, is higher. The results are 47% increase between 200 and 1000 N/s force rate and 59% between 200 and 2000 N/s. Comparing original model and prototype in heel deflection, the prototype shows very similar stiffness at high force rate as the original, and unexpectedly slightly stiffer. This could be due to difference in force rate as some time dependent force response is present in the resin material in the leaf spring and foot shell. For the forefoot, the original model shows stiffer response than the prototype at highest force rate. This is consistent with the factor three higher extension force in forefoot loading than compressive force in hindfoot loading.

The stiffness increase presented here is somewhat understated as the test equipment fails to adhere to the set control values at higher force rates. This affects the testing on the toe more than the heel.

### 5.4.3 Prosthetic foot roll-over testing

Results from the roll-over testing are presented in an ankle moment vs ankle angle plot in Figure 5.14. The heel-strike is at ~2 deg ankle angle. Progression through the cycle is represented with arrows in the plot. As the heel is loaded, the ankle rotates in plantar flexion (negative angle) and negative moment reaction. At minimum moment, the quasi-stiffness increase in hindfoot loading is 14 %, between slowest and fastest cycles (0.25 and 1.0 Hz). At the maximum forefoot loading, the quasi-stiffness increase is slightly less or 12%, for the same rates. The counterclockwise hysteresis curve illustrates the energy dissipation in the cycle. The decrease in hysteresis for higher rates shows that the damping coefficient exceeds value of maximum energy dissipation in the system and approaches force coupling.

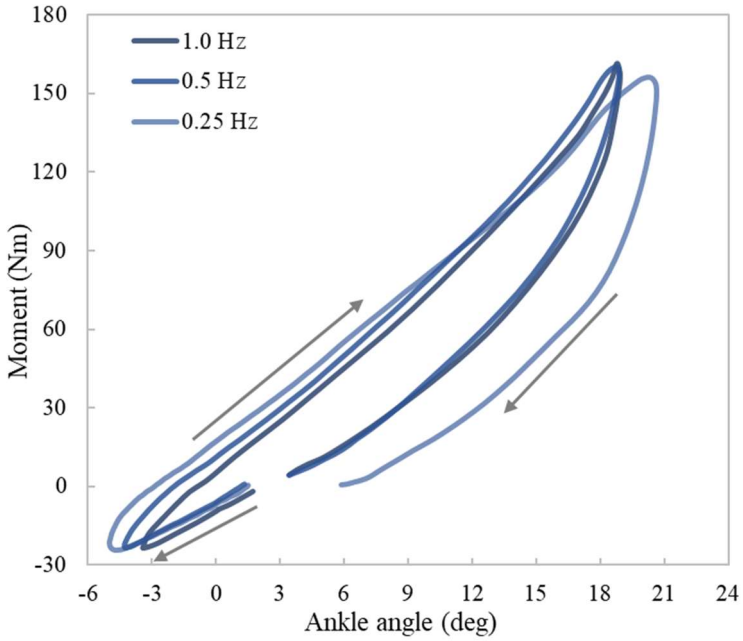


*Figure 5.14 Ankle moment vs ankle angle for three different cycle rates. Arrows indicate progression through the cycle.*

The angle at the end of the curve, at toe-off, varies from 3 deg to 6 deg. In the swing phase, between heel strike (~2 deg) and toe-off, the foot is being pulled to the neutral angle by the springs, retained by the damper. This shows that the toe is slightly raised in the swing phase. This effect is beneficial as it increases clearance for the user in the swing phase, reducing risk of tripping (Barrett, Mills, & Begg, 2010). At the same time, it reduces the push-off available in the unloading of the foot.

The difference between 1.0 Hz and 0.5 Hz runs is mostly in response of the hindfoot loading, while following roughly the same curve shape in forefoot loading. For numerical comparison between the different rates the average slope through the data set is calculated. The results are 6.2, 7.1 and 7.2 Nm/ deg for 0.25, 0.5 and 1.0 Hz, respectively. This results in a 14.5% and a 16.1% quasi-stiffness increase from the slowest cycle speed. This change in quasi-stiffness is close to the range intended, 10% - 15%, or roughly one stiffness category.

The rate of movement where the stiffness increases in both uniaxial loading and roll-over testing can be considered slow compared to the rate of ankle movement during normal, or

even slow walking. The load rate in the standard roll-over test at 1.0 Hz reaches values of 8000 N/s compared to the 200 - 2000 N/s load rate in the uniaxial loading test. The greater change in stiffness in the uniaxial load test than the roll-over test, shows that the capacity of the prototype to vary stiffness is not fully represented at the normal roll-over test rate.

The slower cycle speeds in the roll-over tests are again much slower than the range of normal walking pace. Walking pace range between slow and fast has been reported to range from 1.3 s/step to 0.85 s/step (Cunningham, Rechnitzer, Pearce, & Donner, 1982) or roughly 0.77 to 1.18 Hz. On the other hand, the roll-over cycle exaggerates the rotation and forces for slow walking so the cycle rate does not fully represent the walking speed.

Stiffness change at these low rates can also be considered relevant to users. Although focus of prosthetic feet design is on normal walking on level surface and inclines, other tasks are also considered. Slower movements like ambulation in a standing position, maneuvering in tight spaces, shifting weight between feet etc. is a considerable part of the everyday tasks.

## 5.5 Summary

In this chapter we described the design objectives and requirements for a bi-functional STF piston damper. It is intended as an adaptable element in the variable stiffness system. The STF damper, shows velocity dependent behavior that shifts from compliant damping to force transfer at critical velocity, representing DST in the STF. The dependency of critical velocity and force response to orifice gap dimension and shape was mapped. Tests showed reaction forces meeting the criteria for the application. The initiation of the shift from damping to coupling, for these gap dimensions, occurred at a piston velocity below the required value (~ 4 mm/s). The DST effect was apparent in the tests, but further modifications are required to the damper to obtain control of the transition velocity.

Testing of varying solids concentration in the STF showed that reaction forces dropped with reduced DST effect but had only a small effect on the piston velocity at which the DST effect occurred. A prototype prosthetic foot, incorporating the STF damper, showed variable stiffness at varying load rates.

Velocity dependent stiffness was demonstrated in the prototype foot incorporating the STF damper. The stiffness change induced by roll-over motion at a higher rate was measured, meeting the objectives of stiffness change corresponding to one foot category. A greater change was measured in a linear deflection at lower load rates. This indicates that more stiffness change could be induced, but at a rate that is lower than was aimed for.

# 6 Improved coupling function

While the proof of concept was reached in the previous chapter, the coupling force is lower than desired, especially for the piston geometry whose critical speed is close to the value aimed for. This chapter presents a design of a coupling that shows an improved force transfer, resulting in a more acute change in stiffness. The design is based on the same simple symmetric piston damper and the dependency to the rate of motion is again gained from the non-linear properties of the STF. The thickening of the STF at a critical speed and the resulting piston force is used to affect the geometry of a soft, elastic piston. The deformation of the piston closes the orifice gap, resulting in full coupling.

Here the background of the current design is detailed and how the STF coupling developed from results of previous work. The material chosen for the deformable piston is characterized. The function of the assembled coupling is tested over a range of velocities in a uniaxial force-displacement testing. Assembly of a prototype foot is described, and the quasi-stiffness measured in a test bench, in a roll-over motion at varying speed. Finally, the prototype foot is tested by a single user over a range of walking speed, characterizing the prototype foot and comparing it to the original model. The coupling operation ranges from providing added damping to the ESR mechanism at low activity levels to a rigid coupling at higher impact levels.

## 6.1 Design concept

### 6.1.1 Speed dependent stiffness

The same STF as before is used. The discontinuous increase in viscosity of over 50-fold ("Data Sheet: STF SG - Standard," 2015) can be seen in the results from previous chapter. Also, evident in the gradually reduced rise in force as shear rate is further increased beyond the critical value, indicates the shear thinning region following the discontinuous thickening. This shear thinning has been explained by the particles being forced into a micro structured layers of flow (Galindo-Rosales et al., 2011). This gradual rise in force with higher piston velocity does not correspond to the desired trend of full lock.

A more potent effect is needed at higher velocity of movement of the element. Figure 6.1 reviews the results for the different gap sizes from previous chapter (from Figure 5.6). In addition, a preferred force reaction curve has been plotted for comparison. The aim is an exponential growth in force around the target velocity of 4 ± 0.5 mm/s, previously determined. The preferred critical velocity was previously seen at a gap of 720 µm. The goal of a new approach to the design is to produce a coupling function rather than damping. Furthermore, the forces acting over the mechanical link in a normal walking profile are found to be higher than 3 kN. The preferred force response of the device was thereby defined as

minimum force for velocities below this critical value, increasing rapidly but continuously around the critical value to a full lock.

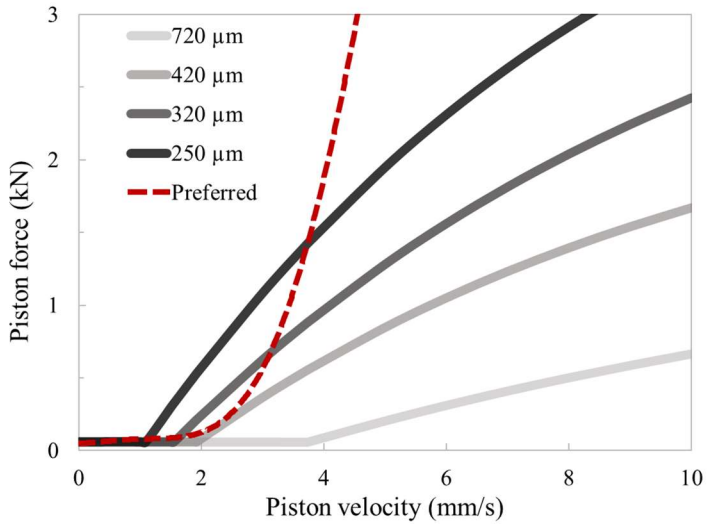


*Figure 6.1 Trends for piston force vs piston velocity for a rigid piston for different gap dimensions, compared to the preferred curve.*

### 6.1.2 Elastic piston coupling

For the more effective force transfer, the rigid piston design is modified by replacing the piston section with an elastic material. A sudden pressure increase, acting on the piston at velocities above the critical velocity of DST, compresses the piston axially. Axial compressive deformation of the elastic piston results in a radial expansion. This effect leads to a decreased gap dimension of the annular orifice between the piston and the cylinder wall, which induces further increase in pressure. Given enough force on the piston, this effect will block the piston movement relative to the cylinder, in a coupling action. According to the results from previous work shown in Figure 6.1, the initial gap dimension is set to 750 µm.

Figure 6.2 shows the section view of the STF coupling. The piston rod is assembled of four parts: upper rod (inside threaded nut), elastic piston, washer and a lower rod (threaded end). The piston and washer sit on a turned part of the lower rod, fixed between the collar of the upper rod and facing on the lower rod. The washer acts as a sliding collar for the piston, while the collar on the upper rod is fixed. This design makes the coupling function asymmetrical, so the force coupling is higher in the direction of tension than compression. Therefore, the foot is expected to lock-in at lower velocities, and more aggressively on forefoot load than it will on hindfoot load. The assembly is fixed by threading the lower rod into the upper rod. The piston rod assembly is guided by bushings and sealed to the outside with hydraulic seals, fitted in the cylinder and cylinder-cap.

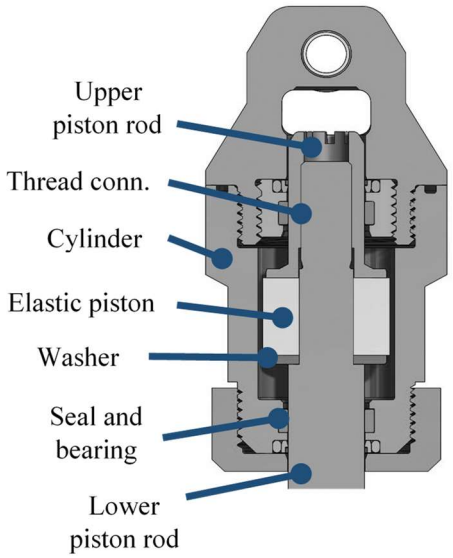


*Figure 6.3 Section view of the STF coupling, showing piston assembly.*

The coupling function is explained in Figure 6.3. The left side depicts the reaction at low force and velocity (blue arrows). The fluid will flow through the gap between chambers (red arrows) in the cylinder and very little pressure build-up is on the washer. The right side of Figure 6.3 shows the deformation of the piston under high force on the piston rod. Pressure builds up as the thickening of the fluid resists the flow between chambers. Axial compression and consequential radial expansion of the piston closes the gap and couples the force between rod and cylinder. The design also allows for pre-compression of the piston material by tightening the threaded rod parts and thereby controlling the initial gap dimension.

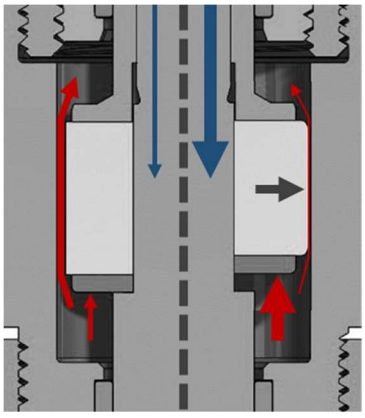

*Figure 6.2 Section view of the coupling in two states; left side shows fully open at low velocity and force. Right side shows coupling function of the elastic piston at higher force and velocity, causing in the annular orifice to close. Blue arrows show force and direction of piston travel. Red arrows show fluid pressure and flow. Thickness of arrows indicate intensity.*

The prototype foot is again assembled, replacing the rigid mechanical link with the STF coupling and parallel C-springs. The foot is the same modified category as before, cat. 6 sole/top-blade and cat. 7 mid-blade and is compared to a cat. 5 original model. The STF coupling has the same range of motion as previously, ± 5 mm (ankle rotation of ± 6 deg)

New, softer C-springs were made for the new prototype, 3D printed with a fiber reinforced nylon composite (Markforged, Watertown, USA). To further increase the potential for stiffness change the springs are made weaker than in previous prototype, resulting in more motion over the springs. The springs were tested in a uniaxial force deflection test and the spring constant determined 118 N/mm for both springs combined. Resulting moment, calculated in the pivot point with a moment arm perpendicular from the link to pivot point, translates to 4.7 to 5.1 Nm/deg angular stiffness, for fully extended to fully compressed, as the moment arm shortens as the link extends. This angular stiffness is chosen so the combined stiffness of the springs in series will be ~20% lower than that of a cat.5 of the original model (see below in section 6.2.3). Here, the goal for change of stiffness has been increased to the range over two stiffness categories as defined for the original model. The weight of the prototype foot is 1080 g, with the foot cover, while the original model weighs 920 g.

# 6.2 Design prototyping and testing

## 6.2.1 Characterization of elastic piston

The material properties required for the elastic piston, are derived from the geometry of the previous STF damper and the condition that a ~1.0 kN force results in a radial expansion that will close the gap between piston and cylinder. The material selected for the piston is an ether-based polyurethane (PU) of hardness 90 Shore A (Misumi, USA). The material is commercially available in a cylindrical form with a through hole, with outer and inner diameters 20.0 ± 0.1 mm and 8.5 ± 0.1 mm, respectively. The material was machined to the set piston length, 13.0 ± 0.1 mm.

The PU piston was tested in compression under constant speed, with a hydraulic testing machine, Instron 8503 (Instron, USA). A pin is placed in the through hole to replicate the support of the piston rod. The setup of the test is shown in Figure 6.4 a). The figure shows the piston unstrained on the left and under a 2.0 mm compression on the right. The relation between axial compression, Δz, and radial expansion, ΔD, is shown in Figure 6.4 b). In the

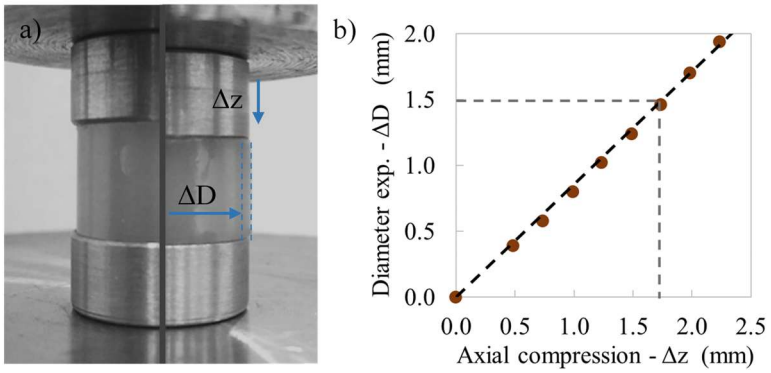


*Figure 6.4 a) Combined image of PU-piston. Left side: unstrained of initial dimensions; length 13.0 mm and diameter 20.0 mm. Right side: axial compression of 2.0 mm, resulting in radial expansion of ΔD = 1.7 mm. b) Relation between axial displacement (compr.) and expansion in diameter.*

range tested, and for the given geometry, the relation can be considered linear, as $\Delta D = 0.85 \Delta z$. According to this result the piston would be expected to fill the orifice gap at $\Delta z \sim 1.75$ mm ($\rightarrow \Delta D = 1.5$ mm).

The force loading profile, resulting from the compression is measured at loading rates in the range from 0.5 to 8.0 mm/s. The loading rates were constant through compression and relaxation. The material exhibits a typical viscoelastic effect where the force response increases with increased test velocity. The relaxation of the material also shows a hysteresis loop; see Figure 6.5. This viscoelastic effect will have a slight adverse effect as one of the design objectives of the coupling is to engage faster at increasing velocity.

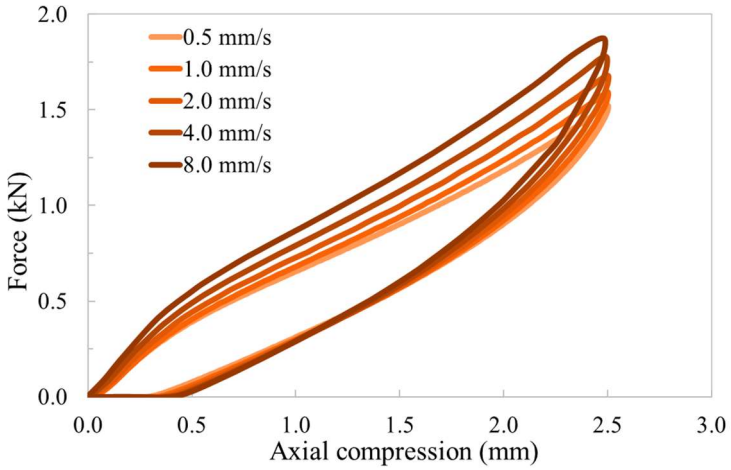


*Figure 6.5 Development of piston force over the measured stroke for increasing velocity.*

### 6.2.2 Uniaxial testing of STF coupling

The STF coupling is assembled and filled with fluid (STF Technologies LLC, Delaware, USA) ("Data Sheet: STF SG - Standard," 2015). The characteristics of the coupling are mapped in a uniaxial force-displacement test, performed over a range of velocity. The testing is done with a hydraulic test machine, Instron 8503 (Instron, USA). The fixtures for the coupling allow for rotation around a ball joint on one end to eliminate any horizontal forces. The test procedure from previous prototype is repeated. The displacement for each run is set to 7 mm, over the middle of the available 11 mm stroke. For each run, the coupling is first pulled at a constant velocity and then pushed back at the same velocity. The test is continued for consecutive runs at velocity increments of 0.5 mm/s. Again, the test is paused for up to 5 seconds between each stroke, to avoid heating and allowing the fluid to recover from thickened state. As the coupling effect is stronger than in the STF damper the test is run until the coupling force exceeds a 4 kN limit, set to prevent over straining the device. Testing is then resumed for velocities up to 7 mm/s, obtaining the piston travel needed to trip the force limit. Tests are performed at room temperature (21 ± 1°C).

Figure 6.6 shows the development of the coupling force over the stroke of the piston for given velocities. Low velocities result in a low constant force over the full stroke. As the velocity of the piston exceeds the critical value for the DST effect in the fluid, the pressure buildup starts affecting the piston geometry, resulting in a progressively increasing coupling

force. Eventually, at a high enough velocity, the force measured exceeds the 4 kN test limit in a shorter displacement than the set value of displacement. The test is continued for higher velocities and the resulting displacement measured. As shown in Figure 6.6, the negative force from compression does not result in a force coupling at the velocities tested. The force remains relatively constant, though a slight increase is present at the end of the back-stroke for the highest velocities. This is due to the asymmetry in the piston design where the fixed collar on the piston rod on the pressure side in compression does not allow the deformation seen on the washer in tension.

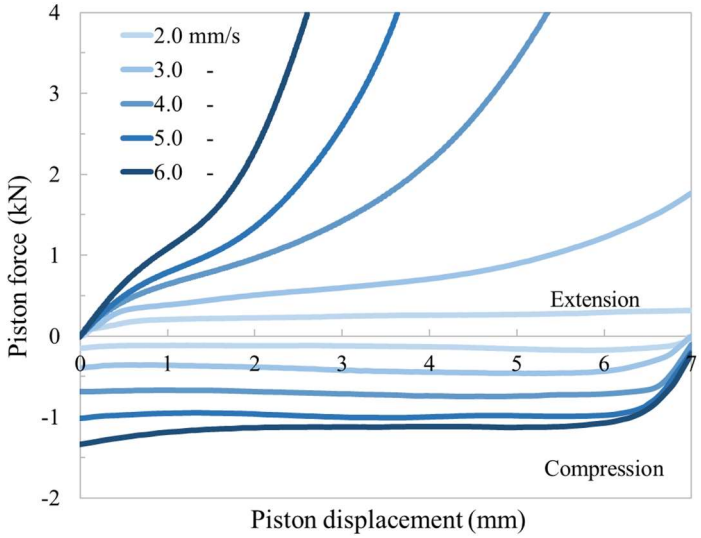


*Figure 6.6 Development of piston force over the measured stroke for increasing piston velocity. Positive force values for extension of coupling (forefoot load) and negative values for compression (heel load). Non-compressed setting of coupling.*

The coupling is also tested in the pre-compressed settings as described in section 6.1.2. The top piston rod is turned a third of a revolution and the measurement repeated for three pre-compressed settings. The pitch of the threads is 1.0 mm. The pre-compression tested is therefore: 0.33, 0.67 and 1.0 mm.

For the general trend for force vs. velocity, the average piston force is calculated over each stroke. Figure 6.7 shows the trend lines through these averages for the coupling in four settings; no pre-compression and the three pre-compressed settings. The curve for non-pre-compressed setting of the coupling approaches the criteria for the preferred curve introduced in section 6.1.1 above (Figure 6.1). A progressive force response is initiated at ~3 mm/s, in tension (forefoot-loading), with full coupling for velocities >4 mm/s. The force response in compression (heel loading) is lower and can be described as non-linear damping.

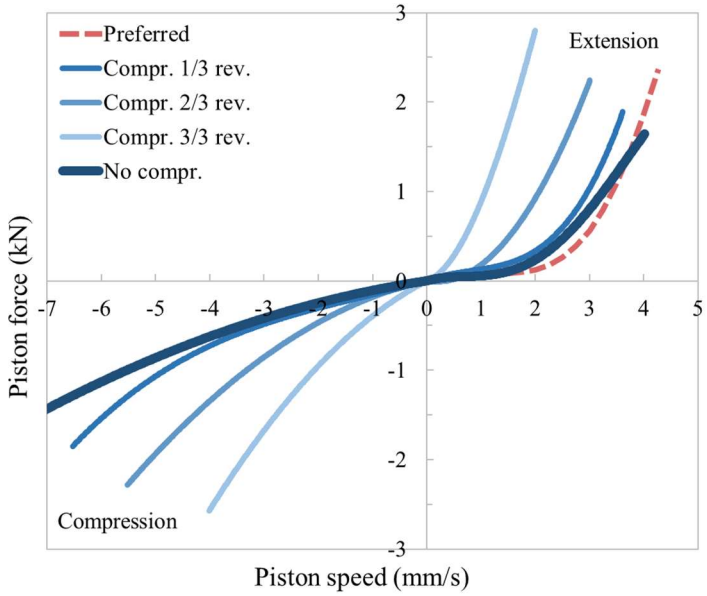


*Figure 6.7 Average coupling force vs velocity. Lines shown for pre-compressed piston in revolution (1 mm/rev.). Comparison made to the preferred profile shown in Figure 6.1*

The displacement needed to exceed 3 kN was measured for increasing velocities. This force value is expected to be exerted on the link during normal walking of a prosthetic user, using a category 5 foot (89 - 100 kg). Figure 6.8 shows the results for the pre-compression settings described above. For no pre-compression the displacement drops and stabilizes at around 2 mm at a velocity of 6 mm/s. This displacement is approximately the axial compression needed on the elastic piston to close the annular gap. For increasing pre-compression this value decreases as the pre-compression itself partially closes the annular gap.

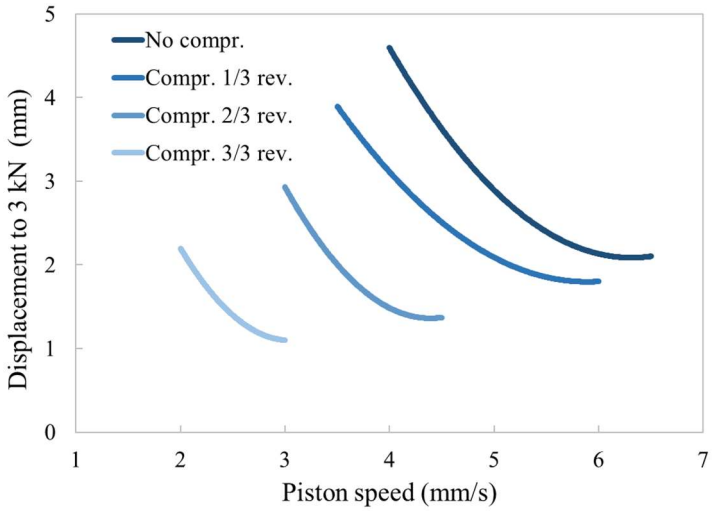


*Figure 6.8 Displacement of piston to reach a 3 kN force for different pre-compression settings.*

Visual inspection of the parts after the testing showed no sign of friction between the piston and cylinder wall. It can therefore be assumed that the piston is at full stop as it is pressed

against the cylinder wall. The different settings tested herein show the ability to allow for adjustments in the performance characteristics of the device. The most progressive reaction, and highest reaction velocity, is with no pre-compression. For testing of rate dependent change in stiffness of the prototype foot this setting is chosen to investigate the full capacity to rate dependent stiffness.

### 6.2.3 Mechanical test of prototype foot at varying speed

The method for mechanical testing of the prototype foot is altered from previous procedure. For the uniaxial force-displacement testing (section 2.4.1), the control loop of the test equipment is unable to keep a constant load rate for the displacement of the test. This effects the higher test rate more than lower. The cyclic testing of ISO/TS 16955 (section 2.4.2) is more reliant when varying the rate of the test. On the other hand, the input curves exaggerate the conditions of the walking cycle. Evaluating the stiffness of the foot through a whole roll-over cycle is also problematic. Taking this into account, a more moderate cyclic testing is adopted. Instead of full roll through a step, the foot is rolled under constant load through rotation over a smaller angle around mid-stance. The controlled dorsiflexion through mid-stance will be the section of the walking cycle where the speed dependent coupling will have the biggest effect on the foot stiffness.

The geometrical dimensions of the test setup are based on ("ISO/TS 16955:2016 ", 2016) described in section 2.4.2 and are carried out on the foot with a foot-cover. The foot sample is attached to the rod, and the anterior/posterior alignment adjusted. A constant 400 N force is applied on the ball joint pressing the foot flat down on the tilt table. The tilt table is then rotated with a sinusoidal waveform, ±4 deg.

The setup of the test is meant to imitate a standing person, in a motion of leaning back and forth. It gives a good representation of the stiffness of the foot in roll-over through mid-stance. The test is set up for a wide range on rate, to capture the value of the initiation of the force coupling. The test is performed at four different wave frequencies: 0.25, 0.5, 1.0 and 1.5. These frequencies result in a maximum angular velocity through the 0 deg of: 6.3, 12.6, 25.1, 37.7 deg/s, respectively. The ankle moment is calculated, from the forces and moments measured in the load cell, to a point on the tilt table directly under the pylon. The ankle angle is captured graphically with 2D video analyzer (TEMA, Image Systems, Linköping, Sweden) as the angle between the pylon and the sole of the foot-cover. The same test is performed on the original model foot for comparison.

Figure 6.9 shows the foot angular stiffness as ankle moment vs ankle angle. Plotted up for the four test rates on the STF prototype foot, showing stiffer response at increasing rates. The same is plotted for the original model for comparison. Inset image shows the test setup. Over the presented range of angular motion, the calculated ankle moment is close to linear for an effective ESR foot as the original model. The curves for original model in Figure 6.9, for different rates, show that the force response is largely unaffected by the rate of motion. The slope of the curve describes the quasi-stiffness of the foot. The oval shape of the curves for the prototype foot describes the hysteresis from the viscose damping of the STF flow over the piston. It is noted that this hysteresis reduces for higher rates showing a more effective coupling action. The small hysteresis in the original model curves can be accounted for by the visco-elastic material in the foot-cover and friction in joints and connections.

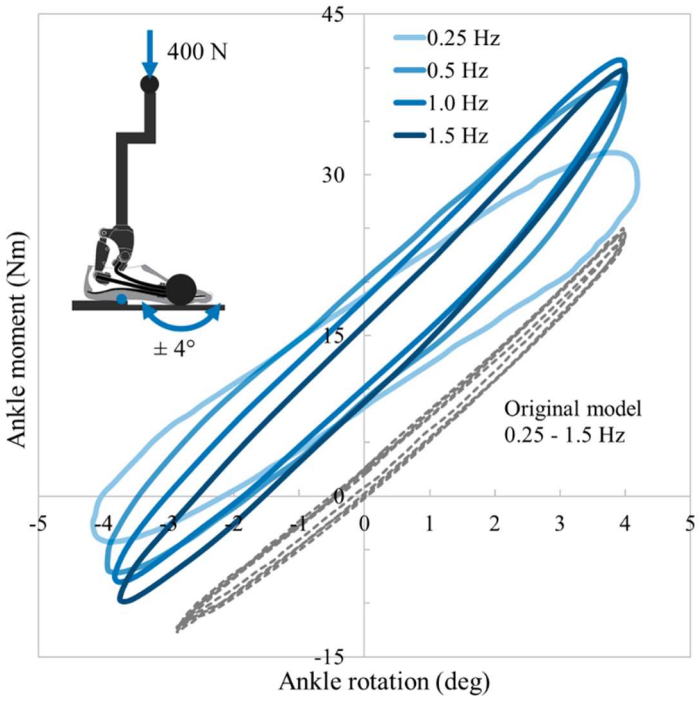


*Figure 6.9 Stiffness of prototype foot, measured in rolling motion for varying rates, compared to the original model. Curve direction is clockwise, higher moments in roll from heel to toe than rolling back from toe to heel.*

For a numerical evaluation of the stiffness, the slope of a linear regression line through the data points of each curve is calculated. For the prototype foot, this slope is 3.9, 5.4, 6.0 and 6.2 Nm/deg for frequencies 0.25, 0.5, 1.0 and 1.5 Hz, respectively. The stiffness increase from the lowest frequency is therefore 38%, 54% and 59%. For comparison, the slope calculated for the original model is same for all speeds, 5.3 Nm/deg. Same measurements were conducted on a cat. 4 and cat. 6 of the original model. These yield a slope of 4.6 Nm/deg and 5.9 Nm/deg, respectively (13% lower and 11 % higher, compared to cat. 5). The measurements are done on individual samples of feet. Some deviation is to be expected within different samples of same category, not captured here.

The positive offset in moment values in the curves for the prototype foot compared to the original foot are due to alignment adjustment in the spring and damper movement. As the foot starts reciprocating in the rolling motion, the neutral point moves to plantarflexion, resulting in an overall higher moment. The measurement of absolute moment values is quite sensitive to this angle, but the slopes of the curves are unaffected. This effect is not seen in the user testing, where the feet are aligned by a prosthetist, with feedback from the user.

### 6.2.4 User testing with prototype foot

A case study is presented to obtain biomechanical data, comparing the quasi-stiffness of the prototype to the original model. The test user (42 years old, weighs 100 kg, height of 1.77 m, amputee for 9 years) underwent 3D analysis, while walking at varying speeds at level ground. The test was performed on an instrumented dual belt treadmill (Bertec, Ohio, USA) (400 Hz) and an eight camera-based 3D motion capture system (Qualisys AB, Gothenburg,

Sweden) used to measure body kinematics (400 Hz). A 6DoF model was constructed and data processed and analyzed in Visual 3D (C-motion, Germantown, USA). A fourth-order low-pass Butterworth filter was applied for the kinematic and kinetic data with a cut-off at 10 Hz and 6 Hz, respectively. The tested feet were set up and aligned to the subject's current socket by a certified prosthetist. No other components of the prostheses were altered. The protocol for the user testing was approved by the Icelandic National Bioethics Committee and the subject gave an informed written consent to participation in the study.

The test was performed at three walking speeds: 0.4, 0.7 and 1.0 m/s (slow, moderate, normal). These speeds were selected to give a wide range of ankle angular velocity in order to capture the rate dependent change in stiffness of the prototype foot. The slowest speed of 0.4 m/s can be described as leisurely ambulation, while the fastest speed can be considered a normal walking speed, for this particular subject. For the test, the subject started walking at the slowest speed. The speed of the treadmill was then increased in two steps, during the test. The test was run at each speed long enough to capture 15 steps on each side at constant speed, in total for 90 s. The data were separated for each walking speed and average and deviation calculated.

The ankle angle is measured between the foot segment and shank segment, negative for plantar-flexion and positive for dorsi-flexion. In Figure 6.10 the angular velocity of the ankle joint is plotted over the gait cycle for the three walking speeds, on the prototype foot. The average angular velocity over the controlled dorsiflexion is calculated between 15% and 55% of the gait cycle; 22.9, 36.6 and 48.1 deg/s for slow, moderate and normal walking speed, respectively. Comparing these angular velocities to the rate settings in the rolling test (section III.B) and the stiffness results from Figure 6.9, reveals that the most prominent stiffness change occurs at an angular velocity that is lower than measured at slow walking.

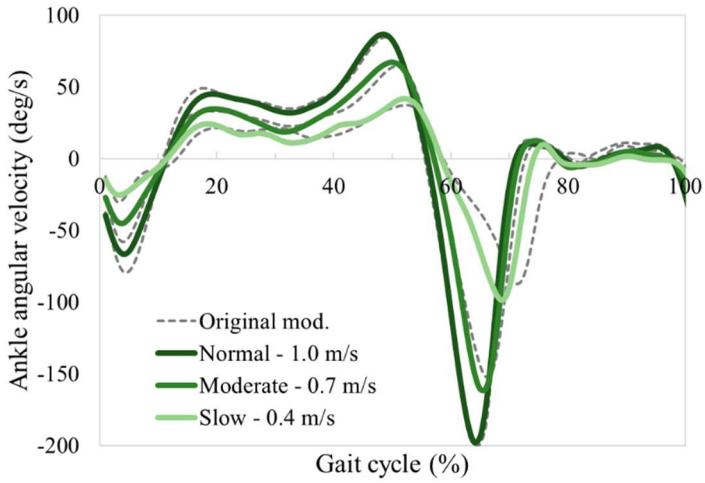


*Figure 6.10 Ankle angular velocity in gait analysis for the three different walking speeds.*

The resulting ankle moment-angle curves, characterizing the stiffness of the prototype foot in comparison to the original model, are shown in Figure 6.11. The slope of the curves increases with increased walking speed for the prototype foot as well as there is a shift to higher moment for increased speed. Calculating a linear regression line to represent the slope yields; 4.97, 5.44 and 5.72 Nm/deg for walking speeds 0.4, 0.7 and 1.0 m/s, respectively. The quasi-stiffness increase from the slow speed is thus 9.5% for moderate and 15.1% for normal speed. For the original model, the moment vs angle curves coincide over the larger share of the angular motion, while showing increasing moment at maximum dorsi-flexion. The regression line slope values for the original model are: 4.93, 5.04 and 5.18 for walking speeds 0.4, 0.7 and 1.0 m/s, respectively, resulting in an increase of 2.2% for moderate and 5.1% for normal speed, from the slow speed. It can thus be stated, accounting for the increase seen in the original model, that over this range of walking speed there is a 10% speed-induced increase in stiffness of the prototype foot, or approximately the equivalent of one stiffness category.

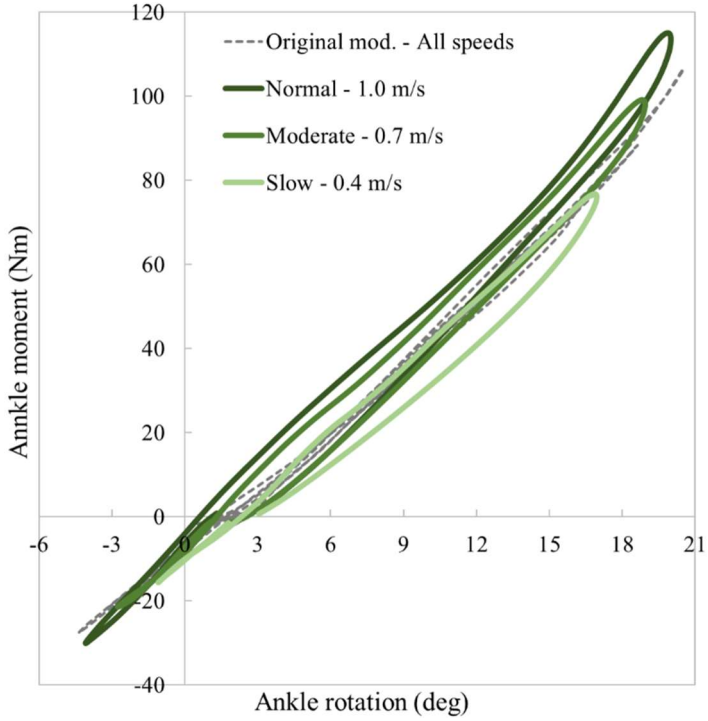


*Figure 6.11 Ankle quasi-stiffness (ankle moment vs angle) from gait analysis, measured at three different walking speeds. Results for STF prototype foot compared to original model.*

The difference in slope between the curves (stiffness) is most noticeable between -4 and 4 deg, at the low angular velocities for both plantarflexion during weight acceptance and the controlled dorsiflexion through mid-stance. The increased ankle moment, early in the stance phase, remains high through the late stance. Hence, the quasi-stiffness curve is shifted towards increased dorsiflexion with slower pace, allowing for a more compliant roll-over.

The quasi-stiffness profiles of Figure 6.11 show that while the original model shows negligible hysteresis, there is dissipation of energy in the profile for the prototype. In effort to quantify this, work input and output during dorsiflexion are calculated as the product of

moment and rotation. The results indicate that ~80% (79% for slow, 81% for mod. and norm.) of the work input is retrieved during the push-off from peak moment.

## 6.3 Summary

In this chapter we introduce a different design approach to obtain a greater coupling effect in the speed adaptable device. The design of the coupling is described, adding to the function from device presented in previous chapter, with a more effective force transfer. The novelty of the design is the interaction of non-Newtonian fluid flow and elastic components, where material properties are employed for a rate dependent function. Adjustability of the coupling, towards a full lock was demonstrated.

The change in stiffness of a prototype, with changing rate of motion, is mapped in mechanical testing. Over the range tested, a 59% increase in stiffness was observed. Compared to different stiffness categories of the original model, this covers the range of over three categories. Clinical user testing shows that the quasi-stiffness change, over the walking speeds tested, is equivalent to one stiffness category as defined for the original model (10%). The novel design adds function to the prosthetic foot with little added weight, compared to the original model (17%). On the other hand, an energy dissipation of ~20% is seen in the hysteresis of the quasi-stiffness profiles from user testing.

# 7 Conclusions and future work

The primary goal of this work was to design and prototype a prosthetic foot, achieving variable stiffness using smart materials. A speed adaptable, variable stiffness prosthetic foot has been presented. The variable stiffness of the system is obtained by coupling forces acting on the system, over one spring connected in series to a second one. The system response thus varies from the combined stiffness of two springs connected in series, to the stiffness of one spring. The dependency to the speed of movement is realized by employing the highly non-linear, shear rate dependent properties of an STF in the coupling element.

The design of the coupling element was described, prototyped, and tested mechanically. The novelty of the design is the use of non-Newtonian fluid for a rate dependent function. The design of the coupling was iterated for a more effective force transfer using elastic components for geometric change of the piston. Adjustability of the coupling, towards a full lock was demonstrated. A proven ESR prosthetic foot model was modified, including the coupling device, and a prototype prosthetic foot set up.

The basis for the development of the variable stiffness system was set in a couple of initial steps of the work:

- A review of some smart materials for the application, result revealed that more compliant materials show greater change in properties. A simple fluid filled piston-damper design was chosen, due to the level of robustness needed for the application, providing a light weight, compact device, capable of transferring large forces. While the coupling effect could be reached with a controlled MR device, STF was favored as a solution that could adapt the response of the prosthetic to the rate of movement of the user.
- The FE model of the original prosthetic foot proved useful. Design changes were simulated in the model, obtaining the initial parameters for the design of the speed adaptable coupling. The concept of variable stiffness and initial design of the system could be validated in the model. Furthermore, the dissipation of the coupling element could be quantified.

The mechanical testing of the prototype indicated a more compliant force response at speeds below then what was realized at slow walking speed in user testing. It can be concluded that for ambulation tasks of lower angular velocity of the ankle, the prototype foot will be more compliant. Examples of such tasks would be: shifting of weight in a standing position, balancing on inclined surface, and standing up from a seated position. Whether a more compliant foot would be beneficial in these tasks remains a topic for further user testing. On the other hand, it has been reported that prosthesis stiffness needed for standing is three times higher than needed for walking (Hansen & Wang, 2010). The compliant reaction in the prototype could be unfavorable for this purpose. A fully controlled coupling, in place of an adaptable one, would address this issue.

Viscosity of the liquid phase of the STF will decrease with increased temperature, and consequently, the critical shear rate of discontinuous shear thickening will increase. Effectively the coupling in the STF device will happen at higher speeds in higher temperatures. This effect is known, so all measurements were conducted at constant room temperature and no heating was experienced in the STF device during the testing. Appendix A presents measurements made on the STF damper at different temperatures. These give an indication on how much the function of the device changes.

## 7.1 Recommendation for future work

Future work should be aimed at mapping the effect on the stiffness transition in the device at varying temperatures. This work could include efforts to explore STFs that are less temperature dependent, in the temperature range of most common use (5 - 25°C). As stated before this is highly dependent on the viscosity of the liquid phase and a fluid that shows less temperature dependency in this range might reduce this effect. Likewise, the fatigue of the STF needs to be studied. The fluid is abrasive and experience with the device indicated that the fluid slightly erodes softer metals and seals, so analysis of different build materials is needed.

Further work on FE analysis would include simulations with changed boundary conditions. Force vector data from gait analysis could be used to dictate vertical force curves and tilt table rotations in order to better imitate normal walking. Furthermore, data could be gathered to produce different gait patterns, such as ascent and descent of ramps and stairs.

The focus of this work has been the proof of concept and realizing a working prototype. Some iterations are needed to investigate how the foot can be improved. Further testing of function could include different material properties of the elastic piston to investigate if a more rapid coupling effect can be reached with a softer piston. Furthermore, different spring stiffness of the parallel springs as well as the stiffness of components of the original model should be investigated. Further clinical user testing should be aimed at different tasks such as ramp walking and stability, for a more thorough characterization of the novel foot, and user preferences for speed dependent stiffness.

# References


Adamczyk, P. G., Roland, M., & Hahn, M. E. (2017). Sensitivity of biomechanical outcomes to independent variations of hindfoot and forefoot stiffness in foot prostheses. *Human movement science, 54*, 154-171. doi:10.1016/j.humov.2017.04.005

Aldridge, J. M., Sturdy, J. T., & Wilken, J. M. (2012). Stair ascent kinematics and kinetics with a powered lower leg system following transtibial amputation. *Gait and Posture, 36*(2), 291-295. doi:10.1016/j.gaitpost.2012.03.013

ANSYS Mechanical APDL Element Reference. (2018). In. Canonsburg, PA: ANSYS, Inc.

Barnes, H. A. (1989). ShearThickening (“ Dilatancy ”) in Suspensions of Nonaggregating Solid Particles Dispersed in Newtonian Liquids. *Journal of Rheology, 33*, 329-366. doi:10.1122/1.550017

Barrett, R. S., Mills, P. M., & Begg, R. K. (2010). A systematic review of the effect of ageing and falls history on minimum foot clearance characteristics during level walking. *Gait & Posture, 32*, 429-435. doi:10.1016/j.gaitpost.2010.07.010

Bayram, H. A., & Bayram, M. B. (2018). Dynamic Functional Stiffness Index of the Ankle Joint During Daily Living. *J Foot Ankle Surg, 57*(4), 668-674. doi:10.1053/j.jfas.2017.11.034

Beck, O. N., Taboga, P., & Grabowski, A. M. (2016). Characterizing the Mechanical Properties of Running-Specific Prostheses. *PLoS ONE, 11*. doi:10.1371/journal.pone.0168298

Belluco, P. (2007). EAP - A Short Introduction to Robotics Applications. In: Plotecnico di Milano.

Bonnet, X., Pillet, H., Fode, P., Lavaste, F., & Skalli, W. (2012). Finite element modelling of an energy – storing prosthetic foot during the stance phase of transtibial amputee gait. *Proceedings of the Institution of Mechanical Engineers, Part H: Journal of Engineering in Medicine, 226*, 70-75. doi:10.1177/0954411911429534

Bovi, G., Rabuffetti, M., Mazzoleni, P., & Ferrarin, M. (2011). A multiple-task gait analysis approach: kinematic, kinetic and EMG reference data for healthy young and adult subjects. *Gait Posture, 33*(1), 6-13. doi:10.1016/j.gaitpost.2010.08.009

Brady, J. F., & Bossis, G. (1985). The rheology of concentrated suspensions of spheres in simple shear flow by numerical simulation. *Journal of Fluid Mechanics, 155*, 105-129.

Brown, E., & Jaeger, H. M. (2012). The role of dilation and confining stresses in shear thickening of dense suspensions. *Journal of Rheology, 56*, 875-923.

Brown, E., & Jaeger, H. M. (2014). Shear thickening in concentrated suspensions: Phenomenology, mechanisms and relations to jamming. *Reports on Progress in Physics, 77*. doi:10.1088/0034-4885/77/4/046602

Cagle, J. C., Reinhall, P. G., Allyn, K. J., Mclean, J., Hinrichs, P., Hafner, B. J., & Sanders, J. E. (2018). A finite element model to assess transtibial prosthetic sockets with elastomeric liners. *Medical and Biological Engineering and Computing, 56*, 1227-1240. doi:10.1007/s11517-017-1758-z

Carlson, J. D., & Jolly, M. R. (2000). MR fluid, foam and elastomer devices. *Mechatronics, 10*(4), 555-569. doi:10.1016/S0957-4158(99)00064-1

Cherelle, P., Grosu, V., Cestari, M., Vanderborght, B., & Lefeber, D. (2016). The AMP-Foot 3, new generation propulsive prosthetic feet with explosive motion characteristics: design and validation. *BioMedical Engineering OnLine, 15*(145). doi:10.1186/s12938-016-0285-8

Childers, W. L., & Takahashi, K. Z. (2018). Increasing prosthetic foot energy return affects whole-body mechanics during walking on level ground and slopes. *Scientific Reports, 8*. doi:10.1038/s41598-018-23705-8

Collins, J. D., Arch, E. S., Crenshaw, J. R., Bernhardt, K. A., Khosla, S., Amin, S., & Kaufman, K. R. (2018). Net ankle quasi-stiffness is influenced by walking speed but not age for older adult women. *Gait Posture, 62*, 311-316. doi:10.1016/j.gaitpost.2018.03.031

Comtet, J., Chatté, G., Nigués, A., Bocquet, L., Siria, A., & Colin, A. (2017). Pairwise frictional profile between particles determines discontinuous shear thickening transition in non-colloidal suspensions. *Nature Communications, 8*. doi:10.1038/ncomms15633

Cunningham, D., Rechnitzer, P., Pearce, M., & Donner, A. (1982). Determinants of Self-Selected Walking Pace across Ages 19 to 66. *Journal of Gerontology, 37*, 560-564.

D3O: Impact protection. (2019). *D3O*.

Darter, B. J., Bastian, A. J., Wolf, E. J., Husson, E. M., Labrecque, B. A., & Hendershot, B. D. (2017). Locomotor adaptability in persons with unilateral transtibial amputation. *PLoS ONE, 12*(7). doi:10.1371/journal.pone.0181120

Data Sheet: STF SG - Standard, STF Technologies LLC (2015).

De Asha, A. R., Munjal, R., Kulkarni, J., & Buckley, J. G. (2013). Walking speed related joint kinetic alterations in trans-tibial amputees: impact of hydraulic 'ankle' damping. *J Neuroeng Rehabil, 10*(107). doi:10.1186/1743-0003-10-107

De Asha, A. R., Munjal, R., Kulkarni, J., & Buckley, J. G. (2014). Impact on the biomechanics of overground gait of using an 'Echelon' hydraulic ankle-foot device in unilateral trans-tibial and trans-femoral amputees. *Clinical Biomechanics, 29*(7), 728-734. doi:10.1016/j.clinbiomech.2014.06.009

Decker, M. J., Halbach, C. J., Nam, C. H., Wagner, N. J., & Wetzel, E. D. (2011). Stab resistance of shear thickening fluid ( STF ) - treated fabrics. *Recent Patents on Materials Science, 4*, 565-578. doi:10.1016/j.compscitech.2006.08.007

Ding, J., Tracey, P. J., Li, W., Peng, G., Whitten, P. G., & Wallace, G. G. (2013). Review on shear thickening fluids and applications. *Textiles and Light Industrial Science and Technology, 2*, 161-173.

Dziaduszewska, M., & Wekwejt, M. (2018). Composites in energy storing prosthetic feet. *European Journal of Medical Technologies, 3*, 16-22.

Fey, N. P., & Hargrove, L. J. (2014). Controlling Knee Swing Initiation and Ankle Plantarflexion With an Active Prosthesis on Level and Inclined Surfaces at Variable Walking Speeds. *IEEE Journal of Translational Engineering in Health and Medicine, 2*. doi:10.1109/JTEHM.2014.2343228

Fey, N. P., Klute, G. K., & Neptune, R. R. (2011). The influence of energy storage and return foot stiffness on walking mechanics and muscle activity in below-knee amputees. *Clin Biomech (Bristol, Avon), 26*, 1025-1032. doi:10.1016/j.clinbiomech.2011.06.007

Galindo-Rosales, F. J., Rubio-Hernández, F. J., & Sevilla, A. (2011). An apparent viscosity function for shear thickening fluids. *Journal of Non-Newtonian Fluid Mechanics, 166*, 321-325. doi:10.1016/j.jnnfm.2011.01.001

Gao, F., Liu, Y. N., & Liao, W. H. (2017). Optimal design of a magnetorheological damper used in smart prosthetic knees. *Smart Materials and Structures, 26*. doi:10.1088/1361-665X/aa5494

Gates, D. H., Aldridge, J. M., & Wilken, J. M. (2013). Kinematic comparison of walking on uneven ground using powered and unpowered prostheses. *Clinical Biomechanics, 28*, 467-472. doi:10.1016/j.clinbiomech.2013.03.005

Genin, J. J., Bastien, G. J., Franck, B., Detrembleur, C., & Willems, P. A. (2008). Effect of speed on the energy cost of walking in unilateral traumatic lower limb amputees. *European journal of applied physiology, 103*.

Giddings, P. F., Bowen, C. R., Salo, A. I. T., Kim, H. A., & Ive, A. (2010). Bistable composite laminates: Effects of laminate composition on cured shape and response to thermal load. *Composite Structures, 92*, 2220-2225. doi:10.1016/j.compstruct.2009.08.043

Glanzer, E. M., & Adamczyk, P. G. (2018). Design and Validation of a Semi-Active Variable Stiffness Foot Prosthesis. *IEEE Trans Neural Syst Rehabil Eng, 26*, 2351-2359. doi:10.1109/tnsre.2018.2877962

Grimmer, M. (2015). *Powered Lower Limb Prostheses.* (Doctoral). Technical University of Darmstadt, Darmstadt.

Gudmundsson, I., Jonsdottir, F., & Gudmundsson, K. H. (2011, October 10-12). *Fabrication and Characterization of Magnetorheological Elastomers for an Adaptive Spring Element.* Paper presented at the ICAST2011: 22nd International Conference on Adaptive Structures and Technologies, Corfu, Greece.

Gudmundsson, K. H., Jonsdottir, F., Thorsteinsson, F., & Gutfleisch, O. (2011). An Experimental Investigation of Unimodal and Bimodal Magnetorheological Fluids with an Application in Prosthetic Devices. *Journal of Intelligent Material Systems and Structures, 22*, 539-549. doi:10.1177/1045389X11403821

Guo, Y., Wei, Y., Zou, J., Huang, C., Wu, X., Liu, Z., & Yang, Z. (2018). Impact and usage of the shear thickening fluid (STF) material in damping vibration of bolted flange joints. *Smart Materials and Structures*. doi:10.1088/1361-665X/aaef6c Manuscript

Guy, B. M., Hermes, M., & Poon, W. C. K. (2015). Towards a Unified Description of the Rheology of Hard-Particle Suspensions. *Physi, 115*. doi:10.1103/PhysRevLett.115.088304

Hansen, A. H., Childress, D. S., & Knox, E. H. (2004). Roll-over shapes of human locomotor systems: Effects of walking speed. *Clinical Biomechanics, 19*, 407-414. doi:10.1016/j.clinbiomech.2003.12.001

Hansen, A. H., Childress, D. S., Miff, S. C., Gard, S. A., & Mesplay, K. P. (2004). The human ankle during walking: implications for design of biomimetic ankle prostheses. *Journal of Biomechanics, 37*, 1467-1474. doi:10.1016/j.jbiomech.2004.01.017

Hansen, A. H., & Starker, F. (2016). Prosthetic Foot Principles and Their Influence on Gait. In B. Müller & S. I. Wolf (Eds.), *Handbook of Human Motion* (1 ed., pp. 1343-1358). Stuttgart: Springer International Publishing AG.

Hansen, A. H., & Wang, C. C. (2010). Effective rocker shapes used by able-bodied persons for walking and fore-aft swaying: Implications for design of ankle–foot prostheses. *Gait & Posture, 32*, 181-184.

Harrison, J. S., & Ounaies, Z. (2001). *Piezoelectric Polymers* (2001-43). Retrieved from Langley Research Center, Hampton, Virginia:

Hedrick, E. A., Malcolm, P., Wilken, J. M., & Takahashi, K. Z. (2019). The effects of ankle stiffness on mechanics and energetics of walking with added loads: a prosthetic emulator study. *Journal of NeuroEngineering and Rehabilitation, 16*(148). doi:10.1186/s12984-019-0621-x

Heitzmann, D. W. W., Salami, F., De Asha, A. R., Block, J., Putz, C., Wolf, S. I., & Alimusaj, M. (2018). Benefits of an increased prosthetic ankle range of motion for individuals with a trans-tibial amputation walking with a new prosthetic foot. *Gait & Posture, 64*, 174-180. doi:10.1016/j.gaitpost.2018.06.022

Herr, H. M., & Grabowski, A. M. (2012). Bionic ankle-foot prosthesis normalizes walking gait for persons with leg amputation. *Proceedings. Biological sciences, 279*, 457-464. doi:10.1098/rspb.2011.1194

Imam, B., Miller, W. C., Finlayson, H. C., Eng, J. J., & Jarus, T. (2017). Incidence of lower limb amputation in Canada. *Canadian Journal of Public Health, 108*, 374-380. doi:10.17269/CJPH.108.6093

ISO 10328:2016. (2016). In *Prosthetics — Structural testing of lower-limb prostheses — Requirements and test methods*: International Organization for Standardization.

ISO/TS 16955:2016 (2016). In *Prosthetics - Quantification of physical parameters of ankle foot devices and foot units*: International Organization for Standardization.

Jamali, S., & Brady, J. F. (2019). Alternative Frictional Model for Discontinuous Shear Thickening of Dense Suspensions : Hydrodynamics. *Physical Review Letters, 123*, 138002. doi:10.1103/PhysRevLett.123.138002

Jin, L., Adamczyk, P. G., Roland, M., & Hahn, M. E. (2016). The Effect of High- and Low-Damping Prosthetic Foot Structures on Knee Loading in the Uninvolved Limb Across Different Walking Speeds. *Journal of Applied Biomechanics, 32*, 233-240. doi:10.1123/jab.2015-0143

Johnson, L., De Asha, A. R., Munjal, R., Kulkarni, J., & Buckley, J. G. (2014). Toe clearance when walking in people with unilateral transtibial amputation: Effects of passive hydraulic ankle. *The Journal of Rehabilitation Research and Development, 51*, 429-438. doi:10.1682/JRRD.2013.05.0126

Kalman, D. P., Merrill, R. L., Wagner, N. J., & Wetzel, E. D. (2009). Effect of particle hardness on the penetration behavior of fabrics intercalated with dry particles and concentrated particle-fluid suspensions. *ACS Applied Materials and Interfaces, 1*(11), 2602-2612. doi:10.1021/am900516w

Kandil, A. H. (2016). Finite Element based Model of Modified Niagara Foot and its Effect on Stiffness. *International Journal of Computer Applications, 134*. doi:10.5120/ijca2016907837

Ke, M.-J., Huang, K.-C., Lee, C.-H., Chu, H.-Y., Wu, Y.-T., Chang, S.-T., . . . Su, K.-C. (2017). Influence of Three Different Curvatures Flex-Foot Prosthesis While Single-leg Standing or Running : A Finite Element Analysis Study. *Journal of Mechanics in Medicine and Biology, 17*, 1750055-1750051-1750012. doi:10.1142/S0219519417500555

Kern, A. M., Papachatzis, N., Patterson, J. M., Bruening, D. A., & Takahashi, K. Z. (2019). Ankle and midtarsal joint quasi-stiffness during walking with added mass. *PeerJ, 7*, e7487. doi:10.7717/peerj.7487

Klenow, T. D., Kahle, J. T., & Highsmith, M. J. (2016). The dead spot phenomenon in prosthetic gait: Quantified with an analysis of center of pressure progression and its velocity in the sagittal plane. *Clinical Biomechanics, 38*, 56-62. doi:10.1016/j.clinbiomech.2016.08.013

Klodd, E., Hansen, A., Fatone, S., & Edwards, M. (2010). Effects of prosthetic foot forefoot flexibility on gait of unilateral transtibial prosthesis users. *Journal of rehabilitation research and development, 47*(9), 899-910. doi:10.1682/JRRD.2010.01.0003

Koehler-McNicholas, S. R., Nickel, E. A., Barrons, K., Blaharski, K. E., Dellamano, C. A., Ray, S. F., . . . Hansen, A. H. (2018). Mechanical and dynamic characterization of prosthetic feet for high activity users during weighted and unweighted walking. *PLoS ONE, 13*(9), e0202884. doi:10.1371/journal.pone.0202884

Kuder, I. K., Arrieta, A. F., Raither, W. E., & Ermanni, P. (2013). Variable stiffness material and structural concepts for morphing applications. *Progress in Aerospace Sciences, 63*, 33-55. doi:10.1016/j.paerosci.2013.07.001

Lee, Y. S., & Wagner, N. J. (2003). Dynamic properties of shear thickening colloidal suspensions. *Rheologica Acta, 42*, 199-208. doi:10.1007/s00397-002-0290-7

Lin, Y., Shaffer, J. W., & Sodano, H. A. (2010). Electrolytic deposition of PZT on carbon fibers for fabricating multifunctional composites. *Smart Materials and Structures, 19*(12), 124004-124004. doi:10.1088/0964-1726/19/12/124004

Mahmoodi, P., Aristodemou, S., & Ransing, R. S. (2016). Prosthetic foot design optimisation based on roll-over shape and ground reaction force characteristics. *Proceedings of the Institution of Mechanical Engineers, Part C: Journal of Mechanical Engineering of science, 231*, 3093-3103. doi:10.1177/0954406216643110

Maranzano, B. J., & Wagner, N. J. (2001). The effect of particle size on reversible shear thickening of concentrated colloidal dispersions. *The Journal of Chemical Physics, 114*, 10514-10527. doi:10.1063/1.1373687

Mari, R., Seto, R., Morris, J. F., & Denn, M. M. (2014). Shear thickening , frictionless and frictional rheologies in non- Brownian suspensions. *Journal of Rheology, 58*, 1693-1724. doi:10.1122/1.4890747

McGimpsey, G., & Bradford, T. C. (2008). *Limb prosthetics services and devices*. Retrieved from

Mei, Z., Guerrero, V. H., Kowalik, D. P., & Chung, D. D. L. (2002). Reverse piezoelectric behavior of carbon fiber thermoplastic-matrix composite. *Polymer Composites, 23*(5), 697-701. doi:10.1002/pc.10470

Moody, M. J., Marvin, C. W., & Hutchison, G. R. (2016). Molecularly-doped polyurethane foams with massive piezoelectric response. *J. Mater. Chem. C, 4*(20), 4387-4392. doi:10.1039/C6TC00613B

Moriana, A. D., Tian, T., Sencadas, V., & Li, W. (2016). Comparison of rheological behaviors with fumed silica-based shear thickening fluids. *Korea-Australia Rheology Journal, 28*, 197-205. doi:10.1007/s13367-016-0020-9

Muhammad, A., Yao, X.-l., & Deng, Z.-c. (2006). Review of magnetorheological (MR) fluids and its applications in vibration control. *Journal of Marine Science and Application, 5*(3), 17-29. doi:10.1007/s11804-006-0010-2

Mujika, F. (2007). On the effect of shear and local deformation in three-point bending tests. *Polymer Testing, 26*, 869-877. doi:10.1016/j.polymertesting.2007.06.002

Noroozi, S., Rahman, A. G. A., Khoo, S. Y., Zahedi, S., Sewell, P., Dyer, B., & Ong, Z. C. (2014). The dynamic elastic response to impulse synchronisation of composite prosthetic energy storing and returning feet. *Proceedings of the Institution of Mechanical Engineers, Part P: Journal of Sports Engineering and Technology, 228*, 24-32. doi:10.1177/1754337113501491

Olabi, A. G., & Grunwald, A. (2007). Design and application of magneto-rheological fluid. *Materials & Design, 28*(10), 2658-2664. doi:10.1016/j.matdes.2006.10.009
Omasta, M., Paloušek, D., Návrat, T., & Rosický, J. (2012). Finite element analysis for the evaluation of the structural behaviour, of a prosthesis for trans-tibial amputees. *Medical Engineering & Physics, 34*, 38-45. doi:10.1016/j.medengphy.2011.06.014
Palmer, R. M., & Green, P. C. (2008).
Park, J., Yoon, G.-h., Kang, J.-w., & Choi, S.-b. (2016). Design and control of a prosthetic leg for above-knee amputees operated in semi- active and active modes. *Smart Materials and Structures, 25*. doi:10.1088/0964-1726/25/8/085009
Peters, I. R., Majumdar, S., & Jaeger, H. M. (2016). Direct observation of dynamic shear jamming indense suspensions. *Nature Letter, 532*, 214-217. doi:10.1038/nature17167
Phulé, P. P. (2001). Magnetorheological (MR) fluids : Principles and applications. *Smart Materials Bulletin(February),* 7-10.
Pickle, N. T., Wilken, J. M., Aldridge, J. M., Neptune, R. R., & Silverman, A. K. (2014). Whole-body angular momentum during stair walking using passive and powered lower-limb prostheses. *Journal of Biomechanics, 47*(13), 3380-3389. doi:10.1016/j.jbiomech.2014.08.001
Piezoelectric Actuators. (2014). In I. Physik (Ed.): PI Ceramic GmbH.
Pro-Flex Catalog. (2019). Retrieved from res.cloudinary.com/ossur/image/upload/v1573570065/product-documents/en-us/PN20158/catalogs/PN20158_Pro-Flex_Pivot.pdf
Quesada, P., & Skinner, H. B. (1991). Analysis of a below-knee patellar tendon-bearing prosthesis: A finite element study. *The Journal of Rehabilitation Research and Development, 28*. doi:10.1682/JRRD.1991.07.0001
Ramadan, K. S., Sameoto, D., & Evoy, S. (2014). A review of piezoelectric polymers as functional materials for electromechanical transducers. *Smart Materials and Structures, 23*(3), 033001-033001. doi:10.1088/0964-1726/23/3/033001
Raschke, S. U., Orendurff, M. S., Mattie, J. L., Kenyon, D. E., Jones, O. Y., Moe, D., . . . Kobayashi, T. (2015). Biomechanical characteristics, patient preference and activity level with different prosthetic feet: a randomized double blind trial with laboratory and community testing. *J Biomech, 48*(1), 146-152. doi:10.1016/j.jbiomech.2014.10.002
Ray, M. C., & Batra, R. C. (2009). Effective Properties of Carbon Nanotube and Piezoelectric Fiber Reinforced Hybrid Smart Composites. *Journal of Applied Mechanics, 76*(3), 034503-034503. doi:10.1115/1.3063633
Rigney, S. M., Simmons, A., & Kark, L. (2017). Mechanical characterization and comparison of energy storage and return prostheses. *Medical Engineering and Physics, 41*, 90-96. doi:10.1016/j.medengphy.2017.01.003
Rouse, E. J., Gregg, R. D., Hargrove, L. J., & Sensinger, J. W. (2013). The difference between stiffness and quasi-stiffness in the context of biomechanical modeling. *IEEE Trans Biomed Eng, 60*(2), 562-568. doi:10.1109/tbme.2012.2230261
Rouse, E. J., Hargrove, L. J., Perreault, E. J., & Kuiken, T. A. (2014). Estimation of human ankle impedance during the stance phase of walking. *IEEE Trans Neural Syst Rehabil Eng, 22*(4), 870-878. doi:10.1109/tnsre.2014.2307256
Saavedra Flores, E. I., Friswell, M. I., & Xia, Y. (2013). Variable stiffness biological and bio-inspired materials. *Journal of Intelligent Material Systems and Structures, 24*(5), 529-540. doi:10.1177/1045389X12461722

Safaeepour, Z., Eshraghi, A., & Geil, M. (2017). The effect of damping in prosthetic ankle and knee joints on the biomechanical outcomes: A literature review. *Prosthetics and Orthotics International, 41*, 336-344. doi:10.1177/0309364616677651

Safaeepour, Z., Esteki, A., Ghomshe, F. T., & Osman, N. A. A. (2014). Quantitative analysis of human ankle characteristics at different gait phases and speeds for utilizing in ankle-foot prosthetic design. *BioMedical Engineering OnLine, 13*.

Safety Data Sheet: STF, STF Technologies LLC (2015).

Saunders, M. M., Schwentker, E. P., Kay, D. B., Bennett, G., Jacobs, C. R., Verstraete, M. C., & Njus, G. O. (2003). Finite Element Analysis as a Tool for Parametric Prosthetic Foot Design and Evaluation. Technique Development in the Solid Ankle Cushioned Heel (SACH) Foot. *Computer Methods in Biomechanics and Biomedical Engineering, 6*, 75-87. doi:10.1080/1025584021000048974

Schnall, B. L., Dearth, C. L., Elrod, J. M., Golyski, P. R., Koehler-McNicholas, S. R., Ray, S. F., . . . Hendershot, B. D. (2020). A more compliant prosthetic foot better accommodates added load while walking among Servicemembers with transtibial limb loss. *Journal of Biomechanics, 98*, 109395. doi:10.1016/j.jbiomech.2019.109395

Shell, C. E., Segal, A. D., Klute, G. K., & Neptune, R. R. (2017). The effects of prosthetic foot stiffness on transtibial amputee walking mechanics and balance control during turning. *Clinical Biomechanics, 49*, 56-63. doi:10.1016/j.clinbiomech.2017.08.003

Shepherd, M. K., Azocar, A. F., Major, M. J., & Rouse, E. J. (2018). Amputee perception of prosthetic ankle stiffness during locomotion. *Journal of NeuroEngineering and Rehabilitation, 15*. doi:10.1186/s12984-018-0432-5

Shepherd, M. K., Gunz, D., Lecomte, C., & Rouse, E. J. (2019). *Methods for Describing and Characterizing the Mechanical Behavior of Running-Specific Prosthetic Feet*. Paper presented at the IEEE 16th International Conference on Rehabilitation Robotics (ICORR), Toronto, Canada.

Shepherd, M. K., & Rouse, E. J. (2017). The VSPA Foot: A Quasi-Passive Ankle-Foot Prosthesis With Continuously Variable Stiffness. *IEEE Transactions on Neural Systems and Rehabilitation Engineering, 25*(12), 2375-2386. doi:10.1109/TNSRE.2017.2750113

Shorter, A. L., & Rouse, E. J. (2020). Ankle Mechanical Impedance During the Stance Phase of Running. *IEEE Trans Biomed Eng, 67*(6), 1595-1603. doi:10.1109/tbme.2019.2940927

Sinitski, E. H., Hansen, A. H., & Wilken, J. M. (2012). Biomechanics of the ankle-foot system during stair ambulation: Implications for design of advanced ankle-foot prostheses. *Journal of Biomechanics, 45*(3), 588-594. doi:10.1016/j.jbiomech.2011.11.007

Spaggiari, A. (2012). Properties and applications of magnetorheological fluids. *Frattura ed Integrita Strutturale, 23*, 57-61. doi:10.3221/IGF-ESIS.23.06

Stuhlenmiller, F., Schuy, J., Beckerle, P., & Rinderknecht, S. (2017). A user-specific human-machine interaction strategy for a prosthetic shank adapter. *Current Directions in Biomedical Engineering, 3*(2), 493-496.

Sun, S., Yang, J., Li, W., Deng, H., Du, H., & Alici, G. (2015). Development of a novel variable stiffness and damping magnetorheological fluid damper. *Smart Materials and Structures, 24*. doi:10.1088/0964-1726/24/8/085021

Tian, T., Li, W., Ding, J., Alici, G., & Du, H. (2013). *Study of the temperature effect of shear thickening fluid*. Paper presented at the IEEE/ASME International Conference on Advanced Intelligent Mechatronics (AIM), Wollongong, Australia.
Tian, T., & Nakano, M. (2017). Design and testing of a rotational brake with shear thickening fluids. *Smart Materials and Structures, 26*. doi:10.1088/1361-665X/aa5a2c
Tian, T., Nakano, M., & Li, W. (2018). Applications of shear thickening fluids : a review. *International Journal of Hydromechatronics, 1*(2), 238-257.
Tryggvason, H., Starker, F., Armannsdottir, A. L., Lecomte, C., & Jonsdottir, F. (2020). Speed adaptable prosthetic foot; concept description, prototyping and initial user testing. *IEEE Transactions on Neural Systems and Rehabilitation Engineering, 28*(12), 2978-2986. doi:10.1109/TNSRE.2020.3036329
Tryggvason, H., Starker, F., Lecomte, C., & Jonsdottir, F. (2020a). Use of Dynamic FEA for Design Modification and Energy Analysis of a Variable Stiffness Prosthetic Foot. *Applied Sciences, 10*(2), 650. doi:10.3390/app10020650
Tryggvason, H., Starker, F., Lecomte, C., & Jonsdottir, F. (2020b). Variable stiffness prosthetic foot based on rheology properties of shear thickening fluid. *Smart Materials and Structures, 29*(9). doi:10.1088/1361-665X/ab9547
Ventura, J., Klute, G., & Neptune, R. (2011). The effect of prosthetic ankle energy storage and return properties on muscle activity in below-knee amputee walking. *Gait & Posture, 33*, 220-226. doi:10.1016/j.gaitpost.2010.11.009
Versluys, R., Beyl, P., Damme, M. V., Desomer, A., Ham, R. V., & Lefeber, D. (2009). Prosthetic feet : State-of-the-art review and the importance of mimicking human ankle – foot biomechanics. *Disability and Rehabilitation: Assistive Technology, 4*, 65-75. doi:10.1080/17483100802715092
Villani, M., Delmonte, D., Culiolo, M., Calestani, D., Coppedè, N., Solzi, M., . . . Zappettini, A. (2016). Turning carbon fiber into a stress-sensitive composite material. *J. Mater. Chem. A, 4*(27), 10486-10492. doi:10.1039/C6TA02646J
Vinney, J., Noroozi, S., Rahman, A. G. A., Sewell, P., Chao, O. Z., Kuan, K. K., & Dupac, M. (2012). Analysis of Composite Prosthetic Energy-Storing-and-Returning (ESR) feet: A comparison between FEA and the experimental analysis. *International Journal of COMADEM, 15*, 19-28.
Wagner, N. J., & Brady, J. F. (2009). Shear thickening in colloidal dispersions. *Phys. Today, 62*, 27-32. doi:10.1063/1.3248476
Wegener, M. (2010, April 2010). *Piezoelectric polymer foams: transducer mechanism and preparation as well as touch-sensor and ultrasonic-transducer properties.* Paper presented at the Procedings of the SPIE.
Wereley, N. M., & Pang, L. (1998). Nondimensional analysis of semi-active electrorheological and magnetorheological dampers using approximate parallel plate models. *Smart Materials and Structures, 7*, 732-743.
White, F. M. (1991). *Viscous fluid flow* (L. Beamesderfer & J. M. Morriss Eds. 2nd ed.). Singapore: McGraw-Hill, Inc.
Williams, R. J., Hansen, A. H., & Gard, S. A. (2009). Prosthetic Ankle-Foot Mechanism Capable of Automatic Adaptation to the Walking Surface. *Journal of Biomechanical Engineering, 131*(3), 035002 035001-035007. doi:10.1115/1.3005335

Womac, N. D., Neptune, R. R., & Klute, G. K. (2019). Stiffness and energy storage characteristics of energy storage and return prosthetic feet. *Prosthet Orthot Int, 43*(3), 266-275. doi:10.1177/0309364618823127

Yeh, F.-y., Chang, K.-c., & Chen, T.-w. (2012). *Smart Viscous Dampers utilizing Shear Thickening Fluids with Silica Nanoparticles*. Paper presented at the 15th World Conference on Earthquake Engineering, Lisbon, Portugal.

Zelik, K. E., Collins, S. H., Adamczyk, P. G., Segal, A. D., Klute, G. K., Morgenroth, D. C., . . . Kuo, A. D. (2011). Systematic variation of prosthetic foot spring affects center-of-mass mechanics and metabolic cost during walking. *IEEE Trans Neural Syst Rehabil Eng, 19*(4), 411-419. doi:10.1109/tnsre.2011.2159018

Zhang, X. Z., Li, W. H., & Gong, X. L. (2008). The rheology of shear thickening fluid (STF) and the dynamic performance of an STF-filled damper. *Smart Materials and Structures, 17*(3). doi:10.1088/0964-1726/17/3/035027

Zhou, H., Yan, L., Jiang, W., Xuan, S., & Gong, X. (2016). Shear thickening fluid–based energy-free damper: Design and dynamic characteristics. *Journal of Intelligent Material Systems and Structures, 27*, 208-220. doi:10.1177/1045389X14563869

Ziegler-Graham, K., MacKenzie, E. J., Ephraim, P. L., Travison, T. G., & Brookmeyer, R. (2008). Estimating the Prevalence of Limb Loss in the United States: 2005 to 2050. *Archives of Physical Medicine and Rehabilitation, 89*(3), 422-429. doi:10.1016/j.apmr.2007.11.005

Zmitrewicz, R. J., Neptune, R. R., Walden, J. G., Rogers, W. E., & Bosker, G. W. (2006). The effect of foot and ankle prosthetic components on braking and propulsive impulses during transtibial amputee gait. *Archives of Physical Medicine and Rehabilitation, 87*(10), 1334-1339.

# Appendix A

# Details on FEA of roll-over test

Section 2.4.2 describes testing methods for evaluating prosthetic foot performance in a mechanical test setup, standardized in ISO/TS 16955:2016. Figure 2.3 shows the schematic setup of the test equipment and control functions for the equipment. These include the M-shaped force curve and the rotation of the tilt table as functions of time over the stance duration. The FEM simulation of the roll-over test imitates these in a transient analysis.

The parts of the test equipment, rod and tilt table, are modeled in the 3D space along with the model of the foot. Both parts are defined fully rigid and aligned internally in accordance to the standard. The foot is aligned to the end of the rod and defined fixed to the rod. Contact is defined between the elements of the bottom sole blade and the tilt table. The friction is set to prevent sliding. Constraints are defined to the test equipment parts. A translational joint is defined between “ground” and the ball joint at the top of the rod, so the rod is free to rotate around all axes but constrained to movement along the y-axis in the space (i.e. up/down) (see “Ball joint” in Figure 2.3). A rotational joint is defined between “ground” and the tilt table in the rotation axis (marked in Figure 2.3) so it is fixed in the space but free to rotate. The boundary conditions are then defined to the two parts in their degree of freedom. The M-shaped force curve is applied on the ball joint of the rod, in the y-direction, as a function of time. Likewise, the function described in the curve for the rotation, from -20° decline rolling over to 40° incline is defined to the tilt-table.

The analysis is run for the stance phase of 0.6 s according to the boundary condition functions, corresponding to a 1.0 s normalized step time. The program determines the sub-step sizes (function of time) and calculates each step in several iterations. Generally, the calculations for simulations of the roll-over testing are done in 50-70 sub-steps, rendering all results as continuous curves as a function of time.

# Appendix B

# Effects of temperature on the STF

As discussed in sections 3.5 and 3.6, the shear thickening properties of the STF are assumed to be temperature dependent. The effect of this dependency was avoided in the measurements presented in chapters 5 and 6, by performing all measurements at controlled room temperature of 21-22°C. To investigate the effect of varying temperature on the STF piston, some additional measurements were made at different temperatures. The temperature was controlled by submersing the damper into water bath at controlled temperature for 25 minutes. The damper was then taken out of the bath and insulation wrapped around the cylinder. The damper was then setup in the uniaxial testing machine and the test sequence run, as described in section 5.3.1. Figure B.1 shows the results for a STF damper with a gap dimension of 320µm. Measurements were carried out for temperatures of 15, 25, 35 and 45°C.

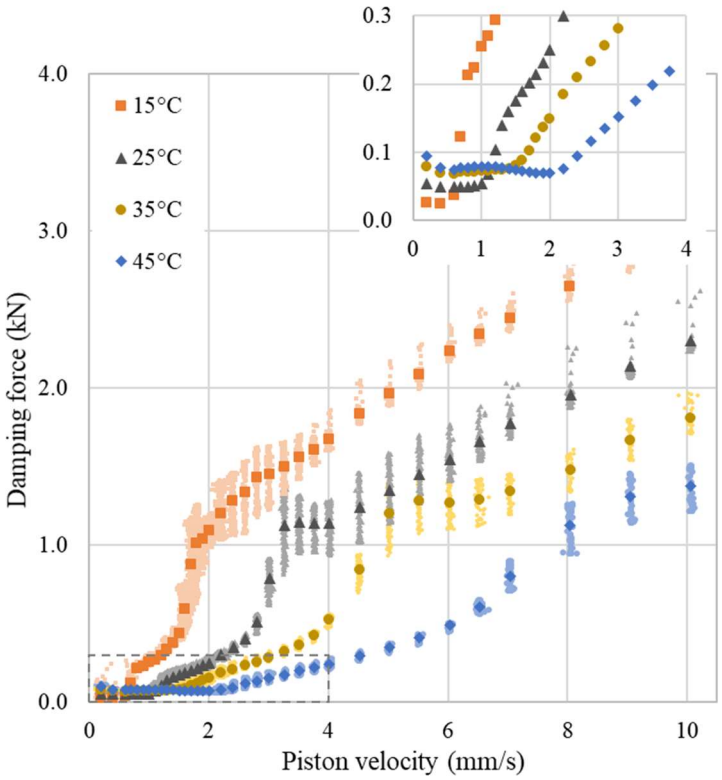


*Figure B.1 Damping force vs. piston velocity for an STF damper of 320 µm piston gap at different temperatures.*

As anticipated, the results clearly show a higher critical velocity and overall lower damping forces with increased temperature. The damping force below the critical piston velocity seems to be consistently lower for lower temperature. The opposite would be expected as

the force should be governed by the liquid phase viscosity in this flow region. At these low velocities, the frictional forces of the rod's seals and bearings are high compared to the forces from the pressure gradient of the fluid flow. Thermal expansion in damper components could therefore explain this effect.

There is a clear turning point in the curves at a damping force 1.0 to 1.2 kN, following the exponential increase in force from the critical point. In the data set for 25 and 35°C there is a clear plateau in the force before it continues to increase linearly with higher velocity. It is assumed that this plateau represents the maximum viscosity value and starting of shear thinning after the DST.

The results for 15 and 25°C would be relevant for ambient temperature change that could be experienced in the use of the device. The higher temperatures are more indicative on behavior of the fluid, in the case where it would heat up due to excessive shearing. It is clear from these results that the force response in an STF filled device would change according to the ambient temperature. Quick adjustments would be needed on the device to compensate for this change.

# Appendix C

# Effects of pressure on STF properties

As described in section 5.2.4, an effort was made in the filling process of the STF damper to limit the amount of air bubbles trapped in the fluid. The parts of the damper assembly were primed with fluid before assembly and filled syringes were filled and stored at room temperature for at least 24 hours before use, to allow small air bubbles to gather. The fluid chamber was flushed with STF before closing the filling holes with the plug screws. As this process became more effective in eliminating air, an increase in force reaction and lower critical velocity of the damper was noticed. The reason for the unexpected rise in force was soon presumed to be due to increased pressure in the fluid chamber, created by volume displacement of the screws when blocking the filling holes (3 mm in diameter and 8 mm long). To map this effect, some additional measurements were made on an STF damper where pressure was put on the fluid in the chamber, compared to the same damper after the pressure had been relieved.

An STF damper was assembled and filled as described above. In the assembly the upper endcap was not tightened fully, leaving a 0.5 mm displacement available in the cap threading (see Figures 5.4 and 6.3 for drawings of damper). Before measuring the damper in the uniaxial testing machine, the endcap was tightened into the O-ring used to seal the chamber. Reducing the volume of the chamber increased the pressure. The damper was then measured repeatedly in the test sequence. The pressure was then relieved through the filling holes and the damper measured again, for comparison. Unfortunately, the pressure in the chamber could not be measured.

The results for the first test run showed that the pressure decreased throughout the run and this run was discarded. The following test runs showed consistent results as the pressure had dropped to a value that the rod seals could hold. Figure C.1. shows the results for a test run where the fluid chamber is pressurized, compared to the results where the pressure had been relived from the chamber. The higher damping forces for velocity below critical value could be higher friction forces from the rod seals under pressure (see inset in Figure C.1). The damping forces are higher in the pressurized damper and the critical piston velocity is lower, showing an overall stronger shear thickening effect. The increased pressure will cause an increased viscosity of the liquid phase of the STF, so much like the temperature change, this will affect the shear thickening properties of the STF.

Consequently, the filling procedure for the STF damper was adapted to this finding and care taken not to pressurize the fluid chamber with the plug screws for the filling holes.

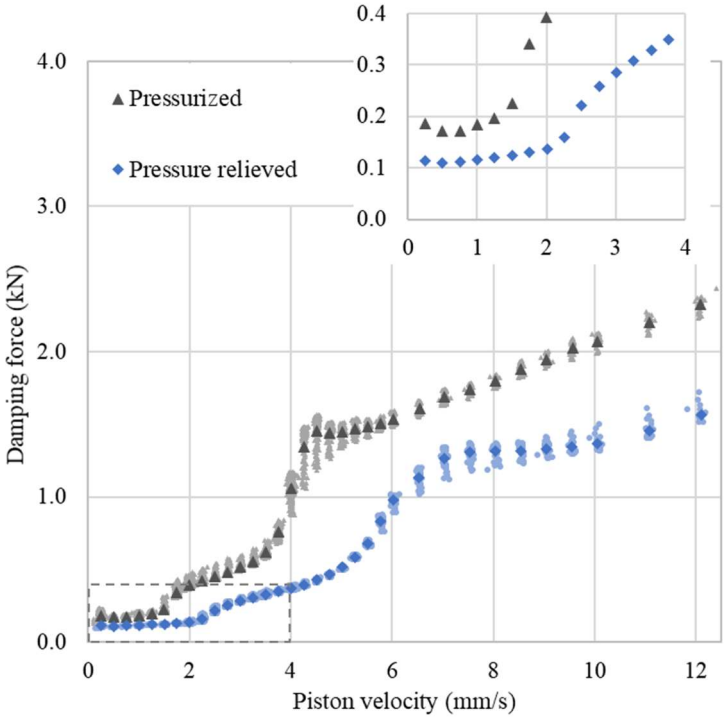


*Figure C.1 Damping force vs. piston velocity for an STF damper with 420 µm piston gap, measured at two different pressures.*